

7-14-2021

## Creation of Hand Sensors and Orthotics to Capture and Replicate Human Movement and Forces

Edward Frank Austin Jr.

*Louisiana State University and Agricultural and Mechanical College*

Follow this and additional works at: [https://repository.lsu.edu/gradschool\\_dissertations](https://repository.lsu.edu/gradschool_dissertations)

---

### Recommended Citation

Austin, Edward Frank Jr., "Creation of Hand Sensors and Orthotics to Capture and Replicate Human Movement and Forces" (2021). *LSU Doctoral Dissertations*. 5616.

[https://repository.lsu.edu/gradschool\\_dissertations/5616](https://repository.lsu.edu/gradschool_dissertations/5616)

This Dissertation is brought to you for free and open access by the Graduate School at LSU Scholarly Repository. It has been accepted for inclusion in LSU Doctoral Dissertations by an authorized graduate school editor of LSU Scholarly Repository. For more information, please contact [gradetd@lsu.edu](mailto:gradetd@lsu.edu).

# CREATION OF HAND SENSORS AND ORTHOTICS TO CAPTURE AND REPLICATE HUMAN MOVEMENT AND FORCES

A Dissertation

Submitted to the Graduate Faculty of the  
Louisiana State University and  
Agricultural and Mechanical College  
in partial fulfillment of the  
requirements for the degree of  
Doctor of Philosophy

in

The School of Electrical and Computer Engineering

by

Edward Frank Austin, Jr., PT, LOT  
B.S., Northeast Louisiana University, 1999  
M.P.T, University of Texas Medical Branch, 2003  
August 2021

## **Acknowledgements**

Gratitude is in order for a few people in my life. First off, thanks to my committee members. A thank you is in order for Dr. Heather Lucas for sacrificing your time to be a part of the committee. Gratification to Drs. Todd Monroe, Nikita Kuznetsov, and Kidong Park for assisting me in this endeavor and offering a helping hand and advice for various portions of this research. Thanks to the staff at Baton Rouge General Medical Center for being flexible with my work schedule and to all my co-workers for the constant encouragement. A thank you to the graduate and undergraduate students that have assisted me through the BioMEMS lab. A special thanks to Young Ho Shinn (Glenn), Pedro J. Chacon, Tallis Huther de Costa, and Chris O'Loughlin for the instruction and assistance with different technical details. Significant gratitude and credit to William Frischhertz, Charles P. Kearney, III, Grace Dirks, Gabriel Breaux, and Prasanna Acharya for the many hours, failures, and successes that we have experienced in the lab. Special thanks to Dr. Sara Wings for the above and beyond assistance, proofreading, and mentoring that has been provided. A huge thanks is in order for Dr. Jin-Woo Choi for providing an incredible learning and growing experience. Thank you for providing the capability to fail and succeed while imparting just the right amount of criticism and guidance in this creative realm. Finally, an immense amount of thanks to my family. Thanks to my mother-in law Jackie Yancey for sewing the force glove together. Also, a huge thanks for all the babysitting. Thanks to my parents for the support throughout this process and the lifelong encouragement that no obstacle is too big. And to my wife, Jennifer Austin, I am so happy that you are in my life. Without your organization and sacrifices to take on numerous jobs and longer hours, I would not have completed this process. I hope this assists my children, Ashlyn, Tré, and Ava, and their generation in some form or fashion.

# Table of Contents

Acknowledgements.....	ii
List of Tables .....	v
List of Figures.....	vi
Abstract.....	x
1. Introduction.....	1
1.1. Motivation.....	1
1.2. Objectives .....	2
2. Background.....	3
2.1. Introduction.....	3
2.2. Orthotics to Move a Paralyzed Hand.....	4
2.3. Reproducing Human Kinematics – Forces and Motion.....	12
3. Force Gloves – Hand Forces.....	17
3.1. Introduction.....	17
3.2. Glove Fabrication.....	17
3.3. Force Glove Calibration with Codamotion System.....	20
3.4. Force Glove Used During Activities of Daily Living (ADL).....	23
3.5. Force Glove Discussion.....	30
4. Force Glove – Motion Capture .....	32
4.1. Introduction.....	32
4.2. Wrist Movements.....	33
4.3. Thumb Movements .....	37
4.4. Index, Middle, Ring and Little Finger Movements .....	46
4.5. Motion Capture Calibration Results and Linearity Values.....	65
4.6. Motion Capture with Force Glove Used During Activities of Daily Living (ADL) .....	66
5. Suggestions on Soft Elastomer Sensors and Actuators for the Hand .....	78
5.1. Introduction.....	78
5.2. Background of a Hand Sensor Design.....	79
5.3. Sensor Characteristics.....	82
5.4. Force Sensor Fabrication, Preliminary Findings, and Encountered Problems .....	85
5.5. Devices to Actuate the Hand and Wrist – Soft Robotics and Mechanical Gear Orthosis .	94
5.6. Summary of Sensors and Actuators.....	100

6. Conclusion .....	102
Appendix A. IRB Approval .....	104
Appendix B. Questionnaire.....	105
Bibliography .....	106
Vita.....	114

## List of Tables

Table 4.1. Linearity ( $R^2$ ) of Goniometric Values Compared to Codamotion Values.....	65
Table 4.2. Can Grasp Task.....	70
Table 4.3: Key turn task ROM.....	73

## List of Figures

Figure 2.1. a) Percutaneous functional electrode system[2] and b) Bioness H200 device.....	7
Figure 2.2. a) Freehand system and b) Saeboflex device .....	8
Figure 2.3. Exomusculature glove: a) all components, and cables on b) dorsum and c) palmar regions.....	9
Figure 2.4. Sixth finger device.....	10
Figure 2.5. Braingate: a) cortical implant, b) DEKA/LUKE arm, c) testing procedure[1] .....	11
Figure 2.6. Types of grasp patterns: a) nonprehensile pointer swipe, b) hook grasp, c) spherical grasp, d) cylindrical grasp, e) tripod grasp, f) tip-to-tip pinch, g) lateral pinch .....	12
Figure 2.7. Manual muscle testing chart and procedures.....	14
Figure 2.8. Dynamometer .....	15
Figure 2.9. Cyberglove .....	16
Figure 3.1. FlexiForce glove fabrication: (a) glove with flexiforce sensors, (b) glove with flexiforce sensors and membranes viewable, (c) PCB, and (d) PCB with attachments of flexiforce (green arrow), 1 M $\Omega$ resistor (red arrow), and output wire (orange arrow).....	17
Figure 3.2. Force sensor positions .....	18
Figure 3.3. Voltage divider circuit of FlexiForce sensor .....	19
Figure 3.4. Calibration of FlexiForce sensors: a.) calibration pedestal with flexiforce sensor, b) Winware weight added, and c) graph of weight to Codamotion units.....	20
Figure 3.5. Calibration curve of each sensor embedded in the force glove.....	22
Figure 3.6. a) Can grasp and b) key turn activities with force glove.....	24
Figure 3.7. Can grasp and key turn calibration: a) Fast fourier transform of force glove sensor, b) unfiltered sensor data, and c) low pass 10 Hz filter.....	25
Figure 3.8. Can grasp results and analysis: (a) graphs of force during can grasp task with 3 subjects and 3 trials and (b) average maximum value during those 3 trials with a heat map of forces represented at each phalanx. ....	26
Figure 3.9. Key turn results a) graphs of force during key turn task with 3 subjects and 3 trials, and b) average maximum value during those 3 trials with a heat map of forces represented at each phalanx.....	27

Figure 4.1. 26 sensors placed on the hand .....	32
Figure 4.2. Motions of the wrist.....	33
Figure 4.3. a) Sensor position of the forearm and hand, b) forearm plane with out-of-plane vector, and c) forearm plane with perpendicular vector .....	34
Figure 4.4. a) Wrist in extension and radial deviation, b) components of vector $FI$ , c) relation of vector $BA$ to $FI$ , and d) radial/ulnar deviation ( $\angle\alpha$ ) and flexion/extension ( $\angle\beta$ ) angles. ...	36
Figure 4.5. Calibration graphs: a) wrist radial deviation and b) flexion.....	37
Figure 4.6. Motions of the thumb CMC joint: a) abduction/adduction, b) flexion/extension, and c) opposition.....	38
Figure 4.7. a) Forearm plane on hand with right hand rule and b) forearm plane with perpendicular vector.....	39
Figure 4.8. a) Thumb CMC hand plane and vectors, b) perpendicular and parallel vectors of $EH$ , c) out of plane (abduction/adduction) angles, and D) in-plane (flexion/extension) angles. 40	
Figure 4.9. Thumb CMC calibration: a) full extension and adduction, b) neutral thumb, c) full thumb flexion, and d) full thumb abduction .....	42
Figure 4.10. Calibration values of a) CMC flexion/extension and b) CMC abduction/adduction	43
Figure 4.11. a) Thumb MCP flexion and extension and b) IP flexion/extension .....	44
Figure 4.12. a) Thumb MCP flex, b) illustration of MCP vector planes, c) thumb IP flex, and d) illustration of IP vector planes .....	45
Figure 4.13: a) Thumb MCP Calibration and b) Thumb IP Calibration .....	46
Figure 4.14. MCP motions: a) abduction/adduction and b) flexion/extension .....	47
Figure 4.15. a) Index finger plane and b) perpendicular vector, c) middle finger plane and d) perpendicular vector, e) ring finger plane and f) perpendicular vector, and g) little finger plane and h) perpendicular vector.....	48
Figure 4.16. a) Index finger hand plane and vectors, b) perpendicular and parallel vectors of $IN$ , c) out-of-plane angle (flexion/extension), and d) in-plane angles (abduction/adduction)...	49
Figure 4.17. Digits 2-5 MCP flexion/extension and abduction/adduction calibration graphs.....	60
Figure 4.18. Digit 2-5 a) PIP flexion/extension and b) DIP flexion/extension.....	61
Figure 4.19. Digits 2-5 a) PIP flexion/extension sensors, b) DIP flexion/extension .....	63

Figure 4.20. Digits 2-5 PIP and DIP flexion/extension calibration graphs.....	64
Figure 4.21. a) Sensor positions without filter with zero marks, b - c) sensor positions zeroes removed unfiltered, d-e) fourier transform of sensor positions, and f-g) sensor positions with 0.001-10 Hz bandpass filter .....	67
Figure 4.22. Can grasp mean results for a) subject 1, b) subject 2, c) subject 3, and (d) between subjects.....	69
Figure 4.23: Key turn grasp mean results for a) subject 1, b) subject 2, c) subject 3, and (d) between subjects .....	71
Figure 5.1. CNT finger sensor .....	79
Figure 5.2. Graphene, single-walled, and multi-walled CNT[1] .....	80
Figure 5.3. Considerable motions of the finger .....	82
Figure 5.4. Mechanical properties of silicon rubber and skin: a) Translational and b) rotational	83
Figure 5.5. Three dimensional forces applied to the finger .....	83
Figure 5.6. CNT solution injected into printer cartridge .....	85
Figure 5.7. a) Grid patterns formulated on Fusion 360, b) printed on inkjet printer, and c) resultant transparencies.....	86
Figure 5.8. a) Laser engraver used to cut out transparency aligner board and b) laser engraver transparency cut .....	87
Figure 5.9. a) PLA casting aligners, transparencies, and rings, and b) silicon rubber casting .....	88
Figure 5.10. a) Transparency/SR released from PLA casting aligner, b) placed in an acrylic aligner, c) laser cut to precision, and d) resultant transparency/SR structure.....	89
Figure 5.11. a) Infrared heating of SR/ transparency, b) removal of transparency, and c) aluminum wired adhered to SR with silver epoxy and aluminum adhesive tape .....	90
Figure 5.12. 2D to 3D transformation of SR: a) wrap SR on inner PLA device to form b), combine outer shell around inner PLA/SR, d) pour liquid SR, and e) completed cylindrical device .....	91
Figure 5.13. Recorded resistances of released CNT/SR device related to IR heat exposure .....	92
Figure 5.14. Model of soft robotics: a) inflation and expansion of SR, b) encircled SR allowing linear translation, c) restrictive layer creating cantilever ( <a href="https://softroboticstoolkit.com">https://softroboticstoolkit.com</a> ).....	95

Figure 5.15. Fabrication of SR orthosis: a) MCP PLA piece and valve, b) PIP PLA piece and valve, c) polyethylene glycol (PEG) poured into MCP and PIP cast, d) MCP and PIP with PEG, e) casting with SR, and f) SR completed cast ..... 96

Figure 5.16. SR orthotic: a) independent MCP and PIP chambers, b) inflated device, and c) strain gauge measurements at the distal tip of the PIP/DIP and MCP..... 97

Figure 5.17. Gear orthosis: a) at rest, b) with MCP flexion, c) gearmotor with angle overhang, d) current fabricated device..... 99

## **Abstract**

Paralysis is a debilitating condition affecting as many as 5.4 million in the United States. Upper extremity paralysis/paresis is the most debilitating form of paralysis due to the robust kinematic patterns in our hands and wrist. These forces and movements available at our hand allow us to manipulate objects as small as a sewing needle yet still lift multiple grocery bags at one time on a daily basis. Inability to use the upper extremities usually necessitates 24-hour assistance. Therefore, it is imperative to build devices that are biomimetic to assist those with upper extremity paralysis. To accomplish this feat, this research attempted to capture forces and movement of the hand and wrist during activities of daily living (ADLs). An understanding of the forces and movement is imperative in designing algorithms for orthotics and prosthetics that mimic human movement. As a result of this collected data, flaws in design of sensors attempting to capture force and movement were discovered. Therefore, preliminary research was attempted to create sensors that could lead to better kinematic data. These sensors could also provide sensory feedback to those wearing prosthetics and orthotics. The final portion of the research dealt with the creation of orthotics or actuators of the hand. Two methods including soft robotics and mechanic gear orthotics were attempted. Further research in the actuation portion in order to create a device that is widely used by those who have some form of upper extremity paresis.

# 1. Introduction

## 1.1. Motivation

The motivation for this author came when an opportunity presented itself to work with a patient in his young 20-age range who had recently experienced a spinal cord injury.

Unfortunately for this patient, he suffered a spinal cord injury in the C6 region. This injury has left him with full paralysis in his lower limbs, trunk, and much of his upper extremities. The main motivation for this project was the patient's requirement for assistance with simple activities such as feeding, daily hygiene tasks such as brushing teeth, and using a cellphone to ask for assistance. The initial objective of this dissertation was to develop a device that could provide hand function for those who have suffered hand paralysis. In this author's work history as a physical and occupational therapist, there have been devices, such as prosthetics, that can provide life-altering opportunities to those who have suffered limb loss. (SUCH AS THE C-LEG AND DEKA ARM). There are also the investigative devices that utilize electromyogram (EMG) and electroencephalogram (EEG) human output to control prosthetics. However, there are very few commercially available devices that can attach to a paralyzed human limb and provide compensatory movement for that limb. Most of the current devices on the market with this intention are lower extremity devices that assist with knee and ankle paralysis. There are very few devices that actually assist with hand function. The main motivation for this project was the patient's requirement for assistance with simple activities such as feeding, daily hygiene tasks such as brushing teeth, or even using a cellphone to ask for assistance.

## 1.2. Objectives

In order to create a device, a literature review was initially carried out to determine the kinematics of the hand that occur when moving the hand. After exploration, it was easy to see that there was limited specific data on minimal force requirements and angular kinematics to complete daily tasks such as grasping utensils. Therefore, a force glove was created that contained resistive FlexiForce sensors (FSR) on each of the phalanges (14 sensors in all). On this same glove, LEDs were placed appropriately over each of the wrist and finger joints and recorded with motion sensor technology.

When performing data analysis, it became very evident there were many limitations in this method. Limitations included inability to capture the full breadth of the finger as well as the small distinct features of the finger. An advantage of being in the BioMEMS research group was that other members of the group were developing cheap, robust, and relatively simple resistive sensors using carbon nanotubes. Working in cooperation with those team members, an application was proposed to build a grid of sensors on the fingers and palmar surface of the hand to measure the force of the fingers and palm of the hand more accurately. In this proposed method, a grid of carbon nanotubes was printed onto a transparency and transferred to a silicon rubber substrate through a casting technique. Each grid pattern would then be returned to a microcontroller. This method would allow a better representation of the full surface of the finger as well as better capability of capturing forces when small objects are grasped by the hand.

The last portion of the research related to passive movement of the hand in which the human user would be able to control the movement. The methods attempted to complete this feat have included servomotor exoskeleton and soft robotics. These methods will require more attention even after completion of this dissertation.

## 2. Background

### 2.1. Introduction

Paralysis is a life altering condition that affects nearly 5.4 million in the United States. There are varying causes of paralysis including but not limited to spinal cord injury (SCI), cerebrovascular disease (CVA), peripheral nerve injury, amyotrophic lateral sclerosis (ALS), cerebral palsy (CP) as well as many other neurological diseases.[3]. Those affected with paralysis may lose the ability to perform activities of daily living (ADLs) including walking, dressing, bathing, and evening feeding independently. Economically, the effects of paralysis can be devastating. Depending on the severity of paralysis, individuals may be unable to return to work or may even require a caregiver to assist with the above-mentioned ADLs. The National Spinal Cord Injury Statistical Center (NSCISC) revealed that the mean annual caregiver cost per individual following the first year of SCI was \$114,515 for C1-C4 injury (no extremity function, ventilator assistance). The cost of caregiver assistance decreases to \$61,780 for C5-C8 injury and \$25,524 for T1-S5 injuries.[4]

In C1-C4 injuries, there is no upper extremity (UE) function. Individuals with C5-C8 injuries have impaired UE function and T1-S5 injuries have intact upper extremity function. The reason for increased caregiver assistance relates to the amount of upper extremity impairment not only in SCI but in all types of paralysis. To live independently, upper extremity and most important, hand function is critical. Therefore, it is important to develop assistive devices that restore upper extremity and hand function to those who have paralysis.

## 2.2. Orthotics to Move a Paralyzed Hand

As mentioned previously, absent, or impaired hand function results in a lack of independence. Therefore, it is imperative to develop devices to assist with hand function. Archeologists have found evidence of prosthetics that date as far back as 2700 BC [5]. Early signs of splinting were also unearthed by archeologists around that period. When speaking about prosthetics and orthotics/splints, there is one criterion that differentiates the devices. Prosthetics is the term used to describe a device that substitutes for a missing limb. Prosthetics are devices typically worn by individuals who have lost a limb through either amputation or congenital (birth) anomaly in which a limb did not develop in utero. When referring to orthotics, these are typically devices that assist a remaining but paralyzed limb in movement and/or function. Individuals that wear orthotics typically suffer paralysis because of a neuromuscular or musculoskeletal injury. Examples of those that wear orthotics are survivors of spinal cord injury, stroke, peripheral nerve injury, and/or individuals born with anomalies such as cerebral palsy.

A brief history of electrophysiology is important to understand since paralysis is a recurring topic in this dissertation. This understanding of electrical impulses as the cause of muscle contraction is a field referred to as electromyography. There were scientists dating as far back as the 1600's and 1700's named Jan Swammerdam and Isaac Newton who introduced the concept of electrophysiology. In fact, it is believed that Jan Swammerdam may have been the first scientist to use electrical stimulation on the nerve of a frog leg to create a muscle contraction[6]. Despite this early movement, it was widely accepted in the early 18<sup>th</sup> century that movement was created by "nervous fluids" in the brain that caused "movement spirits." During the 18<sup>th</sup> century, researchers such as Henry

Cavendish, Stephen Hales, and Luigi Galvani attempted to refute this idea. They are responsible for the electrophysiological model in which electrical activity communication between the brain and nerves results in muscular activity. The aforementioned Galvani published the first journal article in which an exogenous electrical stimulation to the peripheral nerve of a frog caused the frog's muscle to contract[7].

As a result of World Wars I and II and the spread of the neuromuscular disease poliomyelitis, significant breakthroughs were made in the fields of electromyography, prosthetics, and orthotics during the early 20<sup>th</sup> century. During this time, it was imperative that more resources be utilized to study these fields across the world. Early and mid-twentieth century devices typically focused on lower extremity devices that assisted with walking. However, there were cable assisted upper extremity devices that did allow the users to manipulate objects with their prosthetics. Significant limitations existed in the early 20<sup>th</sup> century preventing greater advance of upper extremity orthotics to compensate for neuromuscular paralysis. The most significant problem being that the hand and wrist relates to the void of technology that could build dynamic joints in a small region. The problem with the wrist and hand is that there are so many joints in a small region that result in a large amount of motion. Therefore, upper extremity orthotic devices created during this period most often were static splints that prevented injury of the paralyzed hand but did not actually assist with improved function.

Within the field of electrophysiology, there was a plethora of research being published between the 1920's and 1970's. Researchers Sir Charles Sherrington and Edgar Adrian expanded on the brain topography created by Korbinian Brodmann and Wilder Penfield. This led to a great understanding of the sensory (sensations of touch, vibration, hot/cold, etc.) and

motor (muscle contraction) pathways between the brain, spinal cord, and peripheral contents (muscles, skin, etc.) Their work resulted in mapping the portions of the brain that received the sensory information (sensory homunculus) and exported the motor commands (motor homunculus) to and from the brain [8]. During the period of the 1950's to 1980's, researchers Patrick Merton and David Marsden began to explain the "servo theory" in relation to muscle contraction. This theory explains how small sensory organs termed muscle spindles within a muscle result in a reflex arc of muscle contraction. This theory is also customarily known as the stretch reflex in which a reflex hammer contacts a tendon which results in a stretch of the muscle spindles of the tendon. The spindles send an afferent action potential back to the spinal cord. In turn, an efferent action potential is propagated from the spinal cord directly back to the muscle. This results in contraction of the muscle. These researchers revealed that a mechanical force was not the only method to cause this contraction. They also utilized electrical stimulation to the surface of the skin (surface electrodes) to cause this involuntary muscle contraction [8].

As a result of this aforementioned research, the 1970's and 1980's saw a growth in research that involved moving the paralyzed upper extremity. The proposed methods for moving the paralyzed wrist and hand included electrically stimulating the impaired nervous system to create an open-loop muscle contraction/movement of the limb. The initial devices utilized percutaneous electrodes that were injected by a hypodermic needle through the skin into the desired muscles. The needles were connected to a wire that exited the skin and connected to a controller. Early research involved quadriplegics and revealed that stimulating muscles of the forearm and hand improved function with eating and writing[9] as well as improvement in pinch[10] and grip strength[2]. Although there

was some promise with these early devices, problems such as electrode fracture and non-response after short period of time were the initial encounters. There were also problems regarding the method of controlling the stimulation. Early attempts with these electrical stimulation devices utilized an open loop system in which the user had no control over the electrical stimulation. Some devices did attempt closed control systems but utilized

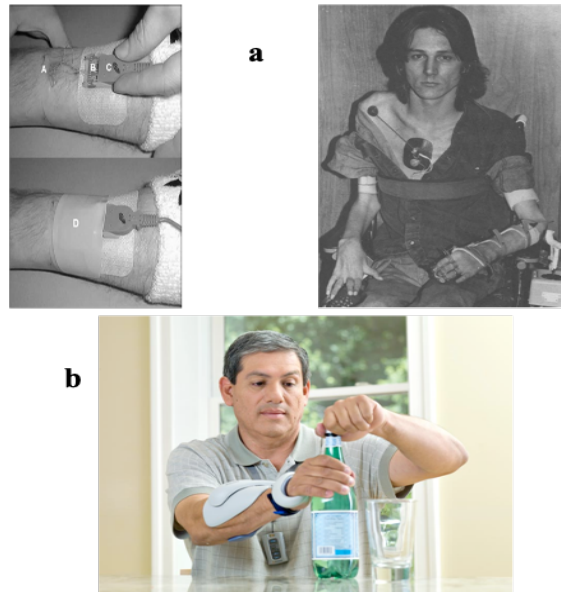


Figure 2.1. a) Percutaneous functional electrode system[2] and b) Bioness H200 device

methods that were not associated with the hand. Examples included using the opposite arm or proximal joints such as the shoulder and neck. This often resulted in significant difficulty controlling the device.

Continued research methods attempted to use less invasive methods to stimulate the hand and wrist. The Bioness H200 was developed and utilized surface electrodes placed over the wrist and hand musculature. This device works on an open loop system. Therefore, the user typically utilized this device as a piece of exercise equipment to stimulate the hand and wrist musculature after a neuromusculoskeletal injury. This device was not intended to be used to assist with ADLs. In a study, this device was utilized to

study its effects on individuals who had suffered a CVA. Participants were separated into two groups. One group received conventional physical therapy treatment. The other group received conventional physical therapy treatment along with treatment time each week using the Bioness H200. After 12 weeks of treatment, the participant in the Bioness H200 group were able to pick up more blocks on the Box and Blocks Test, were faster at completing the Jebsen-Taylor object lift test, and scored better on the Fugl-Meyer test (upper extremity function test).[11]

Another device, termed the Freehand System, utilized a much more invasive approach. Intramuscular electrodes were surgically implanted into wrist and hand musculature and connected, via multiple leads, to a transmitting unit/stimulator (consisting of a processor and power source). This processor was implanted within the body in the chest region. An external controller, a 2-axis joystick sensor, communicated with the internal processor via a radiofrequency coil. It is placed at the opposite and non-affected/paretic upper extremity. The user can control movements of the hand into lateral pinch and gross grasp. Initial testing was performed with four spinal cord injured participants with a C5-C6 lesion. Results of the study demonstrated increased lateral pinch

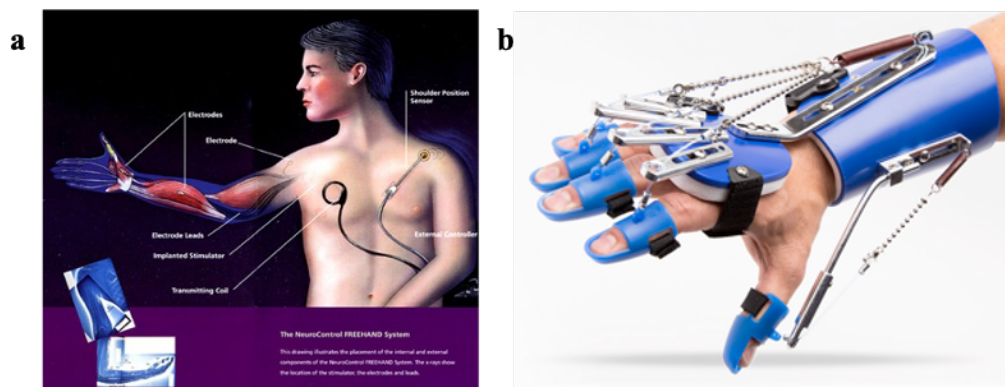


Figure 2.2. a) Freehand system and b) Saeboflex device

and gross grasp of 1.8 and 1.6 kg., respectively, after implantation of the device. This is impressive considering there was no measurable force in either hand position prior to implantation.[12]

There are also orthotic devices that do not rely on electrical stimulation to move the hand. These devices utilize a brace and some type of spring tension or actuator to move the hand. Saebo, Inc. created a few devices that assist those with neuromusculoskeletal injuries. The SaeboFlex is a spring-loaded dynamic splint/exoskeleton that passively pulls the wrist and fingers into extension. The Saeboreach is an extension to the SaeboFlex that passively assists the elbow into extension. These devices are utilized by users who have movement at the hand but have either excessive hand tone or partial paralysis that prevents a functional hand. SaeboMAS was found to enable decreased tone of the proximal shoulder musculature, which also enabled increased activity at the forearm and hand musculature.[13, 14] The limitation with the device is that active elbow flexion and wrist/hand flexion is required to operate the device.

Another design utilized a glove with Bowden cables attached to each finger on the dorsal and palmar sides. The device was termed an “exomusculature glove” and was

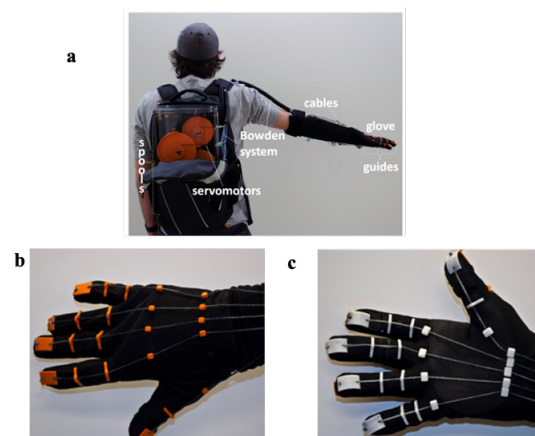


Figure 2.3. Exomusculature glove: a) all components, and cables on b) dorsum and c) palmar regions

controlled via surface electromyography (sEMG) over the wrist and hand musculature. Although this device was never tested on the injured population, the researchers did use the device with a mannequin hand to determine the glove was capable of creating a 15 Newton force.[15] The major problem with this device was the actual hardware of the device weighed approximately 13 pounds.

Another novel device is the Sixth finger. This device is a modular moveable structure composed of servomotors at each module. It is attached to the distal wrist by a rubber strap and acts like an additional thumb. The structure was able to perform a power



Figure 2.4. Sixth finger device

grasp and precision grasp in a non-conventional method. The power grasp was accomplished by securing an object, such as a cup, between the device itself and the radial forearm/wrist region of the user. The precision grasp secured smaller objects, such as a key, between the device and the dorsal thenar eminence of the user. This device was controlled by an on/off switch on a ring that the user wore on the opposite/non-affected hand. By pressing a button on the ring, the Sixth Finger either opened or closed, depending on the mode and button being pressed. Also on that ring was a pressure/force sensor feedback system that relayed information about the force being applied to the object in the Sixth Finger. This feedback system utilized force-sensing resistors applied to each module, which was relayed back to the ring. In this study, one participant with left sided hemiparesis performed the Frenchay Arm Test (FAT) with and without the assistance of the Sixth Finger. The test consisted of five parts: 1) stabilize a ruler, 2) grasp a cylinder, 3)

pick up a glass, 4) remove a clothespin, and 5) comb hair. Without the Sixth finger, the user was only able to stabilize the ruler. With the device, the user was able to stabilize a ruler, grasp a cylinder, and pick up a glass.[16, 17]

A more recent device utilizes a cortical implant to control a prosthesis (DEKA arm). The technology has been termed Braingate. A study utilized a participant who had suffer a brainstem stroke. As a result, she was unable to use her arms and legs. The participant had the implant indwelling in her brain for 5 years. During that time, she had participated in multiple experiments. Therefore, algorithms of movement had been captured over the previous years. During the experiment, the participant was asked to pick up a coffee bottle from a table, bring it to her mouth, drink coffee through the straw in the bottle, and replace the bottle on the table. In the experiment, the DEKA prosthesis was not anchored on the patient's body. Prior to the

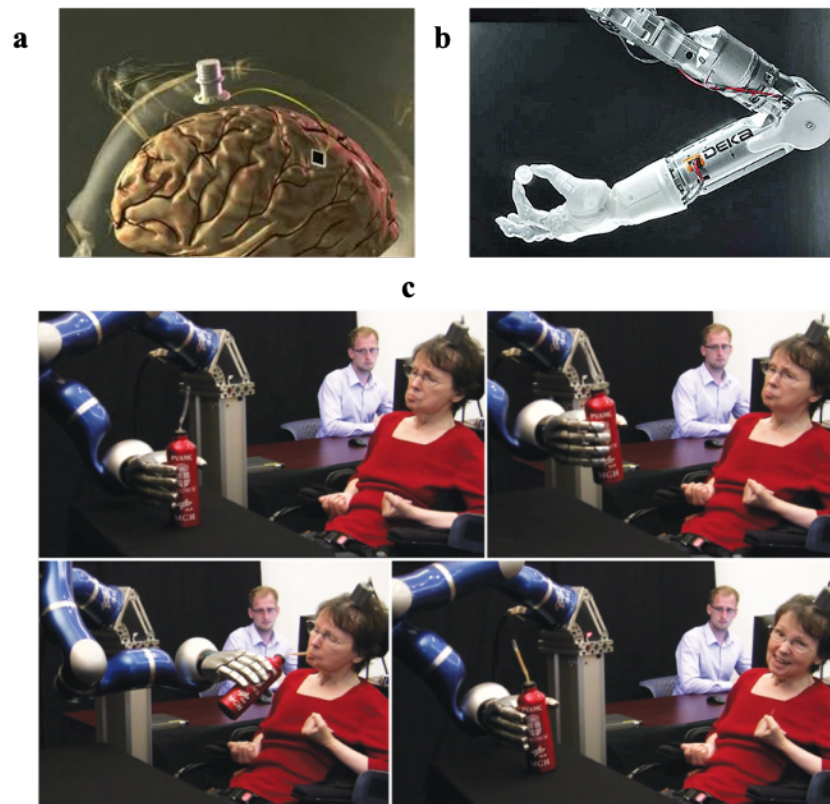


Figure 2.5. Braingate: a) cortical implant, b) DEKA/LUKE arm, c) testing procedure[1]

testing, the patient had 14 minutes of practice with the task before completing the tasks. What is remarkable is that the patient was successful in this task four out of six times in an 8.5-minute testing session. This test is indicative of the ability to control devices with a brain-machine interface[1].

The evidence above proves that there is a distinct interest in improving upper extremity function for those who have suffered some form of paralysis. To create these biomimetic devices, greater understanding of human movement and the forces the hand produces during ADLs is required.

### 2.3. Reproducing Human Kinematics – Forces and Motion

With advances in prosthetic, robotic, and orthotic technology, there is a need for greater knowledge of human hand forces and joint motions during daily activities to mimic human behavior. Classification studies infer that there are as many as 33 different types of hand grasp patterns used by humans [18]. Simpler methods of describing hand grasp positions start with

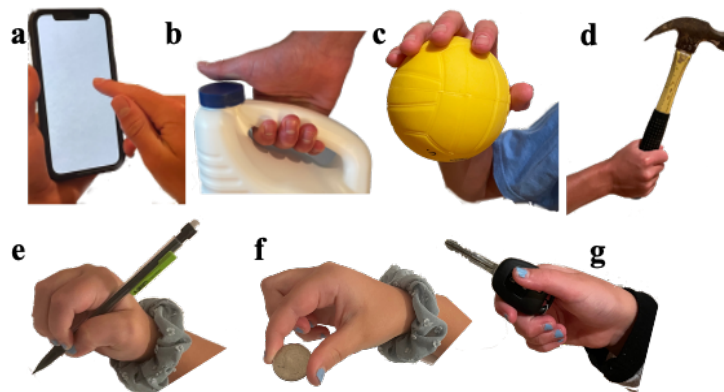


Figure 2.6. Types of grasp patterns: a) nonprehensile pointer swipe, b) hook grasp, c) spherical grasp, d) cylindrical grasp, e) tripod grasp, f) tip-to-tip pinch, g) lateral pinch

classification into prehensile (grasping an object) and non-prehensile (object manipulated but not grasped) movements[19]. Non-prehensile patterns often involve positioning of the fingers to scroll, swipe, stretch and tap touchscreens such as a smart phone. Prehensile movements have

been widely studied and can be subdivided into power and precision grip movements. The power grip movements are categorized as contact between the object, the fingers, and the palm. These positions are usually divided into hook, spherical, and cylindrical grasp positions. Hook grasp results in fingers approximating with an object with the thumb absent from the grasp. Spherical utilizes each finger and the thumb and results in ring and little fingers rotating to wrap around an object. Cylindrical grasp is like spherical grasp, yet the ring and index fingers do not rotate around the object. Precision grasp consists of object manipulation with the fingers and opposing thumb. The precision grasp positions include tripod grasp, tip-to-tip grasp, and lateral pinch positions. These non-prehensile and prehensile hand manipulation positions can be seen in Figure 2.1.

Salter[20] provides an interesting review on the methods utilized to record forces and joint motions leading up to the 1950's. Interest in understanding muscular strength/forces date back as far as the 1800's when diseases such as muscular dystrophy were suspected. According to Salter, the neurologist Dr. Guillaume-Benjamin-Amand Duchenne required ways of assessing neurological weakness. He initially utilized a sling that was positioned around a limb of a participant on one side and attached to a spring on the other side. The participant was asked to push against the sling and the displacement of the spring was utilized to determine the strength of the participant.[21] As a result of injuries suffered by soldiers in World War I and an outbreak of poliomyelitis in the 1920's, methods were attempted to standardize a cheap and efficient method of assessing strength so that multiple practitioners could easily replicate and understand the findings. A subjective method that still utilized the quantitative methods of grading muscle strength on a scale between 0-5 was proposed.[22, 23] At the rank of 0-1, there is no muscle contraction or contraction that produces minimal joint movement. To achieve a score of 2, there

## MANUAL MUSCLE TESTING PROCEDURES

Key to Muscle Grading				
	Function of the Muscle	Grade		
<b>No Movement</b>	No contractions felt in the muscle	0	0	Zero
	Tendon becomes prominent or feeble contraction felt in the muscle, but no visible movement of the part	T	1	Trace
<b>Test Movement</b>	<b>MOVEMENT IN HORIZONTAL PLANE</b>			
	Moves through partial range of motion	1	2-	Poor-
	Moves through complete range of motion	2	2	Poor
	<b>ANTIGRAVITY POSITION</b>			
	Moves through partial range of motion	3	2+	
<b>Test Position</b>	<i>Gradual</i> release from test position	4	3-	Fair-
	Holds test position (no added pressure)	5	3	Fair
	Holds test position against slight pressure	6	3+	Fair+
	Holds test position against slight to moderate pressure	7	4-	Good-
	Holds test position against moderate pressure	8	4	Good
	Holds test position against moderate to strong pressure	9	4+	Good+
	Holds test position against strong pressure	10	5	Normal

**Figure 2.7. Manual muscle testing chart and procedures**

is voluntary movement of the limb. However, there is not sufficient strength to move the limb against gravity. Achieving grades of 3 or greater would mean the participant is able to move the limb against gravity and greater levels of resistance. Further understanding can be understood by referencing figure 2.2.[24] This method is still in use by most medical practitioners today. However, there are limitations in subjectivity which will be discussed later.

In the 1950's, a device called the dynamometer was developed by Rudd in an attempt to create a more objective measure of hand strength.[25] This device utilized a spring strain gauge. This device utilized a spring strain gauge attached to a handle that a participant would grasp with a gross grasp technique. There were studies that date back as far as the 1950's when attempting to measure forces of the hand[26, 27]. In these studies, the dynamometer measurements of those affected by poliomyelitis were recorded to investigate strength improvements during the course of various treatments. Studies dating back to the 1980s were undertaken to build a library of



Figure 2.8. Dynamometer

normative grip and prehensile hand forces per age.[28] However, the dynamometer and pinchmeter record forces produced by the hand as a whole. In order to better understand the hand, a greater understanding of individual phalangeal forces and motion data during activities of daily living (ADLs) is required.

In order to measure finger forces, multiple studies have proposed a variety of gloves and force sensors attached to the hand in a multitude of ways.[29, 30] Asakawa et al[31] did document maximal forces as high as 6.7 Newtons when performing a stretching function on a touchscreen. However, this activity required multiple fingers and the resultant actual force per finger (not phalanx) was only 1.02 N. Another study by Kargov et al. [32] details mean forces of spherical, cylindrical, and tip-to-tip grasp patterns with 17.6 N as a maximal force in spherical grasp. However, the forces measured were also the summed forces of either the phalangeal bones or the summed forces of the three to four sensors on each finger.

With the advent of virtual reality and new sensors, companies such as CyberGlove, Inc. have created products that provide sensory data and feedback for the hands. Products such as the Cyberglove, Cybertouch, Cybergrasp, and Cyberforce are gloves that capture movement patterns of the hand as well as providing sensory feedback of vibration, force, and movement.

This allows users to interact with the virtual world. However, there are limitations to these gloves as they do not capture the forces that the hand imparts on an object when grasping or manipulating the object. These devices are also a bit large and cumbersome on the hand. In order to better mimic the human hand in robotics, orthotics, and prosthetics, a greater understanding of these forces and motions during ADLs is needed. In order to accomplish this goal, this researcher performed an experiment using FlexiForce sensors placed at each of the 14 phalanges and motion capture of the wrist/hand while performing multiple prehensile activities.



Figure 2.9. Cyberglove

### 3. Force Gloves – Hand Forces

#### 3.1. Introduction

As stated previously, a greater understanding of hand forces is required to mimic human movement for future endeavors in robotics, prosthetics, and orthotics. Previous research with Tekscan FlexiForce sensors has been mentioned previously. Due to the low cost and large amount of research performed with these devices, these sensors were chosen for this experiment.

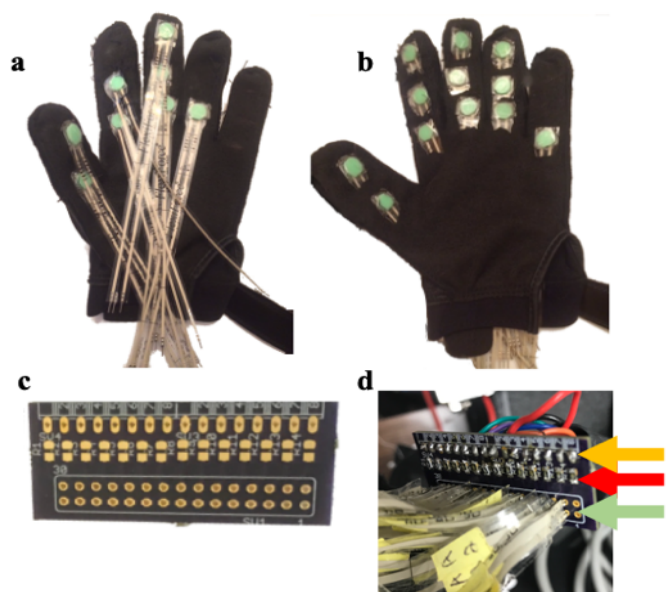


Figure 3.1. FlexiForce glove fabrication: (a) glove with FlexiForce sensors, (b) glove with FlexiForce sensors and membranes viewable, (c) PCB, and (d) PCB with attachments of FlexiForce (green arrow), 1 M $\Omega$  resistor (red arrow), and output wire (orange arrow)

#### 3.2. Glove Fabrication

For the purposes of capturing the individual forces for each of the phalanges (bones of the fingers), fourteen FlexiForce A201(Tekscan, Massachusetts, USA) standard sensors were purchased. These sensors are piezoresistive sensors that demonstrate decreased resistance with increased pressure. Due to the large size of the sensors, each of the sensors was sewn into a

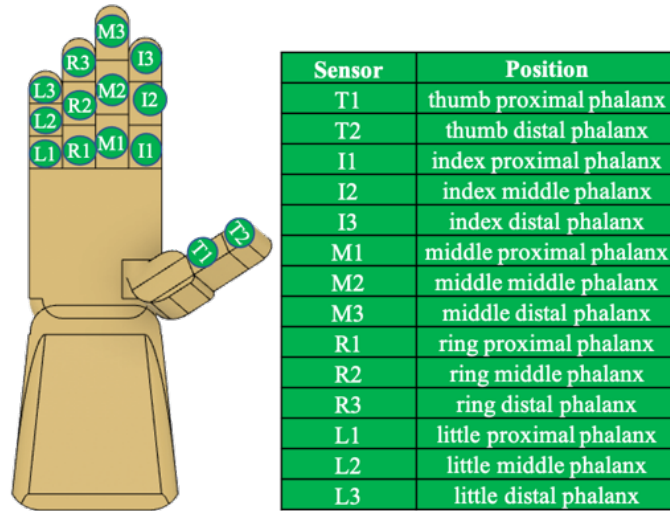


Figure 3.2. Force sensor positions

standard fabric glove. A small, round thermoplastic membrane was adhered onto the FlexiForce sensors to center the forces onto the sensors. The membrane was cut to 0.375-inch diameter so that the full diameter of the FlexiForce sensor was utilized. Each of the sensors distal pins was soldered in parallel to a printable circuit board (PCB) (OSH Park, Oregon, USA) with a 1 MΩ resistor. Output wires were soldered to the PCB and attached on the opposite end to a channel connector provided by Motion Labs Systems (Motion Lab System, Louisiana, USA). The channel connectors consisted of eight ports that were attached to the Ovid Codamotion (Codamotion, Rothley, United Kingdom) hard drive. A 5V input voltage was provided by an Arduino microcontroller in parallel to all FlexiForce sensors.

This circuit created by the 1 MΩ resistor and FlexiForce sensors is a voltage divider. As explained in Figure 3.2, the voltage divider can be explained as a simple circuit:

$$V_{IN} = IR_1 + IR_2$$

In this equation,  $R_1$  is the FlexiForce sensor and  $R_2$  is the 1 M $\Omega$  resistor. Rearranging the formula, we can deduce:

$$I = \frac{V_{IN}}{R_1 + R_2}$$

On the output side of the equation:

$$V_{OUT} = IR_2$$

Substituting  $I$ , we get the equation:

$$V_{OUT} = \left( \frac{V_{IN}}{R_1 + R_2} \right) R_2$$

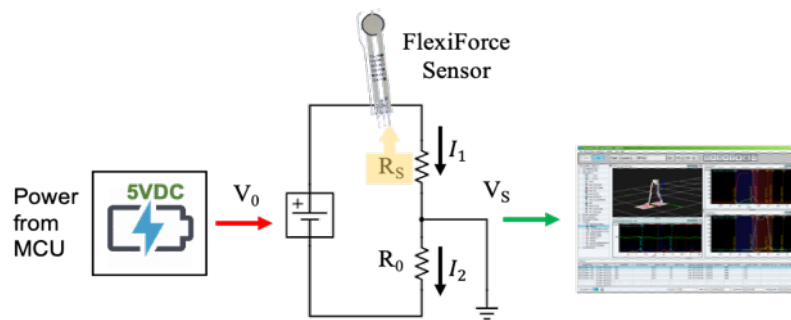


Figure 3.3. Voltage divider circuit of FlexiForce sensor

The FlexiForce sensor ( $R_1$ ) has a resistance greater than 10 M $\Omega$  when there is no pressure applied to the pressure sensor. Therefore, we can infer that when there is no pressure applied to the sensor, the denominator approaches  $\infty$ . From this, we can deduce that  $V_{OUT} \cong 0$  V. When pressure is applied to the sensor,  $R_1$  approaches 0. As  $R_1$  approaches, the equation takes on the form:

$$V_{OUT} = \left( \frac{V_{IN}}{R_2} \right) R_2$$

Therefore,  $V_{OUT} \cong V_{IN} \cong 5$  V. Since the force glove was connected to the Codamotion system, there was an internal analog to digital conversion. Instead of voltage or resistive measurements,

an arbitrary set of numbers were associated with changes in resistance in voltage. This necessitated the calibration of those Codamotion numbers with a standardized set of forces

an arbitrary set of numbers were associated with changes in resistance in voltage. This necessitated the calibration of those Codamotion numbers with a standardized set of forces applied to the FlexiForce sensors.

### 3.3. Force Glove Calibration with Codamotion System

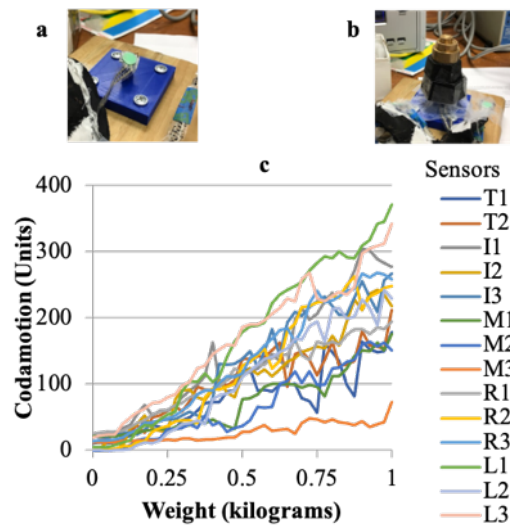


Figure 3.4. Calibration of FlexiForce sensors: a.) calibration pedestal with FlexiForce sensor, b) Winware weight added, and c) graph of weight to Codamotion units

#### 3.3.1. Force Glove Calibration Methods

As stated, the force data collected for the Codamotion system was in a digital format with an arbitrary zero point. Therefore, calibration of the sensors required a standardized format that correlated force applied to the sensors with the appropriate Codamotion numeric value. To accomplish this, a Winware calibration weight set ranging from 0 to 1000 g was applied to the each of the fourteen FlexiForce sensors in increments of 25 grams. A 3D printed pedestal was printed that allowed for the weight set to be placed only on the membrane of the sensor.

Datasheets provided by Tekscan in regards to the FlexiForce sensors have shown that the sensors have linear conductance.[33] While applying the forces to each individual sensor in 25-gram increment, the Codamotion system was utilized to capture each of the forces. The method to perform the task consisted of applying the 25-gram force to the sensor, capturing a 3-5 second period of measurements, and then turning the system off. For each 25 grams of force applied, a 3-5 second recording was captured on each of the sensors. The data was collected at 200 Hz for each recording. These files were saved into a .c3d format and sensors labels and data were then initially analyzed in MATLAB (MathWorks, Massachusetts, USA). The recordings occasionally consisted of short regions where many or even all the sensors gave a zero reading (10 row increments or less). Therefore, those zero points were isolated, and a moving average was utilized to fill in those voids so that the overall average was not skewed. After this averaging, each weight recording was averaged for each of the sensors and the values of Codamotion units (y-axis) was correlated to the weight applied to the sensor (x-axis) in Figure 3.4 as a calibration curve.

### **3.3.2. Force Glove Calibration with Codamotion System - Results**

Calibration curves reveal that the Codamotion signal per force was relatively linear. There were a few exceptions including sensors T1, T2, and M3 where the linearity scores ( $R^2$ ) were slightly poorer compared to most of the sensors. However, those  $R^2$  values were still relatively good at 0.8 or greater. Another other notable issue that occurred during calibration was the variety of values between FlexiForce sensors. A better understanding can be found by looking closely at the graphs. As can be seen, some of the sensors started with Codamotion values at zero whereas others started below and above zero when no weight was applied to the

sensors. On the opposite side of the graphs, some Codamotion values were nearly 400 whereas some ranged only as low as 100 when 10 N of force was applied to the sensor.

### 3.3.3. Force Glove Calibration with Codamotion System - Conclusion

Linearity values were relatively good. Although values were lower for the thumb and middle distal phalanx, those linearity levels were still relatively good at greater than 0.8. A significant problem that occurred with the recordings was the variance in correlating the force

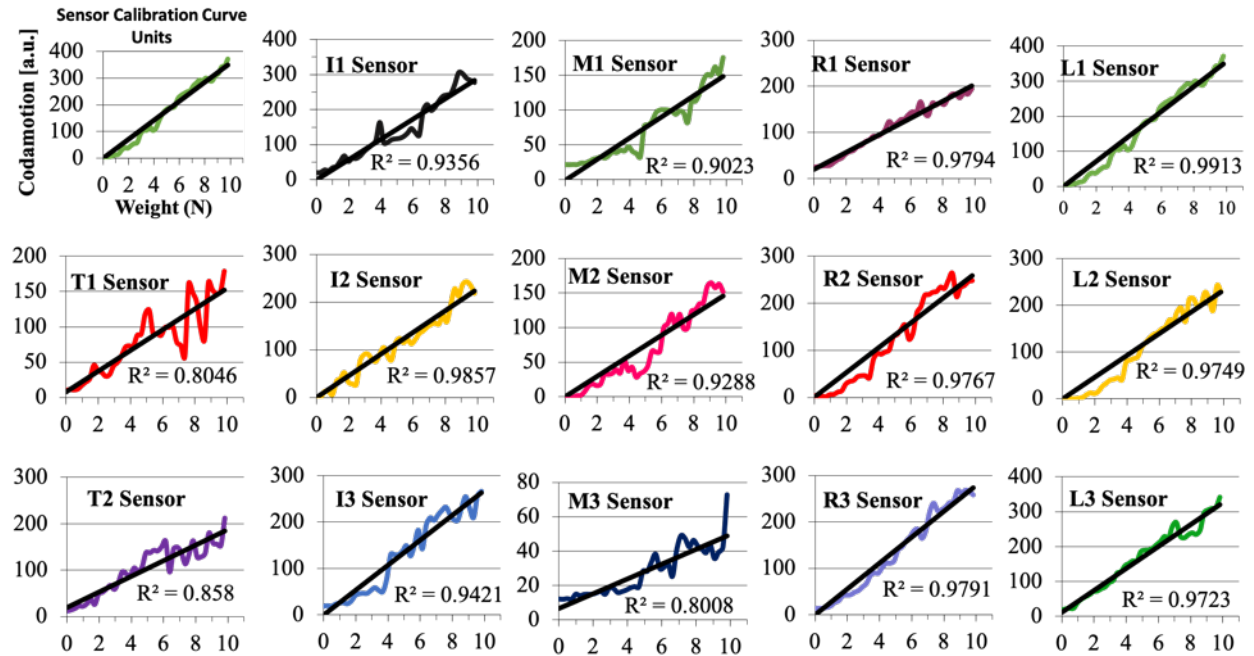


Figure 3.5. Calibration curve of each sensor embedded in the force glove

and Codamotion units between each of the sensors. Specifically, as stated previously, some sensors registered negative Codamotion correlation to a 0 N force whereas other sensors registered values at or greater than zero. As for maximum force values of 10 N, sensor values ranged from 100 Codamotion units compared to 400 Codamotion units between sensors.

Therefore, the y-intercept values were obtained for each of the sensor's results by using the equation:

$$y = mx + b,$$

By rearranging to the formula:

$$x = \frac{y - b}{m}$$

the x-value could be determined resulting in force measurements when a Codamotion value was inserted into the y-value. This method would later be used to convert Codamotion values into force values for future experiments.

### **3.4. Force Glove Used During Activities of Daily Living (ADL)**

As mentioned previously, there is a need to research hand force during ADLs. Therefore, this experiment focused on two ADLs: can grasp and key turning. In these two motions, it is hypothesized that the participants will utilize a spherical gross grasp and lateral pinch grasp, respectively, for each of the activities.

#### **3.4.1. Can Grasp and Key Turn Methods**

Before beginning this experiment, IRB approval (see Appendix) was obtained through Louisiana State University. Three participants voluntarily chose to participate in the experiment and completed a consent form affirming that choice. The participants completed a small questionnaire (see Appendix) obtained information regarding age, race, sex, and information regarding previous hand injury. The participant then donned the force glove. The glove was connected back to the Ovid Codamotion hard drive. Six infrared/near infrared cameras were set up to capture light emitting diode sensors which will further be described in chapter 4. Prior to beginning the experiment, an experimenter applied manual force to each force sensor while another experimenter monitored the Codamotion output values. This procedure was performed prior to testing with each participant to check that each of the sensors was connected to the

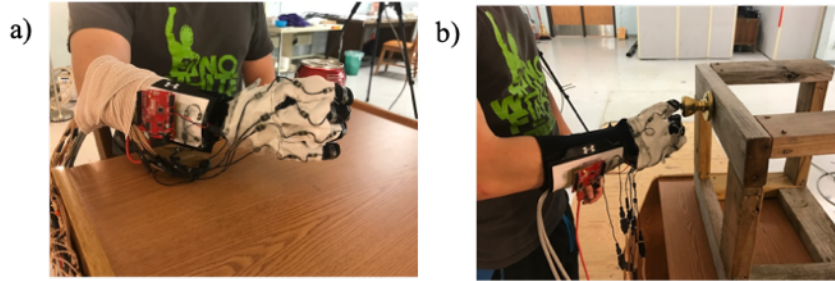


Figure 3.6. a) Can grasp and b) key turn activities with force glove.

Codamotion system. Once this preliminary testing was completed, focus was then turned toward the can grasp and key turn tasks.

In the can grasp task, the participant was asked to grab a full 12-ounce soda can, pick up the soda can and move the can toward his or her mouth (but not touch the mouth). The participant was asked to turn the can as if pouring out the contents into the mouth and then return the can to the table. Prior to using the can for this activity, the participant pantomimed this activity three times. After pantomime, the participant then performed the activity three times while being recorded on the Codamotion system.

Next, the participant took part in a key turn activity. A door handle with a key lock was secured to a wooden frame so that this activity could be performed in front of infrared/near infrared cameras without obstruction. In this activity, the participant was instructed to grab a key that was inserted into a lock and turn the key as far as the lock allowed and then return to neutral. As with the can grasp activity, the participant was first asked to pantomime this activity three times. After completion of pantomime, the participant performed the activity with the key 3 separate time while being recorded on the Codamotion System.

Just as described in the calibration section, the Codamotion system recorded the data at a sampling rate of 200 Hz. That data was collected in a .c3d file format and the data was further analyzed in MATLAB and Microsoft Excel Software Packages. Again, the recordings

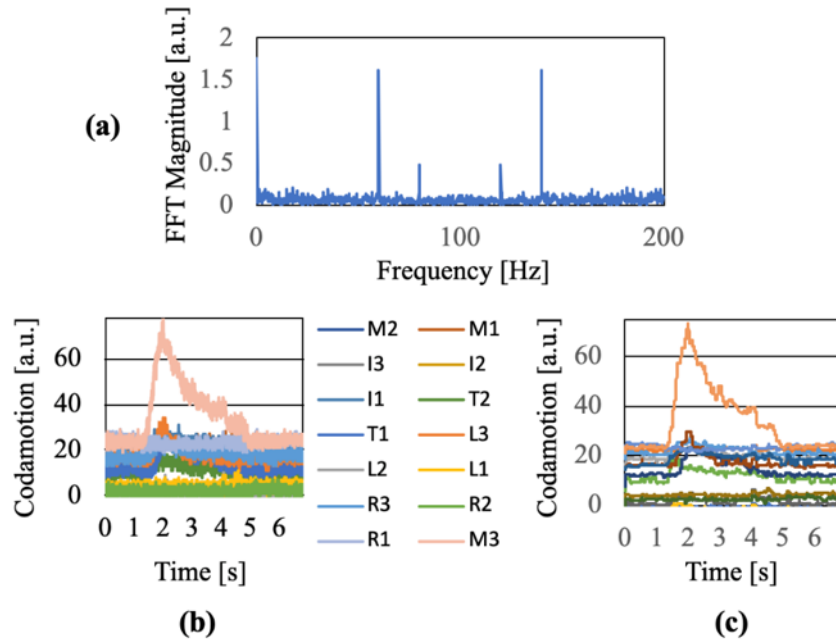


Figure 3.7. Can grasp and key turn calibration: a) Fast fourier transform of force glove sensor, b) unfiltered sensor data, and c) low pass 10 Hz filter

occasionally consisted of short regions where many or even all the sensors gave a zero reading (10 row increments or less). Therefore, those zero points were isolated and eliminated with a moving average product that utilized 5 values above and five values below zero point.

The product was used to avoid a sharp curve in the graphs that could possibly skew the true force values. As can be seen in Figure 3.6, there is still a significant amount noise in our signal that is unrelated to human movement (50-60 Hz AC signals, systolic and diastolic contractions at 120 and 80 Hz, etc.). Therefore, a 10-Hz low pass filter was utilized based on research of human movement and motion capture that demonstrates that normal physiologic movement happens at those lower frequencies[34, 35]. This filtered data was entered into Origin Pro Software (Origin Lab, Massachusetts, USA) in order to create waterfall graphs.

### 3.4.2. Can Grasp and Key Turn Results

Figures 3.8 and 3.9 illustrate the results of force measurements for each sensor in each panel corresponding to different participants and trials. In the can grasp task, for each subject and trial the largest forces were observed at the middle distal phalanx between 8-9

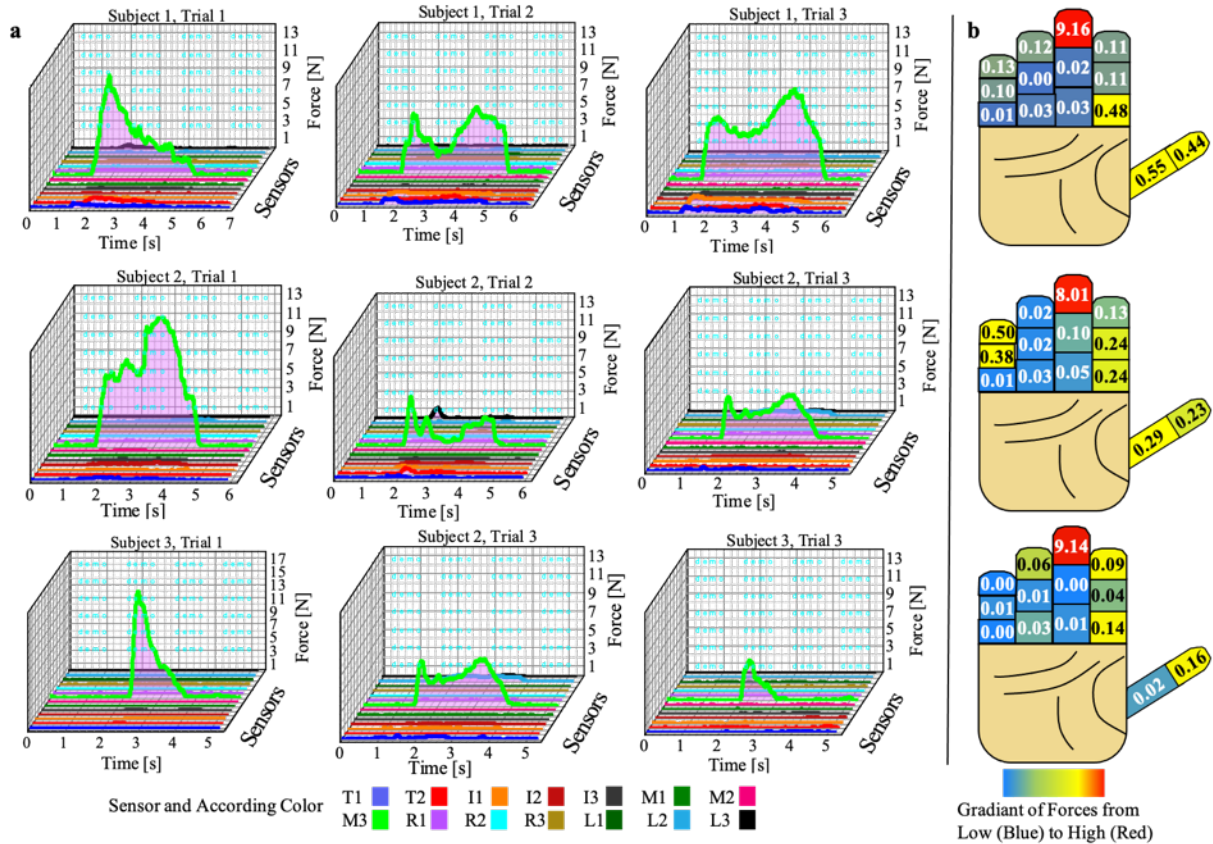


Figure 3.8. Can grasp results and analysis: (a) graphs of force during can grasp task with 3 subjects and 3 trials and (b) average maximum value during those 3 trials with a heat map of forces represented at each phalanx.

N on average. Meaningful but much smaller forces were noted at the thumb and index fingers. As can be seen in participant 2 (second row), there were also small but meaningful forces noted at the little finger. A common occurrence was the lack of force noted little finger proximal phalanx, ring finger proximal, middle, and distal phalanges, and middle finger proximal and distal phalanges.

In the key turn tasks, the largest forces occurred at the distal phalanx of the thumb. The largest forces were a bit more variable than the can grasp task with a range between 14.56 and 23.26 N. Minimal forces occurred at the little, ring, and middle fingers. Each participant did demonstrate meaningful but much smaller force value at the index finger. However, there was some variability in which phalange(s) produced that finger. However, there was some variability in which phalange(s) produced that greater force. Comparing the participants, participant 3 demonstrated greater force at the distal index phalanx whereas participant 2 demonstrated greater force at the index middle phalanx. In contrast, participant 1 demonstrated greater forces at both the index middle and distal phalanges. In

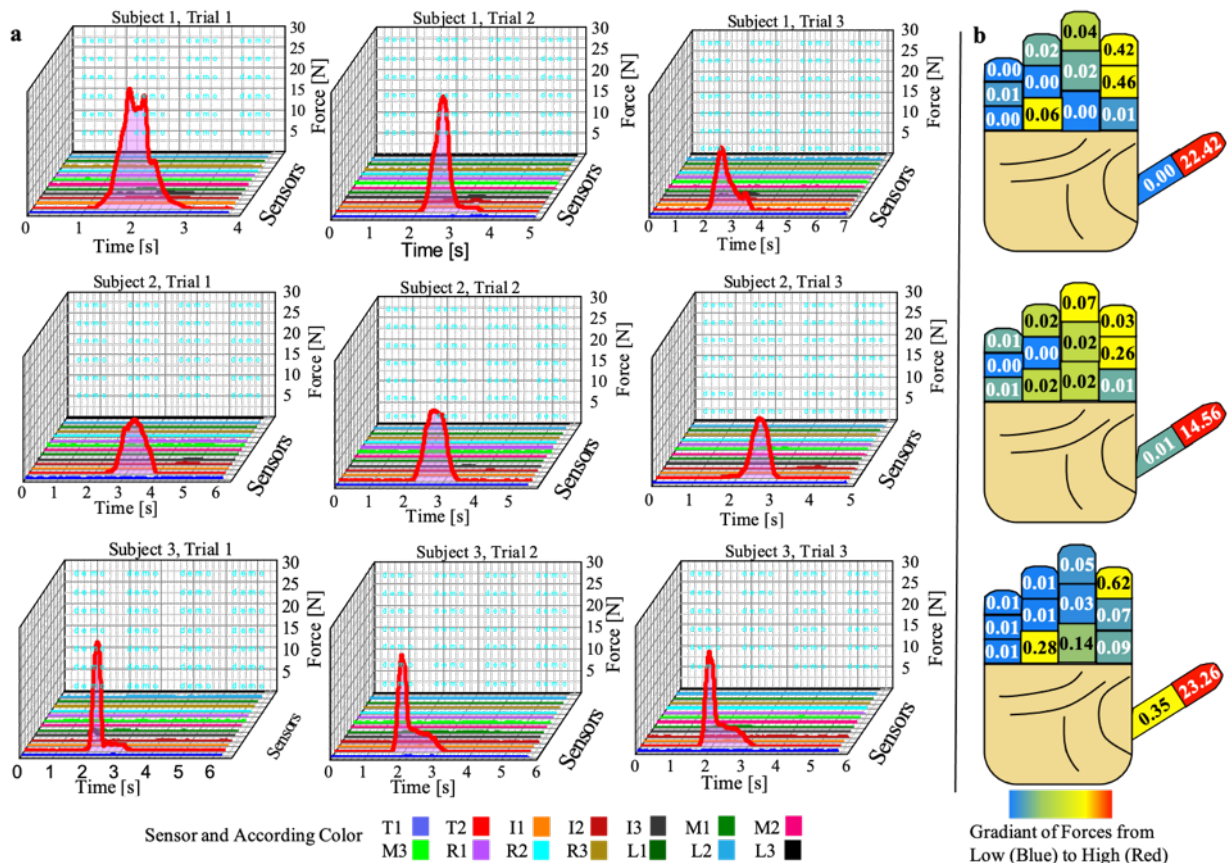


Figure 3.9. Key turn results a) graphs of force during key turn task with 3 subjects and 3 trials, and b) average maximum value during those 3 trials with a heat map of forces represented at each phalanx

the can grasp task, the largest forces were observed at the middle distal phalanx between 8-9 Newtons on average. Significantly smaller but still relatively significant forces were observed at the thumb and index fingers. One more common occurrence was the lack of force noted at the proximal middle, ring, and little phalanges. In the key turn tasks, the largest forces were between 15 and 23 N at the distal thumb phalanx. The only other significant forces were noted at the index middle phalanx. However, those forces were significantly less than the distal thumb phalanx.

### **3.4.3. Can Grasp and Key Turn Discussion**

Results reveal relatively similar maximum values for the can grasp task at the distal middle phalanx between participants. Those findings are somewhat expected since the middle finger is the longest and creates the greatest amount of torque in digits 2-5. An expectation is that the midpoint of the can is in the middle of the hand. With this line of thinking, it makes sense that more control of the can is established by applying more force at the center of the can with the middle finger. However, there is an expectation for an equal and opposite reactionary force on the can from another spot on the hand. This force is necessary to create a sufficient frictional force that would prevent the can from slipping in the hand. In each of the participants, only minimal forces were recorded at other phalanges. Those summed forces of the other fingers did not equal the large force produced by the middle distal phalanx. This leads to two possible reasons for the lack of reaction force. First, the glove did not have enough sensors to accurately measure all the forces. There is an expectation that the hand is in a spherical grasp position when grasping the can. Therefore, the can would be in contact with the metacarpals/palm of the hand as

well as the phalanges. Since there were no sensors placed on the metacarpals, it needs to be considered a portion of the reactional force may have occurred at the palm of the hand.

Another possible reason for the missing reaction forces is related to the specific coverage of the sensors on the phalanges as the sensors have a diameter of 0.375 inches. The small size of the sensors did not completely cover the full palmar surface area on each of the phalanges. Due to the curvature and size of the phalanges, the sides of the phalanges (portions of the fingers between the palmar and dorsal portions of the phalanges) are not covered. Reviewing the second participant's results compared to the first and third participants lead to some insight regarding this problem. The second participant demonstrated small but meaningful forces at the little finger. However, meager forces were noted at the little finger during the first and third participants' trials. It can be suspected that the forces produced by the first and third participants were not captured due to placement of the can in the hand and lack of contact between the sensors and the can.

When exploring the key turn task results, a greater maximal force was observed in this experiment compared to the can task. This is somewhat expected due to small size of the key. Because the key is so small, there is a smaller surface area to focus the force and provide the necessary friction that prevents the key from sliding in the hand. However, compared to the can task, there is a wide range of maximal forces between 14.56 N to 23.26 N. There may exist a few explanations why a wide range of forces existed during this experiment. First, the second participant may have utilized a different grasp type compared to the other two participants. It was hypothesized in this experiment that the participant would either use a lateral pinch or tip-to-tip pinch. Therefore, it was expected

that the thumb and index would create equal and opposite reactional forces for lateral pinch. As for tip-to-tip, the index and middle distal phalanges would create an equal and opposite reactional force to the thumb. The lack of forces recorded at those sensors infers that the current sensors did not properly capture the full force. If the participant utilized a lateral pinch, the radial side of the second finger would most likely register greater forces. If the tip-to-tip method was employed by the participant, the key was more than likely manipulated distal to the placement of the sensors in the glove.

Other limitations that possibly resulted in omission of recorded forces are related to the fabric of the glove and the membrane of the sensor. Although the membrane of the sensor was relatively small (0.0625-inch thickness), the lack of sensory input between the fingers and the object may have altered the method of the participant manipulating the object. Similar to the membrane of the sensor, the fabric may have caused the participant to change their normal method of manipulating the object secondary to altered sensory feedback when grasping the object. The fabric also contains greater flexibility and a decreased frictional coefficient compared to human skin. Both of these properties could result in an altered grasp technique when wearing the glove compared to not wearing the glove and manipulating both objects.

### **3.5. Force Glove Discussion**

This work provided insight toward human biomimetics. In this experiment, forces as large as 23.56 N were observed when grasping and turning a key. Smaller but still meaningful forces of approximately 9 N were observed when grasping a 12-ounce can. This information can be utilized when modeling the minimal forces required for hand prosthetics and orthotics. As mentioned above, there were limitations in force capture due

to sensor size, surface area coverage of the sensors, and properties of the thermoplastic membrane and fabric of the glove. Therefore, further work in this region would require creation of a force sensor that covers a larger surface area of the fingers and palm of the hand. A sensor with grid patterns would be a better method of capturing forces and would be more descriptive to the regions where the force is applied. The materials that would be used to create this grid pattern sensor should also more closely mimic the compression (Young's Modulus) and shear properties of human skin. The sensory feedback to the user should also be considered when fabricating this device because that can alter the grip method.

## 4. Force Glove – Motion Capture

### 4.1. Introduction

To capture movement of the hand and wrist, 26 LED sensors were placed on a glove (Figure 4.1). The wavelength of light emitted by the diodes was slightly different and allowed for tracking of each of the diodes independently. That wavelength was captured by 6 cameras

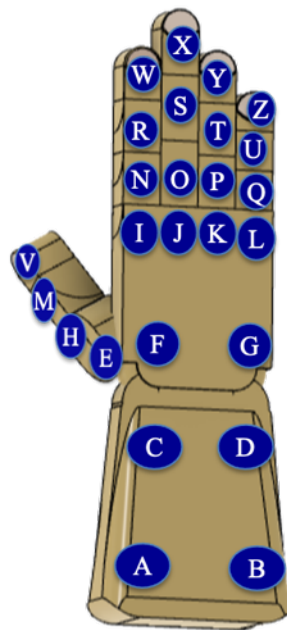


Figure 4.1. 26 sensors placed on the hand positioned around the participant at a sampling rate of 200 Hz. Those cameras transmitted the data to the Codamotion system which allowed for marking of the proper sensors and extraction of the data in a .c3d file. A sample of 0.1s (20 frames) was averaged to create a filtered data set of static sensor movement. Occasionally, zero spots were found in the data. When they were observed, an average of 6 samples (before and after the zero were utilized to replace the zero value. Typically, joint motion is explained in an angular position (degrees) as has previously been explained. A basis for these hand and wrist equations was established in previous literature.[36] However, this research attempts to further explain those vectors and equations for future repetition of similar experiments.

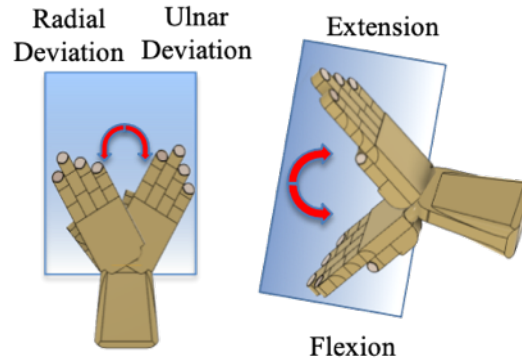


Figure 4.2. Motions of the wrist

## 4.2. Wrist Movements

### 4.2.1. Wrist ROM

The wrist can move into 2 planes: flexion/extension (sagittal plane) and radial/ulnar deviation (frontal plane). In order to determine the angular motion of the wrist in each of these planes, multiple vectors must be considered. First, a reference plane must be established. To accomplish this, three sensors at the forearm (A, B, C) were utilized to create 2 vectors ( $\overrightarrow{BA}$  and  $\overrightarrow{AC}$ ). By utilizing the cross product, these two vectors were utilized to create a forearm plane ( $\vec{n}$ ):

$$\vec{n} = \overrightarrow{BA} \times \overrightarrow{AC}$$

The components of this plane can be explained:

$$\vec{n}_x = (\overrightarrow{BA}_y * \overrightarrow{AC}_z) - (\overrightarrow{BA}_z * \overrightarrow{AC}_y)$$

$$\vec{n}_y = (\overrightarrow{BA}_z * \overrightarrow{AC}_x) - (\overrightarrow{BA}_x * \overrightarrow{AC}_z)$$

$$\vec{n}_z = (\overrightarrow{BA}_x * \overrightarrow{AC}_y) - (\overrightarrow{BA}_y * \overrightarrow{AC}_x)$$

A vector of the hand ( $\vec{FI}$ ) is then projected onto the forearm to create two separate vectors: 1.) in-plane vector ( $\vec{FI}^{\parallel}$ ), and 2.) out-of-plane vector ( $\vec{FI}^{\perp}$ ). The projections of  $\vec{FI}$  can be conceptualized as a shadow of light cast on the forearm plane vectors. Here, the in-plane vector is wrist radial and ulnar deviation while the out-of-plane vector is flexion and extension. To determine the out-of-plane angle, the following equation is utilized:

$$\cos \theta = \frac{\vec{n} * \vec{FI}}{(\|\vec{n}\| * \|\vec{FI}\|)}$$

Rearranging the formula, we find:

$$\angle \theta = \cos^{-1} \left( \frac{\vec{n} * \vec{FI}}{(\|\vec{n}\| * \|\vec{FI}\|)} \right) * \left( \frac{180}{\pi} \right)$$

In order to determine the flexion and extension angle, we start at a neutral reference position between flexion and extension. Since the  $\vec{n}$  is pointed in the flexion position at  $90^\circ$ , the angle must be found by subtracting  $90^\circ$  from  $\theta$ . Therefore, the out-of-plane angle  $\beta$  would be:

$$\angle \beta = \angle \theta - 90.$$

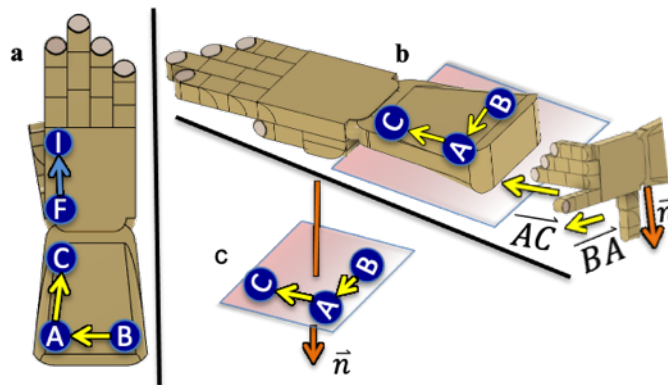


Figure 4.3. a) Sensor position of the forearm and hand, b) forearm plane with out-of-plane vector, and c) forearm plane with perpendicular vector

In this method, we know that if  $\alpha\beta < 0$ , then the motion would be flexion. If  $\alpha\beta > 0$ , the motion would be extension. Utilizing the perpendicular vector  $\vec{n}$ , we can determine the out-of-plane vector:

$$\vec{FI}^\perp = \left[ \frac{(\vec{FI} * \vec{n})}{|\vec{n}|^2} \right] * \vec{n}$$

From linear algebra, we know that vector  $\vec{FI}$  is a product of its components:

$$\vec{FI} = \vec{FI}^\parallel + \vec{FI}^\perp$$

To the determine the in-plane vector, we can rearrange the equation and achieve:

$$\vec{FI}^\parallel = \vec{FI} - \vec{FI}^\perp$$

Next, the dot product can be used to find the angle between a vector used to make up the forearm plane. Here we choose to use  $\vec{BA}$  in the equation:

$$\cos \gamma = \frac{\vec{FI}^\parallel * \vec{BA}}{(\| \vec{FI}^\parallel \| * \| \vec{BA} \|)}$$

By rearranging the equation, we received

$$\angle\gamma = \cos^{-1} \left( \frac{\overline{FI}^{\parallel} * \overline{BA}}{\left( \|\overline{FI}^{\parallel}\| * \|\overline{BA}\| \right)} \right) * \left( \frac{180}{\pi} \right)$$

In order to determine the radial and ulnar deviation angle, we start at a neutral reference position between the two motions. Since the  $\overline{BA}$  is pointed into the radial deviation position of  $90^{\circ}$ , the angle must be found by subtracting  $90^{\circ}$  from  $\angle\gamma$ . Therefore, the out-of-plane angle  $\beta$  would be:

$$\angle\alpha = \angle\gamma - 90.$$

In this method, we know that if  $\angle\alpha < 0$ , then the motion would be radial deviation. If  $\angle\alpha > 0$ , the motion would be ulnar deviation.

#### 4.2.2. Wrist Calibration

To determine correctness of the equations and linearity of the technique, calibration was performed. In this technique, four participants performed five wrist motions: radial

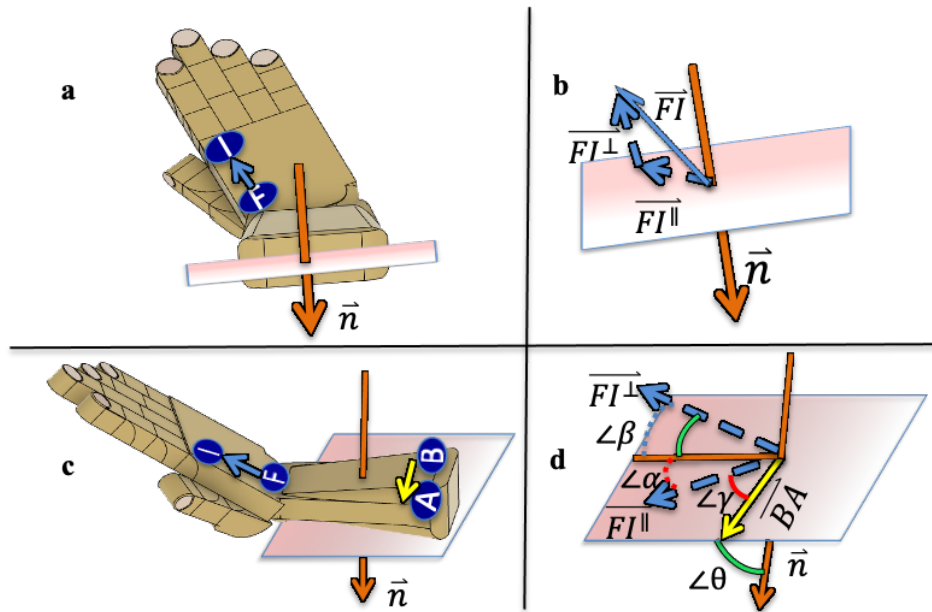


Figure 4.4. a) Wrist in extension and radial deviation, b) components of vector  $\overline{FI}$ , c) relation of vector  $\overline{BA}$  to  $\overline{FI}$ , and d) radial/ulnar deviation ( $\angle\alpha$ ) and flexion/extension ( $\angle\beta$ ) angles.

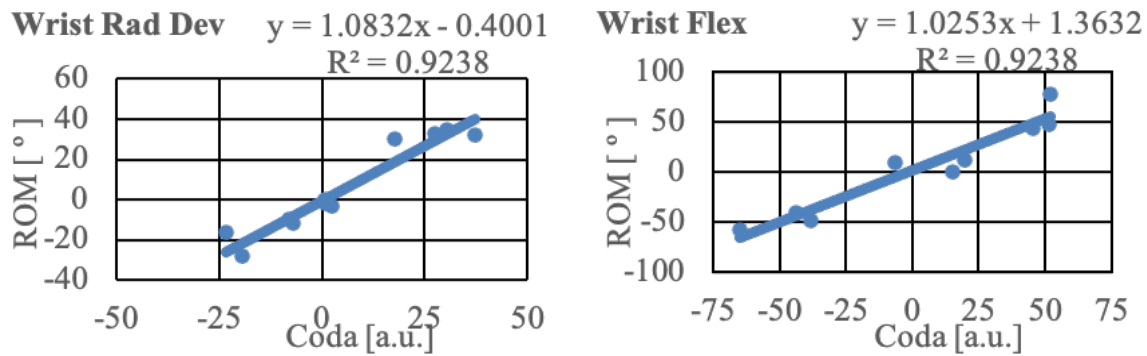


Figure 4.5. Calibration graphs: a) wrist radial deviation and b) flexion

deviation, ulnar deviation, flexion, and extension. The participant statically held the position of the hand, and the sensors were captured using the Codamotion system. After capturing the position of the hand with the Codamotion system, a researcher used a goniometer to capture the range of motion (ROM – angular position) of the hand. The goal of the calibration was to determine if the variance could be described in a linear form. Therefore, the  $R^2$  value as evaluated for the cluster of data obtained. As can be seen in the Figure, the  $R^2$  values are 0.9238 for both radial/ulnar deviation and flexion/extension. Therefore, the method used would be considered a high indicator of a linear measurement. The Y-intercept was also obtained for possible use later to substitute the Codamotion numbers for true ROM (angular position of the wrist) when performing normal daily tasks. This will be described in detail later in this chapter.

### 4.3. Thumb Movements

#### 4.3.1. Thumb CMC ROM

The thumb is one of the more complex joints of the human body. It affords humans the ability to manipulate the environment with greater precision compared to primates. This ability is related to the human hand's longer thumb length and multiple planes of movement.[\[37-39\]](#) The major difference between primates and humans is the carpometacarpal (CMC) joint of the

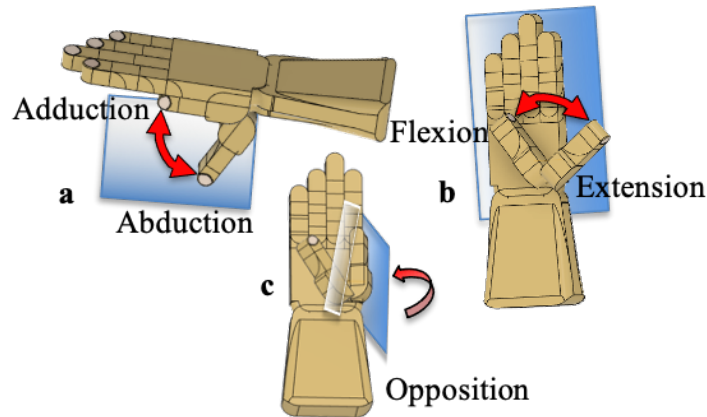


Figure 4.6. Motions of the thumb CMC joint: a) abduction/adduction, b) flexion/extension, and c) opposition

thumb. In primates, this joint only contains 2 planes of movement and moves similarly to the metacarpophalangeal joints of digits 2-5 of humans (will be discussed later). However, the human CMC joint contains three planes of movement: abduction/adduction, flexion/extension, and opposition. Adduction and abduction are motions that occur in the sagittal plane while flexion and extension occur in the frontal plane. Opposition is the movement that differentiates the human hand from primate's hand and it occurs in the transverse plane. Normative ROM of the CMC joint has been found to be 0-70 degrees adduction to abduction and 0-45 degrees flexion and extension. The normative ROM for opposition is not set in an angular measure. Rather it is just the observation of the ability to touch the “pad of the thumb to the pad of the fifth digit.”[24, 40] Opposition can better be described as rotation of the 1<sup>st</sup> metacarpal around the axis of 2 carpal bones (trapezium and trapezoid). The easiest way to see the movement is to watch the thumb fingernail rotate as the thumb moves from neutral flexion beneath the index finger to the little finger as seen in Figure 4.6.

Although there are three movement planes of the hand, two planes of movement are combined secondary to difficulty with separating out the motions. The motions that are combined are flexion/extension and opposition. To determine the angular motion of the thumb CMC joint, a reference plane of the thumb must be determined. Sensors F, I, and J are utilized to create vectors  $\vec{FI}$  and  $\vec{IJ}$ . By using the cross product, these vectors create the thumb plane and the perpendicular thumb plane vector  $\vec{t}$ :

$$\vec{t} = \vec{GF} \times \vec{FI}$$

The components can be explained:

$$\vec{t}_x = (\vec{GF}_y * \vec{FI}_z) - (\vec{GF}_z * \vec{FI}_y)$$

$$\vec{t}_y = (\vec{GF}_z * \vec{FI}_x) - (\vec{GF}_x * \vec{FI}_z)$$

$$\vec{t}_z = (\vec{GF}_x * \vec{FI}_y) - (\vec{GF}_y * \vec{FI}_x)$$

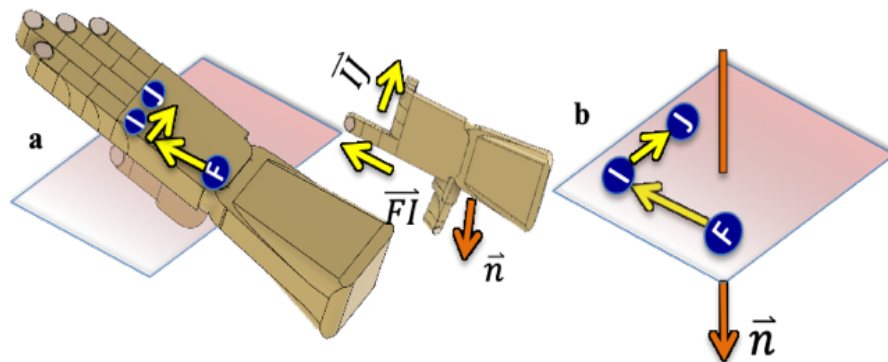


Figure 4.7. a) Forearm plane on hand with right hand rule and b) forearm plane with perpendicular vector

A vector of the thumb ( $\overrightarrow{EH}$ ) is then projected onto perpendicular vector of the hand to create two separate vectors: 1.) in-plane vector ( $\overrightarrow{EH^{\parallel}}$ ), and 2.) out-of-plane vector ( $\overrightarrow{EH^{\perp}}$ ). The projections of  $\overrightarrow{EH}$  can be conceptualized as a shadow of light cast on the hand plane vectors. Here, the in-

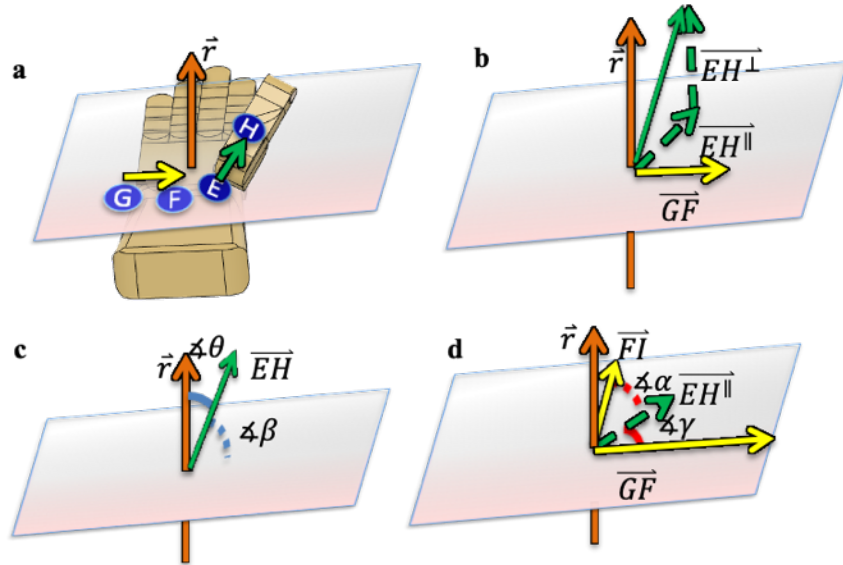


Figure 4.8. a) Thumb CMC hand plane and vectors, b) perpendicular and parallel vectors of  $\overrightarrow{EH}$ , c) out of plane (abduction/adduction) angles, and D) in-plane (flexion/extension) angles.

plane vector represents thumb CMC flexion and extension while the out-of-plane vector represents adduction and abduction. In order to determine the out-of-plane angle, the dot product is utilized to find the angle between the thumb vector ( $\overrightarrow{EH}$ ) and perpendicular thumb plane vector ( $\vec{t}$ ):

$$\cos \theta = \frac{\vec{t} * \overrightarrow{EH}}{(\|\vec{t}\| * \|\overrightarrow{EH}\|)}$$

Rearranging the equation:

$$\theta = \cos^{-1} \left( \frac{\vec{t} * \overrightarrow{EH}}{(\|\vec{t}\| * \|\overrightarrow{EH}\|)} \right) * \left( \frac{180}{\pi} \right)$$

To determine the abduction and adduction angle, we must choose a reference point. Keeping the standard goniometric measurements, the reference point is chosen as parallel to the thumb plane ( $0^\circ$  adduction). Since the  $\vec{r}$  vector is perpendicular to the thumb plane, the angle must be found by subtracting the  $\theta$  angle from  $90^\circ$  (leaving a positive abduction angle). Therefore, the out-of-plane angle  $\alpha\beta$  would be:

$$\alpha\beta = 90 - \angle\theta.$$

In this method, we know that if  $\alpha\beta > 0$ , then the motion would be abduction. If  $\alpha\beta < 0$ , the motion would be adduction. Utilizing the perpendicular thumb plane ( $\vec{r}$ ) vector, we can determine the out-of-plane vector ( $\overrightarrow{EH^\perp}$ ):

$$\overrightarrow{EH^\perp} = \left[ \frac{(\overrightarrow{EH} * \vec{r})}{\|\vec{r}\|^2} \right] * \vec{r}$$

From linear algebra, we know that vector  $\overrightarrow{EH}$  is a product of its components:

$$\overrightarrow{EH} = \overrightarrow{EH^\parallel} + \overrightarrow{EH^\perp}$$

Therefore, the in-plane projection of  $\overrightarrow{EH^\parallel}$  can be found with the equation:

$$\overrightarrow{EH^\parallel} = \overrightarrow{EH} - \overrightarrow{EH^\perp}$$

Next, the dot product can be used to find the angle between the hand plane vector ( $\overrightarrow{GF}$ ) and the in-plane projection vector ( $\overrightarrow{EH^\parallel}$ ):

$$\cos \gamma = \frac{\overrightarrow{EH^\parallel} * \overrightarrow{GF}}{(\|\overrightarrow{EH^\parallel}\| * \|\overrightarrow{GF}\|)}$$

In rearranging the equation, the below is achieved:

$$\angle\gamma = \cos^{-1} \left( \frac{\overline{EH} \parallel * \overline{GF}}{\left( \parallel \overline{EH} \parallel * \parallel \overline{GF} \parallel \right)} \right) * \left( \frac{180}{\pi} \right)$$

In order to determine the flexion and extension angles for the thumb, we start at a neutral reference position between the two motions. In this instance, the placement of the CMC joint makes it a bit more difficult to choose an arbitrary 0° position. The joint is not directly below the second metacarpal ( $\overline{FI}$ ). However, typical goniometric measurements utilize this as the reference point. Since the vector  $\overline{GF}$  is pointed into the extension position of 90° (nearly perpendicular to  $\overline{FI}$ ) the angle must be found by subtracting  $\angle\gamma$  from 90°. Therefore, the in-plane angle  $\angle\alpha$  would be:

$$\angle\alpha = 90 - \angle\gamma.$$

In this method, we hypothesize that if  $\angle\alpha < 0$ , then flexion is occurring. If  $\angle\alpha > 0$ , the motion is extension.

### 4.3.2. Thumb CMC Calibration

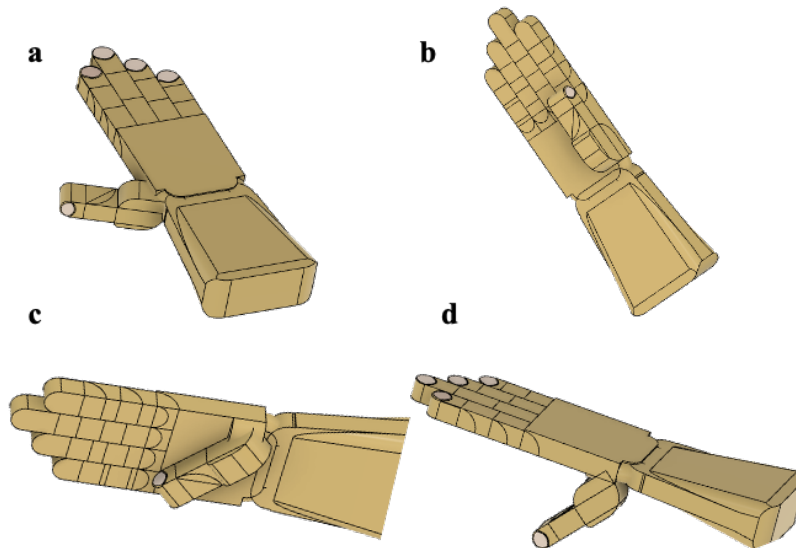


Figure 4.9. Thumb CMC calibration: a) full extension and adduction, b) neutral thumb, c) full thumb flexion, and d) full thumb abduction

Calibration of the thumb utilized the same four participants for wrist calibration. The participants completed four movements: full thumb extension and adduction, thumb neutral (thumb tucked to palm and under second metacarpal), full thumb flexion, and full thumb abduction. The participant statically held the position of the hand, and the sensors were captured using the Codamotion system. After capturing the position of the hand with the Codamotion system, a researcher used a goniometer to capture the range of motion (ROM – angular position) of the hand. Again, the goal of the calibration was to determine if the variance could be described in a linear form. Hence, the  $R^2$  value as evaluated for the cluster of data obtained. As can be seen in the Figure, CMC abduction/adduction resulted in  $R^2$  values are 0.9238 which demonstrates good linearity. However, CMC flexion/extension had poor  $R^2$  at 0.5364. The Y-intercept was also obtained which comes in handy with CMC flexion/extension. Since the CMC never truly reached  $0^\circ$ , it can be utilized in future experiments as a method to multiply the Codamotion values to achieve a true ROM value.

#### 4.3.3. Thumb MCP and IP ROM

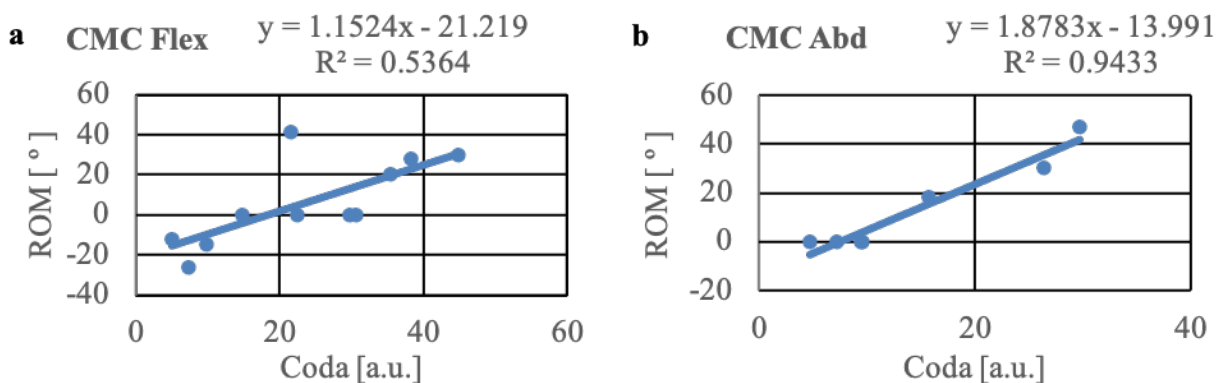


Figure 4.10. Calibration values of a) CMC flexion/extension and b) CMC abduction/adduction

The thumb also contains the metacarpophalangeal (MCP) and interphalangeal (IP) joints. These joints are significantly easier to describe as they contain only one plane of movement. Both of these joints allow for flexion and extension which occurs in the frontal planes. The normative ROM for the MCP joint is 0-50 degrees moving from extension to flexion. The interphalangeal joint's normative ROM is from 0-80 degrees from extension to flexion[24, 40].

Since the MCP only moves in one plane, the geometry is a bit easier. In order to determine the joint angle, the dot product is utilized in the following method:

$$\cos \theta_{MCP} = \frac{\overrightarrow{EH} * \overrightarrow{HM}}{\|EH\| * \|HM\|}$$

Rearranging, we achieve:

$$\theta_{MCP} = \cos^{-1} \left( \frac{\overrightarrow{EH} * \overrightarrow{HM}}{\|EH\| * \|HM\|} \right)$$

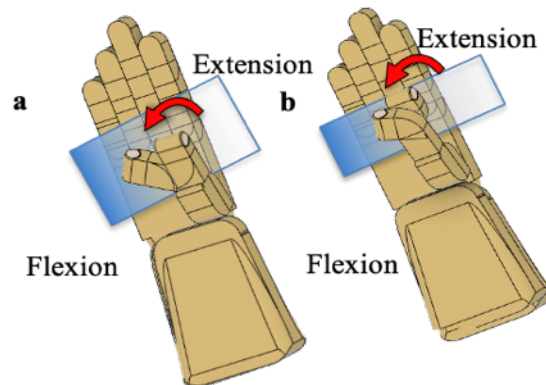


Figure 4.11. a) Thumb MCP flexion and extension and b) IP flexion/extension

Just as the MCP moves only in one plane, so too does the thumb IP joint. To determine the IP joint angle, the dot product is also utilized in the following method:

$$\cos \theta_{IP} = \frac{\overrightarrow{HM} * \overrightarrow{MV}}{\|HM\| * \|MV\|}$$

Rearranging, we achieve:

$$\theta_{IP} = \cos^{-1} \left( \frac{\overline{HM} * \overline{MV}}{\|HM\| * \|MV\|} \right)$$

#### 4.3.4. Thumb MCP and IP Calibration Results and Discussion

To determine correctness of the equations and linearity of the technique, calibration was performed. Again, four participants were asked to actively perform thumb motions. First, the participants were asked to perform extension at the CMC, MCP, and IP joints. This performed. Again, four participants were asked to actively perform thumb motions. First, the participants were asked to perform extension at the CMC, MCP, and IP joints. This motion was taken to be the 0-degree mark of the thumb at both the MCP and IP joints. Next, the patient was asked to

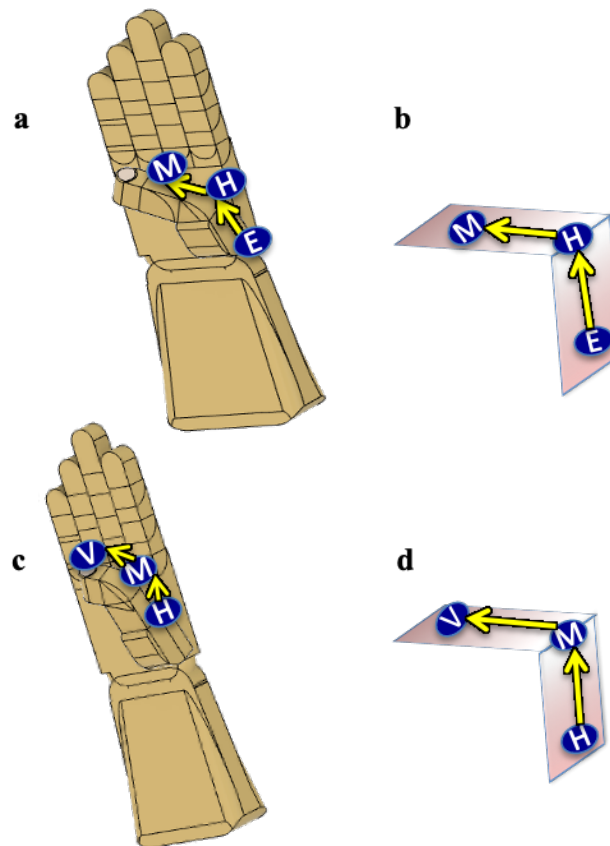


Figure 4.12. a) Thumb MCP flex, b) illustration of MCP vector planes, c) thumb IP flex, and d) illustration of IP vector planes

perform MCP flexion while the thumb CMC remained in extension. Goniometric measurements were taken across the dorsum of the thumb at the MCP joint. Finally, the participants were asked to perform IP flexion with the CMC in extension. The participant was measurements were taken across the dorsum of the thumb at the MCP joint. Finally, the participants were asked to perform IP flexion with the CMC in extension. The participant was encouraged to focus more on flexion of the IP joint and less on MCP joint flexion.  $R^2$  measures revealed that thumb MCP and IP motions are not nearly as linear as wrist motions. This may be due to the small size of the phalanges compared to the larger bones that make up the wrist. This may also be related to the loose fit of the glove and inability to secure the LEDs near to the skin/nail.

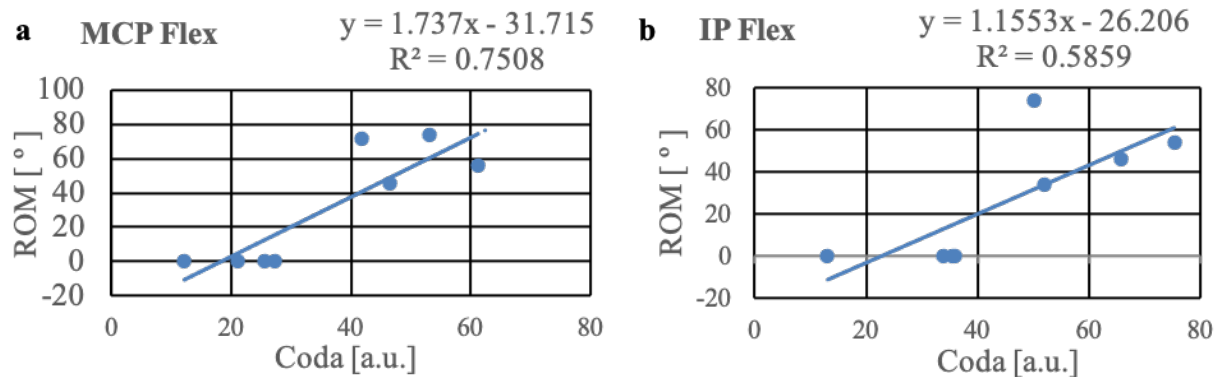


Figure 4.13: a) Thumb MCP Calibration and b) Thumb IP Calibration

#### 4.4. Index, Middle, Ring and Little Finger Movements

##### 4.4.1. Index, Middle, Ring, and Little MCP ROM

The index, middle, ring and little MCP joints will be grouped together since each of the joints contain the same movements. The MCP joint is very different than the MCP of the thumb. It is more like the CMC joint of the thumb. These MCP joints contain 2 planes of movement: adduction/abduction (Figure 4.12) and flexion/extension. Adduction and abduction are motions that occur in the frontal plane while flexion and extension occur in the sagittal plane. Normative

ROM of the MCP joint varies across the literature but is approximately -45 deg to 90 deg moving from hyperextension to flexion. In order to understand abduction and adduction, a midline must first be considered. Abduction is a movement of the finger away from midline whereas adduction is a movement toward midline. Therefore, midline in the anatomical position has been established as the middle finger. The middle finger is considered to only move into

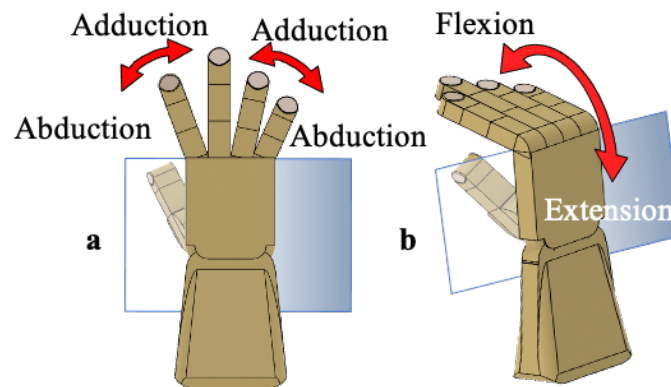


Figure 4.14. MCP motions: a) abduction/adduction and b) flexion/extension

abduction into both directions. However, abduction and adduction for index is the opposite motion of the MCP joint compared to the ring and little fingers. When assessing the ROM into abduction and adduction, the only metacarpal that is directly parallel to the proximal phalanx is the 3<sup>rd</sup> metacarpal. The metacarpals of the index, ring, and little fingers are at a small angle away from parallel. Therefore, there is some difficulty with measuring the abduction and adduction positions. For simplicity's sake, the easiest method in goniometry is to create an arbitrary parallel position (0° abduction/adduction) position. This is accomplished when the hand is in neutral (Figure 4.15A). This allows us to determine a goniometric angle when the metacarpals move away from the middle finger[24, 40]. A problem does occur with Codamotion capture as

the sensors are not arranged to produce parallel vectors while in neutral at each of the fingers. This problem will be further discussed throughout the calibration section.

#### 4.4.2. Index MCP ROM

To determine the angular motion of the index finger MCP joint, a reference plane again must be created since there are two planes of movement. Therefore, an index finger hand plane was created to capture the multiplanar changes that occur at the index MCP (Figure 4.13). To

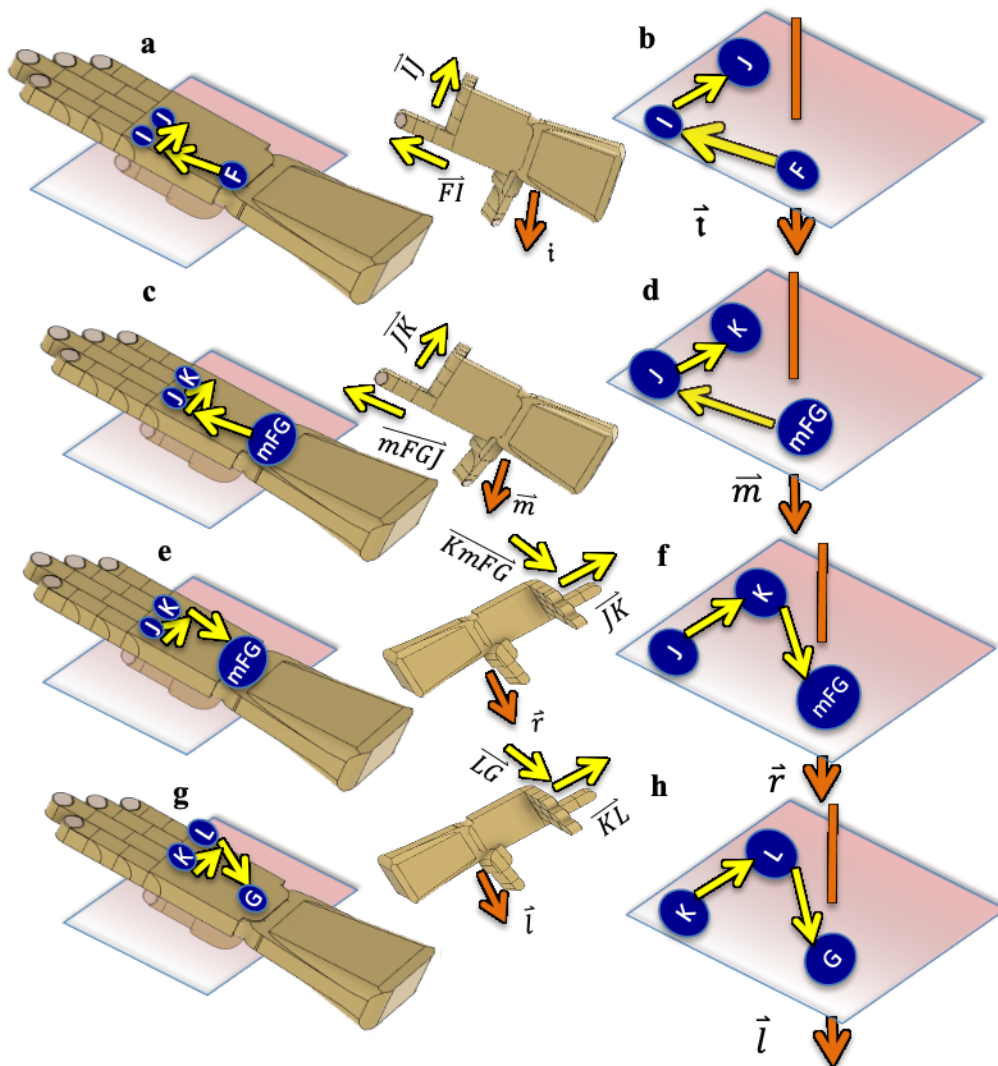


Figure 4.15. a) Index finger plane and b) perpendicular vector, c) middle finger plane and d) perpendicular vector, e) ring finger plane and f) perpendicular vector, and g) little finger plane and h) perpendicular vector

create this plane, sensors F, I, and J were utilized to create vectors  $\overrightarrow{FI}$  and  $\overrightarrow{IJ}$ . By using the cross product, these vectors create the index finger hand plane and the perpendicular vector  $\vec{i}$ :

$$\vec{i} = \overrightarrow{FI} \times \overrightarrow{IJ}$$

The components can be explained:

$$\vec{i}_x = (\overrightarrow{FI}_y * \overrightarrow{IJ}_z) - (\overrightarrow{FI}_z * \overrightarrow{IJ}_y)$$

$$\vec{i}_y = (\overrightarrow{FI}_z * \overrightarrow{IJ}_x) - (\overrightarrow{FI}_x * \overrightarrow{IJ}_z)$$

$$\vec{i}_z = (\overrightarrow{FI}_x * \overrightarrow{IJ}_y) - (\overrightarrow{FI}_y * \overrightarrow{IJ}_x)$$

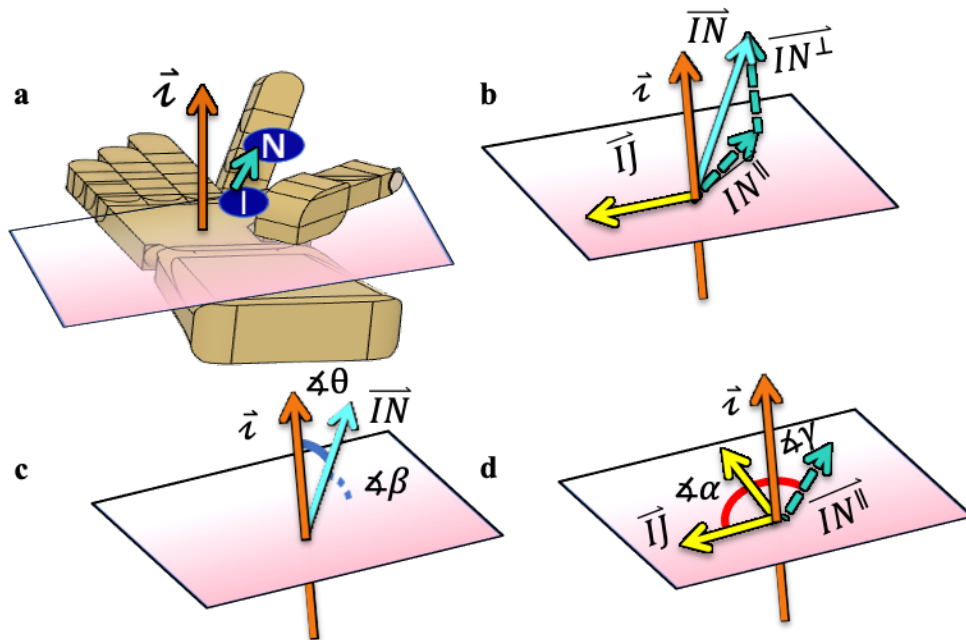


Figure 4.16. a) Index finger hand plane and vectors, b) perpendicular and parallel vectors of  $\overrightarrow{IN}$ , c) out-of-plane angle (flexion/extension), and d) in-plane angles (abduction/adduction)

A vector of the index finger ( $\overrightarrow{IN}$ ) is then projected onto the index hand finger hand plane to create two separate vectors: 1) in-plane vector ( $\overrightarrow{IN}^{\parallel}$ ), and 2) out-of-plane vector ( $\overrightarrow{IN}^{\perp}$ ). The projections of  $\overrightarrow{IN}$  can be conceptualized as a shadow of light cast on the index hand plane vector. Here, the in-plane vector represents index finger MCP adduction and abduction while the out-of-

plane vector represents flexion and extension. In order to determine the out-of-plane angle, the dot product is utilized to find the angle between the index finger vector ( $\overline{IN}$ ) and perpendicular index finger hand plane vector ( $\vec{i}$ ):

$$\cos \theta = \frac{\vec{i} * \overline{IN}}{(\|\vec{i}\| * \|\overline{IN}\|)}$$

Rearranging the equation:

$$\angle \theta = \cos^{-1} \left( \frac{\vec{i} * \overline{IN}}{(\|\vec{i}\| * \|\overline{IN}\|)} \right) * \left( \frac{180}{\pi} \right)$$

In order to determine the difference between flexion and hyperextension, we must choose a reference point. Keeping the standard goniometric measurements, the 0° position occurs when the vector  $\overline{IN}^\perp$  is parallel to the index finger hand plane (0° flexion). Since the vector  $\vec{i}$  is the vector perpendicular to the index finger hand plane, we know that there is a 90° angle between  $\vec{i}$  and the index finger hand plane. Therefore, the angle  $\angle \beta$  must be found by subtracting the  $\theta$  angle from 90° (leaving a positive flexion angle):

$$\angle \beta = 90 - \angle \theta.$$

In this method, we know that if  $\angle \beta > 0$ , then the motion would be flexion. If  $\angle \beta < 0$ , the motion would be hyperextension. Utilizing the perpendicular index finger plane vector ( $\vec{i}$ ), we can determine the out-of-plane vector ( $\overline{IN}^\perp$ ):

$$\overline{IN}^\perp = \left[ \frac{(\overline{IN} * \vec{i})}{\|\vec{i}\|^2} \right] * \vec{i}$$

From linear algebra, we know that vector  $\overline{IN}$  is a product of its components:

$$\overline{IN} = \overline{IN}^\parallel + \overline{IN}^\perp$$

Therefore, the in-plane projection of  $\overline{IN}^{\parallel}$  can be found with the equation:

$$\overline{IN}^{\parallel} = \overline{IN} - \overline{IN}^{\perp}$$

Next, the dot product can be used to find the angle between the hand plane vector ( $\overline{IJ}$ ) and the in-plane projection vector ( $\overline{IN}^{\parallel}$ ):

$$\cos \gamma = \frac{\overline{IN}^{\parallel} * \overline{IJ}}{(\| \overline{IN}^{\parallel} \| * \| \overline{IJ} \|)}$$

In rearranging the equation, the below is achieved:

$$\gamma = \cos^{-1} \left( \frac{\overline{IN}^{\parallel} * \overline{IJ}}{(\| \overline{IN}^{\parallel} \| * \| \overline{IJ} \|)} \right) * \left( \frac{180}{\pi} \right)$$

With this method, calibration will be utilized to differentiate between adduction and abduction.

That subject will be introduced during the calibration portion.

#### 4.4.3. Middle MCP ROM

To determine the angular motion of the middle finger MCP joint, a reference plane again must be created since there are two planes of movement. Therefore, a middle finger hand plane was created to capture the multiplanar changes that occur at the middle MCP (Figure 4.13). To create this plane, a midpoint between sensors F and G was utilized to create one point which we call mFG. Sensors at points the points mFG, J, and K were utilized to create vectors  $\overline{mFGJ}$  and  $\overline{JK}$ . By using the cross product, these vectors create the middle finger hand plane and the perpendicular vector  $\overline{m}$ :

$$\overline{m} = \overline{mFGJ} \times \overline{JK}$$

The components can be explained:

$$\vec{m}_x = (\overrightarrow{mFGJ_y} * \overrightarrow{JK_z}) - (\overrightarrow{mFGJ_z} * \overrightarrow{JK_y})$$

$$\vec{m}_y = (\overrightarrow{mFGJ_z} * \overrightarrow{JK_x}) - (\overrightarrow{mFGJ_x} * \overrightarrow{JK_z})$$

$$\vec{m}_z = (\overrightarrow{mFGJ_x} * \overrightarrow{JK_z}) - (\overrightarrow{mFGJ_y} * \overrightarrow{JK_x})$$

A vector of the index finger ( $\vec{JO}$ ) is then projected onto the middle finger hand plane to create two separate vectors: 1) in-plane vector ( $\vec{JO}^{\parallel}$ ), and 2) out-of-plane vector ( $\vec{JO}^{\perp}$ ). The projections of  $\vec{JO}$  can be conceptualized as a shadow of light cast on the middle hand plane vectors. Here, the in-plane vector represents middle finger MCP adduction and abduction while the out-of-plane vector represents flexion and extension. To determine the out-of-plane motion, the dot product is utilized to find the angle between the middle finger vector ( $\vec{JO}$ ) and perpendicular index finger hand plane vector ( $\vec{m}$ ):

$$\cos \theta = \frac{\vec{m} * \vec{JO}}{(\|\vec{m}\| * \|\vec{JO}\|)}$$

Rearranging the equation:

$$\theta = \cos^{-1} \left( \frac{\vec{m} * \vec{JO}}{(\|\vec{m}\| * \|\vec{JO}\|)} \right) * \left( \frac{180}{\pi} \right)$$

To determine the difference between flexion and hyperextension we must choose a reference point. Keeping the standard goniometric measurements, the 0° position occurs when the vector  $\vec{JO}^{\perp}$  is parallel to the middle finger hand plane (0° flexion). Since the vector  $\vec{m}$  is perpendicular to the middle finger hand plane, we know that there is a 90° angle between  $\vec{m}$  and the middle finger hand plane. Therefore, the angle must be found by subtracting the  $\theta$  angle from 90° (leaving a positive flexion angle):

$$\angle\beta = 90 - \angle\theta.$$

In this method, we know that if  $\angle\beta > 0$ , then the motion would be flexion. If  $\angle\beta < 0$ , the motion would be hyperextension. Utilizing the perpendicular middle finger plane vector ( $\vec{m}$ ), we can determine the out-of-plane vector ( $\vec{JO}^\perp$ ):

$$\vec{JO}^\perp = \left[ \frac{(\vec{JO} * \vec{m})}{\|\vec{m}\|^2} \right] * \vec{m}$$

From linear algebra, we know that vector  $\vec{JO}$  is a product of its components:

$$\vec{JO} = \vec{JO}^\parallel + \vec{JO}^\perp$$

Therefore, the in-plane projection of  $\vec{JO}^\parallel$  can be found with the equation:

$$\vec{JO}^\parallel = \vec{JO} - \vec{JO}^\perp$$

Next, the dot product can be used to find the angle between the hand plane vector ( $\vec{JK}$ ) and the in-plane projection vector ( $\vec{JO}^\parallel$ ):

$$\cos\gamma = \frac{\vec{JO}^\parallel * \vec{JK}}{(\|\vec{JO}^\parallel\| * \|\vec{JK}\|)}$$

In rearranging the equation, the below is achieved:

$$\angle\gamma = \cos^{-1} \left( \frac{\vec{JO}^\parallel * \vec{JK}}{(\|\vec{JO}^\parallel\| * \|\vec{JK}\|)} \right) * \left( \frac{180}{\pi} \right)$$

With this method, calibration will be utilized to differentiate between adduction and abduction.

#### 4.4.4. Ring MCP ROM

In order to determine the angular motion of the ring finger MCP joint, a reference plane again must be created since there are two planes of movement. Therefore, a ring finger hand

plane was created to capture the multiplanar changes that occur at the ring MCP (Figure 4.13). Like middle finger MCP planes, a midpoint between sensors F and G was utilized to create one point which we call mFG. Sensors at points the points mFG, J, and K were utilized to create vectors  $\overrightarrow{KmFG}$  and  $\overrightarrow{JK}$ . The slight difference that occurs in creating ring finger hand plane perpendicular vector ( $\vec{r}$ ) is the order and direction of the vectors. To maintain the perpendicular vector pointing in a downward direction from the palm of the hand, the cross product is written as follows:

$$\vec{r} = \overrightarrow{JK} \times \overrightarrow{KmFG}$$

The components can be explained:

$$\vec{r}_x = (\overrightarrow{JK}_y * \overrightarrow{KmFG}_z) - (\overrightarrow{JK}_z * \overrightarrow{KmFG}_y)$$

$$\vec{r}_y = (\overrightarrow{JK}_z * \overrightarrow{KmFG}_x) - (\overrightarrow{JK}_x * \overrightarrow{KmFG}_z)$$

$$\vec{r}_z = (\overrightarrow{JK}_x * \overrightarrow{KmFG}_y) - (\overrightarrow{JK}_y * \overrightarrow{KmFG}_x)$$

A vector of the ring finger ( $\overrightarrow{KP}$ ) is then projected onto the ring finger hand plane to create two separate vectors: 1) in-plane vector ( $\overrightarrow{KP}^{\parallel}$ ), and 2) out-of-plane vector ( $\overrightarrow{KP}^{\perp}$ ). The projections of  $\overrightarrow{KP}$  can be conceptualized as a shadow of light cast on the ring finger hand plane. Here, the in-plane vector represents ring finger MCP adduction and abduction while the out-of-plane vector represents flexion and extension. In order to determine the out-of-plane motion, the dot product is utilized to find the angle between the ring finger vector ( $\overrightarrow{JO}$ ) and perpendicular ring finger hand plane vector ( $\vec{r}$ ):

$$\cos \theta = \frac{\vec{r} * \overrightarrow{KP}}{(\|\vec{r}\| * \|\overrightarrow{KP}\|)}$$

Rearranging the equation:

$$\sphericalangle\theta = \cos^{-1}\left(\frac{\vec{r} * \overline{KP}}{(\|\vec{r}\| * \|\overline{KP}\|)}\right) * \left(\frac{180}{\pi}\right)$$

In order to determine the difference between flexion and hyperextension, we must choose a reference point. Keeping the standard goniometric measurements, the 0° position occurs when the vector  $\overline{KP^\perp}$  is parallel to the ring finger hand plane (0° flexion). Since the vector  $\vec{r}$  is perpendicular to the ring finger hand plane, we know that there is a 90° angle between  $\vec{r}$  and the ring finger hand plane. Therefore, the angle must be found by subtracting the  $\theta$  angle from 90° (leaving a positive flexion angle):

$$\sphericalangle\beta = 90 - \sphericalangle\theta.$$

In this method, we know that if  $\sphericalangle\beta > 0$ , then the motion would be flexion. If  $\sphericalangle\beta < 0$ , the motion would be hyperextension. Utilizing the perpendicular index finger plane vector ( $\vec{r}$ ), we can determine the out-of-plane vector ( $\overline{KP^\perp}$ ):

$$\overline{KP^\perp} = \left[\frac{(\overline{KP} * \vec{r})}{\|\vec{r}\|^2}\right] * \vec{r}$$

From linear algebra, we know that vector  $\overline{KP}$  is a product of its components:

$$\overline{KP} = \overline{KP^\parallel} + \overline{KP^\perp}$$

Therefore, the in-plane projection of  $\overline{KP^\parallel}$  can be found with the equation:

$$\overline{KP^\parallel} = \overline{KP} - \overline{KP^\perp}$$

Next, the dot product can be used to find the angle between the hand plane vector ( $\overline{JK}$ ) and the in-plane projection vector ( $\overline{KP^\parallel}$ ):

$$\cos \gamma = \frac{\overrightarrow{KP} \parallel * \overrightarrow{JK}}{(\| \overrightarrow{KP} \parallel * \| \overrightarrow{JK} \|)}$$

In rearranging the equation, the below is achieved:

$$\gamma = \cos^{-1} \left( \frac{\overrightarrow{KP} \parallel * \overrightarrow{JK}}{(\| \overrightarrow{KP} \parallel * \| \overrightarrow{JK} \|)} \right) * \left( \frac{180}{\pi} \right)$$

With this method, calibration will be utilized to differentiate between adduction and abduction.

#### 4.4.5. Little MCP ROM

In order to determine the angular motion of the little finger MCP joint, a reference plane again must be created since there are two planes of movement. Therefore, a little finger hand plane was created to capture the multiplanar changes that occur at the little MCP (Figure 4.13). The sensors utilized to define the little finger hand plane slightly differ than the ring and middle fingers. However, the proximal sensor is similar to the index finger sensors. Since there is a sensor placed at the 5<sup>th</sup> carpometacarpal joint (G), that sensor is utilized to create a vector ( $\overrightarrow{LG}$ ) that is more representative of motion that occurs at the little finger. Sensors at points G, K, and L were utilized to create vectors  $\overrightarrow{KL}$  and  $\overrightarrow{LG}$ . By method of the cross product, these vectors create the little finger hand plane and perpendicular vector:

$$\vec{l} = \overrightarrow{KL} \times \overrightarrow{LG}$$

The components can be explained:

$$\vec{l}_x = (\overrightarrow{KL}_y * \overrightarrow{LG}_z) - (\overrightarrow{KL}_z * \overrightarrow{LG}_y)$$

$$\vec{l}_y = (\overrightarrow{KL}_z * \overrightarrow{LG}_x) - (\overrightarrow{KL}_x * \overrightarrow{LG}_z)$$

$$\vec{l}_z = (\overrightarrow{KL}_x * \overrightarrow{LG}_y) - (\overrightarrow{KL}_y * \overrightarrow{LG}_x)$$

A vector of the little finger ( $\overline{LQ}$ ) was then projected onto the little finger hand plane to create two separate vectors: 1) in-plane vector ( $\overline{LQ}^{\parallel}$ ), and 2) out-of-plane vector ( $\overline{LQ}^{\perp}$ ). The projections of  $\overline{LQ}$  can be conceptualized as a shadow of light cast on the little finger hand plane. Here, the in-plane vector represents little finger MCP adduction and abduction while the out-of-plane vector represents flexion and extension. To determine the out-of-plane motion, the dot product is utilized to find the angle between the little finger vector ( $\overline{LQ}$ ) and perpendicular little finger hand plane vector ( $\vec{l}$ ):

$$\cos \theta = \frac{\vec{l} * \overline{LQ}}{(\|\vec{l}\| * \|\overline{LQ}\|)}$$

Rearranging the equation:

$$\sphericalangle \theta = \cos^{-1} \left( \frac{\vec{l} * \overline{LQ}}{(\|\vec{l}\| * \|\overline{LQ}\|)} \right) * \left( \frac{180}{\pi} \right)$$

To determine the difference between flexion and hyperextension, we must choose a reference point. Keeping the standard goniometric measurements, the 0° position occurs when the vector  $\overline{LQ}^{\perp}$  is parallel to the little finger hand plane (0° flexion). Since the vector  $\vec{l}$  is perpendicular to the little finger hand plane, we know that there is a 90° angle between  $\vec{l}$  and the little finger hand plane. Therefore, the angle must be found by subtracting the  $\theta$  angle from 90° (leaving a positive flexion angle):

$$\sphericalangle \beta = 90 - \sphericalangle \theta.$$

In this method, we know that if  $\sphericalangle \beta > 0$ , then the motion would be flexion. If  $\sphericalangle \beta < 0$ , the motion would be hyperextension. Utilizing the perpendicular littlefinger plane vector ( $\vec{l}$ ), we can determine the out-of-plane vector ( $\overline{LQ}^{\perp}$ ):

$$\overrightarrow{LQ^\perp} = \left[ \frac{(\overrightarrow{LQ} * \vec{l})}{\|\vec{l}\|^2} \right] * \vec{l}$$

From linear algebra, we know that vector  $\overrightarrow{KP}$  is a product of its components:

$$\overrightarrow{LQ} = \overrightarrow{LQ^\parallel} + \overrightarrow{LQ^\perp}$$

Therefore, the in-plane projection of  $\overrightarrow{KP^\parallel}$  can be found with the equation:

$$\overrightarrow{LQ^\parallel} = \overrightarrow{LQ} - \overrightarrow{LQ^\perp}$$

Next, the dot product can be used to find the angle between the vector ( $\overrightarrow{KL}$ ) and the in-plane projection vector ( $\overrightarrow{LQ^\parallel}$ ):

$$\cos \gamma = \frac{\overrightarrow{LQ^\parallel} * \overrightarrow{KL}}{(\|\overrightarrow{LQ^\parallel}\| * \|\overrightarrow{KL}\|)}$$

In rearranging the equation, the below is achieved:

$$\gamma = \cos^{-1} \left( \frac{\overrightarrow{LQ^\parallel} * \overrightarrow{KL}}{(\|\overrightarrow{LQ^\parallel}\| * \|\overrightarrow{KL}\|)} \right) * \left( \frac{180}{\pi} \right)$$

With this method, calibration will be utilized to differentiate between adduction and abduction.

#### 4.4.6. Index, Middle, Ring, and Little MCP Calibration Results and Discussion

Calibration of each of the MCP motions consisted of 4 participants moving through three motions. First, the participants were asked to perform extension and adduction, simultaneously, at the MCP joints of digits 2-5. This motion was taken to be the 0-degree mark for MCP extension and abduction/adduction. Next, the participants were asked to abduct MCP joints as far as possible. Goniometric measurements were taken across dorsum of the MCP joints. Lastly,

the participants were asked to perform MCP flexion as far as possible. Again, goniometric measurements were taken across the dorsum of the hand.

$R^2$  measures were calculated to determine the linearity of the values when comparing goniometric ROM to Codamotion values obtained. The linearity varied significantly between MCP flex/extn and abd/add. The  $R^2$  values revealed relatively good linearity for MCP flex/extn of digits 2-5. However, the linearity results were not as good when analyzing abd/add values. There were a few reasons for the lack of linearity and other problems when analyzing the results. An initial problem occurred when recording middle finger MCP goniometric measurements. There was some confusion among testers about abd/add positions since the middle finger is only considered to move into abduction. The recorders were unsure whether to make the value negative when moving them middle finger toward the index finger versus moving it toward the ring finger. Future studies will rectify this problem.

Another problem that occurred with abduction/adduction testing was the lack of adduction testing at the index, ring, and little fingers. The current measurements only cover abduction to neutral positions. Since the motion of abduction and adduction is very minimal, more data would be required to accurately represent these small movements. Finally, the neutral positions of the fingers vary between participants. There are numerous reasons for this variability. First, the Codamotion sensors required replacement on the glove between participants. Other experiments completed in the lab simultaneous to this experiment required disassembly and re-assembly of the LED sensors on the glove. Small changes in placement of the sensors are more likely to cause greater variability in MCP abd/add compared to flex/extn. Another possible reason for the initial variability is fit of the hand in the stretchable glove

relative to hand size. For some of the participants, the glove did not fit snug. Without some tension in the glove, the sensors on the index and little fingers tend to bunch toward the midline. All of the above resulted in poor outcomes when analyzing linearity of Codamotion compared to

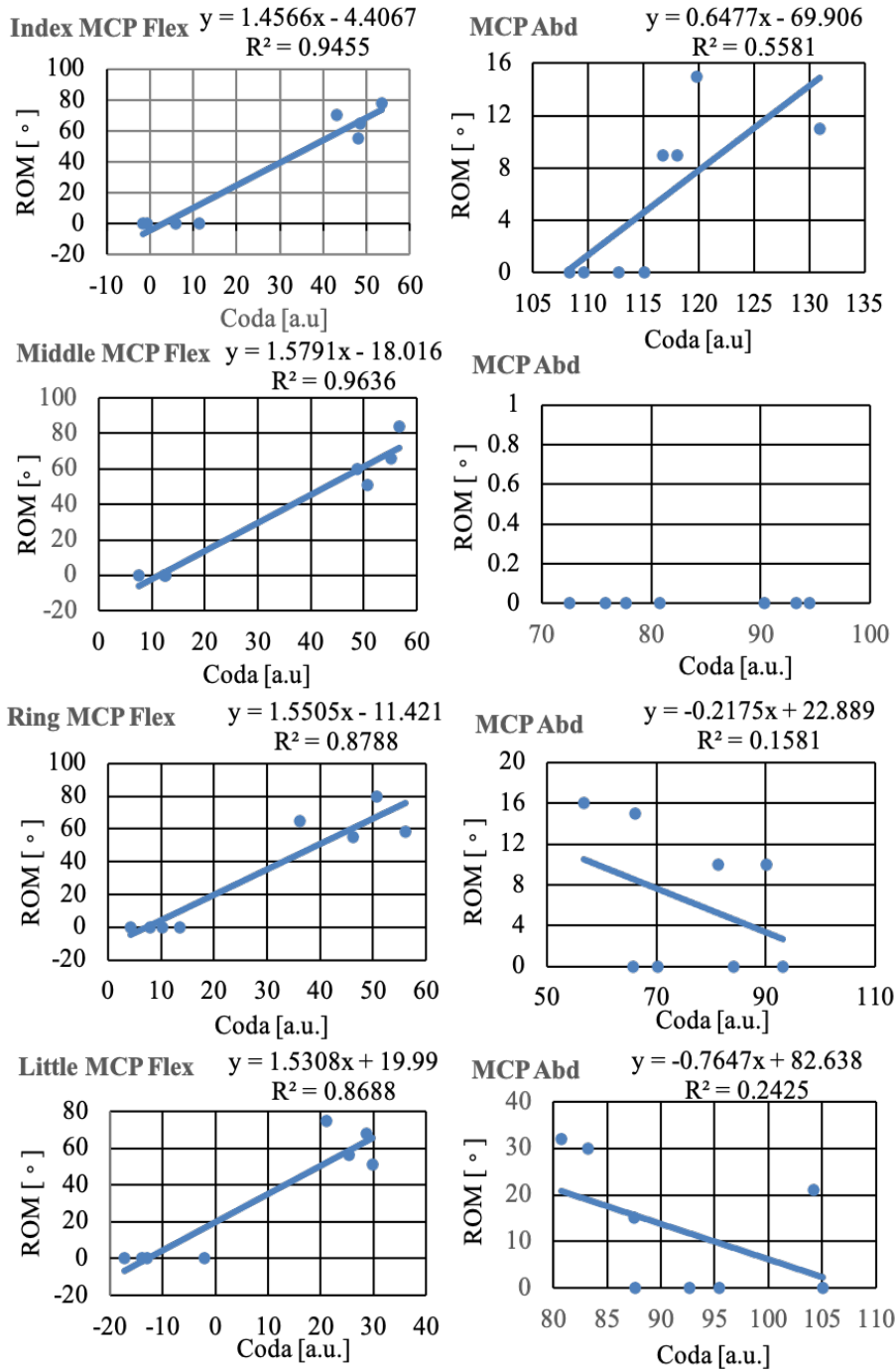


Figure 4.17. Digits 2-5 MCP flexion/extension and abduction/adduction calibration graphs

goniometric motions captured. There, y-intercept values were recorded. With rearrangement in the below equation:

$$y = mx + b$$

$$x = \frac{y - b}{m}$$

Here, the y-value represents the Codamotion values, b is a constant of variability, m is the slope of Codamotion values divided by goniometric values, and the x-value represents goniometric values. For future studies, Codamotion values can be inserted into equation to reveal goniometric measurements when performing ADLs. This will be discussed in the upcoming section.

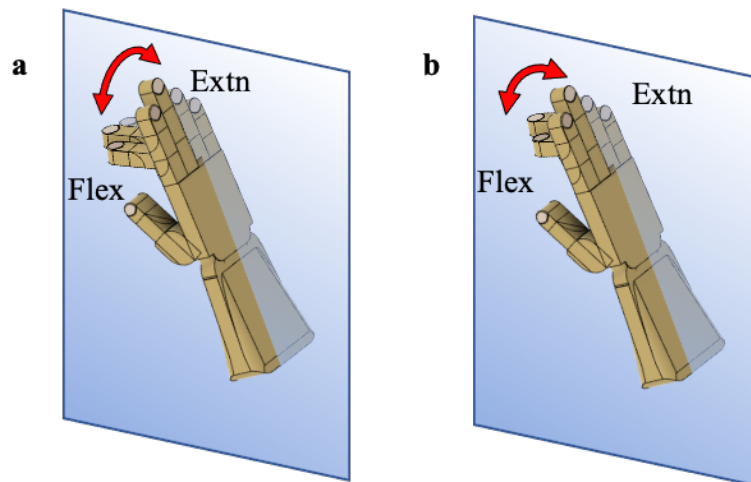


Figure 4.18. Digit 2-5 a) PIP flexion/extension and b) DIP flexion/extension

#### 4.4.7. Index, Middle, Ring, and Little Finger PIP and DIP ROM

Different to the thumb, digits 2-5 contain two interphalangeal joints. These joints are known as the proximal interphalangeal (PIP) and distal interphalangeal (DIP) joints. Like the thumb's interphalangeal joints, this joint contains on one plane of movement. The PIP and DIP joints can perform flexion and extension in the sagittal plane. According to normative data, the ROM available at these joints include 0-100° of PIP flexion and -10 to 90° DIP hyperextension

to flexion[24, 40]. Sensors I, N, and R are utilized to create vectors  $\overline{IN}$  and  $\overline{NR}$  to record measurements of the index PIP joint.

$$\cos \theta_{PIP} = \frac{\overline{IN} * \overline{NR}}{\| \overline{IN} \| * \| \overline{NR} \|}$$

Rearranging, we achieve:

$$\theta_{PIP} = \cos^{-1} \left( \frac{\overline{IN} * \overline{NR}}{\| \overline{IN} \| * \| \overline{NR} \|} \right)$$

Using the same formula, we can find the angular Codamotion values for the PIP joints of the middle finger:

$$\theta_{PIP} = \cos^{-1} \left( \frac{\overline{JO} * \overline{OS}}{\| \overline{JO} \| * \| \overline{OS} \|} \right)$$

ring finger:

$$\theta_{PIP} = \cos^{-1} \left( \frac{\overline{KP} * \overline{PT}}{\| \overline{KP} \| * \| \overline{PT} \|} \right)$$

and little finger:

$$\theta_{PIP} = \cos^{-1} \left( \frac{\overline{LQ} * \overline{QU}}{\| \overline{LQ} \| * \| \overline{QU} \|} \right)$$

The calculations for the DIP joint are exactly the same but with the use of the distal sensors.

Starting with the index finger, we use sensors N, R, and W to make up vectors  $\overline{NR}$  and  $\overline{RW}$ .

Again, we use the dot product to get:

$$\cos \theta_{DIP} = \frac{\overline{NR} * \overline{RW}}{\| \overline{NR} \| * \| \overline{RW} \|}$$

Rearranging, we achieve:

$$\theta_{DIP} = \cos^{-1} \left( \frac{\overline{NR} * \overline{RW}}{\| \overline{NR} \| * \| \overline{RW} \|} \right)$$

Using the same formula, we can find the angular Codamotion values for the PIP joints of the middle finger:

$$\theta_{DIP} = \cos^{-1} \left( \frac{\overline{OS} * \overline{SX}}{\| \overline{OS} \| * \| \overline{SX} \|} \right)$$

ring finger:

$$\theta_{DIP} = \cos^{-1} \left( \frac{\overline{PT} * \overline{TY}}{\| \overline{PT} \| * \| \overline{TY} \|} \right)$$

and little finger:

$$\theta_{DIP} = \cos^{-1} \left( \frac{\overline{QU} * \overline{UZ}}{\| \overline{QU} \| * \| \overline{UZ} \|} \right)$$

Although this method does not differ between hyperextension and flexion, there is limited ROM into hyperextension. Therefore, there is negligible problems with this method. If there is a need

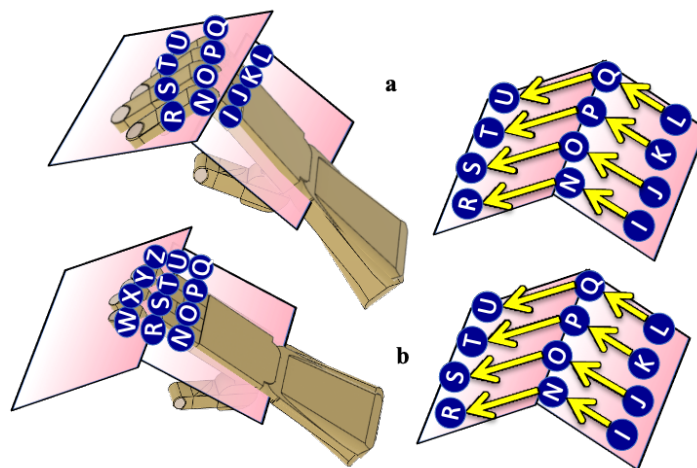


Figure 4.19. Digits 2-5 a) PIP flexion/extension sensors, b) DIP flexion/extension

to differentiate hyperextension from flexion, additional sensors would be needed to create a plane and utilized the cross product.

#### 4.4.8. Index, Middle, Ring, and Little PIP and DIP Calibration

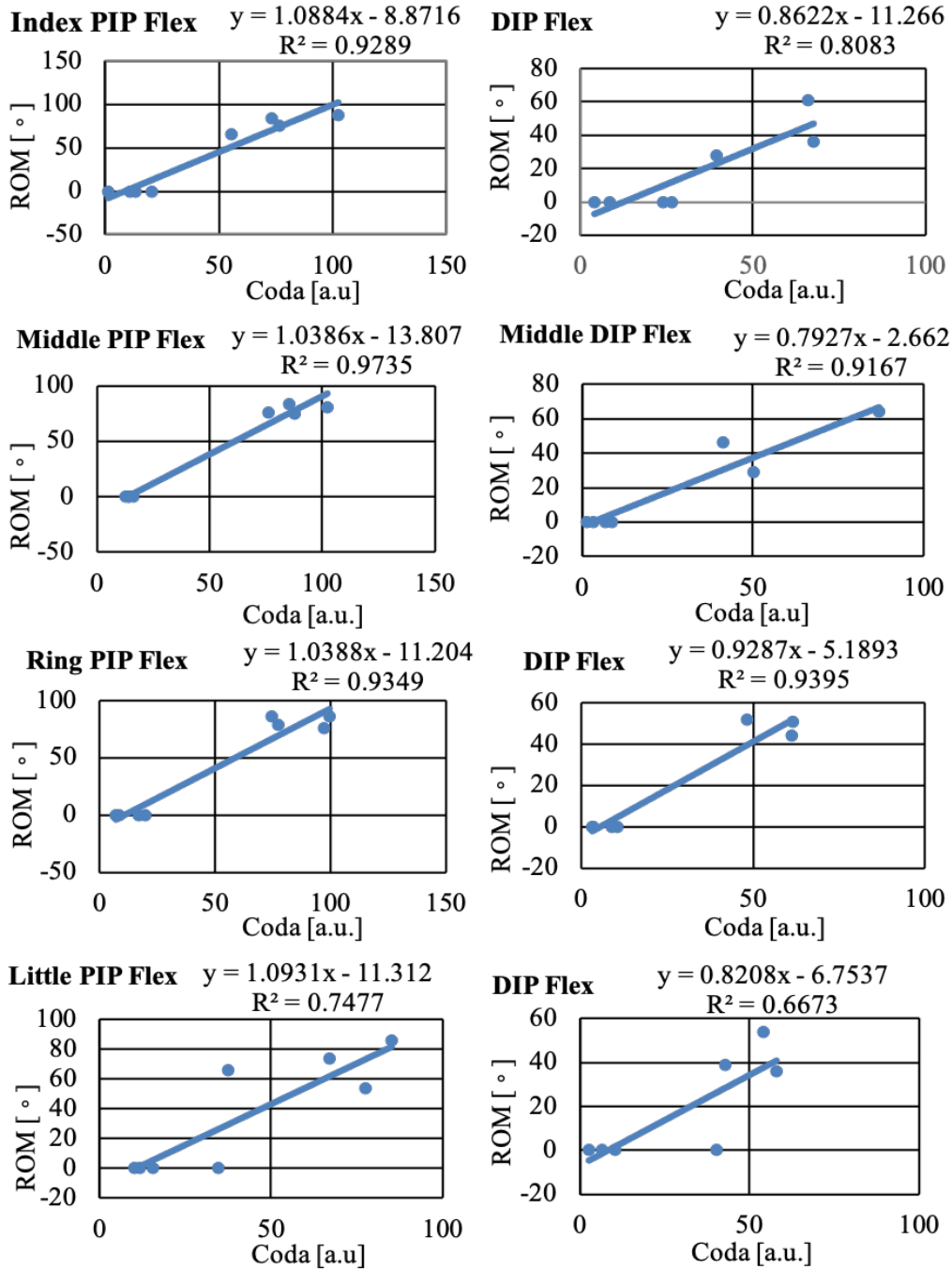


Figure 4.20. Digits 2-5 PIP and DIP flexion/extension calibration graphs

To calibrate PIP and DIP motions of digits 2-5, four participants were asked to perform three movements of the fingers. First, the participants were asked to extend all digits of the hand while Codamotion measurements were captured. Next, the participants were asked to extend the MCP joints and flex the PIP joints as far as possible in an attempt to touch the tips of the fingers to the palm of the hand. Goniometric measurements were captured while performing this activity. Lastly, the participants were again asked to extend the MCP joint while performing PIP and DIP flexion. In this activity, the participants were asked to focus on flexion of the distal joints. Again, goniometric measurements were captured while performing this activity. With the exception of the little PIP and DIP, results of calibration reveal relatively good linear  $R^2$  values. This again is likely related to the loose fit and, hence, lack of representative movement of the sensors.

#### 4.5. Motion Capture Calibration Results and Linearity Values

Table 4.1. Linearity ( $R^2$ ) of Goniometric Values Compared to Codamotion Values

Motion	Wrist	Thumb	Index	Middle	Ring	Little
<b>Flex/Extn</b>	0.9238	n/a	n/a	n/a	n/a	n/a
<b>Abd/Add</b>	0.9238	n/a	n/a	n/a	n/a	n/a
<b>CMC Flex/Extn</b>	n/a	0.5364	n/a	n/a	n/a	n/a
<b>CMC Abd/Add</b>	n/a	0.9433	n/a	n/a	n/a	n/a
<b>MCP Flex/Extn</b>	n/a	0.7508	0.9455	0.9636	0.8788	0.8688
<b>MCP Abd/Add</b>	n/a	n/a	0.5581	n/a	0.1581	0.2425
<b>PIP Flex/Extn</b>	n/a	0.5859	0.9289	0.9735	0.9349	0.7477
<b>DIP Flex/Extn</b>	n/a	n/a	0.8083	0.9167	0.9395	0.6673

CMC = carpometacarpal, MCP = metacarpal, PIP = proximal interphalangeal, DIP = distal interphalangeal, Flex/Extn = flexion/extension, Abd/Add = abduction/adduction

Table 4.1 reveals the linearity ( $R^2$  values) of each of the joints comparing goniometric and Codamotion values. As has been mentioned previously, there were low linearity values for thumb CMC Flex/Extn, thumb PIP flex/extn, and index, ring, and little finger abd/add

movements. There are a variety of reasons as mentioned in the previous sections for these low linearity values. A significant problem with index, ring, and little finger abduction and adduction is the lack of an arbitrary zero point. Therefore, y-intercept values were taken and are multiplied by the Codamotion values to give a ROM value in the ADLs.

#### **4.6. Motion Capture with Force Glove Used During Activities of Daily Living (ADL)**

In the previous chapter, experiments were performed with can grasp and key turn tasks to establish normative force data during ADLs. During the experiment, motion capture data was also collected with the hypothesis that participants would use spherical gross grasp and lateral pinch movements, respectively, for these tasks. The periods where there was greatest force, it is also hypothesized that hand movements were near isometric (no motion but high muscular forces produced). Those time periods were recorded. Below is a recording of the hand position during those highest force periods and the amount of variability in movement.

##### **4.6.1. Can Grasp and Key Turn Motion Capture Methods**

Before beginning this experiment, IRB approval was obtained, a questionnaire was completed, and the force glove was donned by the participant. For further understanding of the preliminary activities and testing methods, refer to section 3.4. Again, three participants performed 2 tasks: can grasp and key turning.

During the can grasp and key turn tasks, motion capture occurred simultaneous to the force capture. On analysis of motion capture data, significant artifact was noticed in the signal of the sensors. First, sudden drops in the sensor (Figure 20A) position toward a 0 position with rapid return to the pre-zero numbers noted. These zero positions were for short periods of time. Therefore, it can be surmised that the sensors were partially obstructed from the view of the Codamotion cameras. Therefore, these data points were removed with an interpolation method.

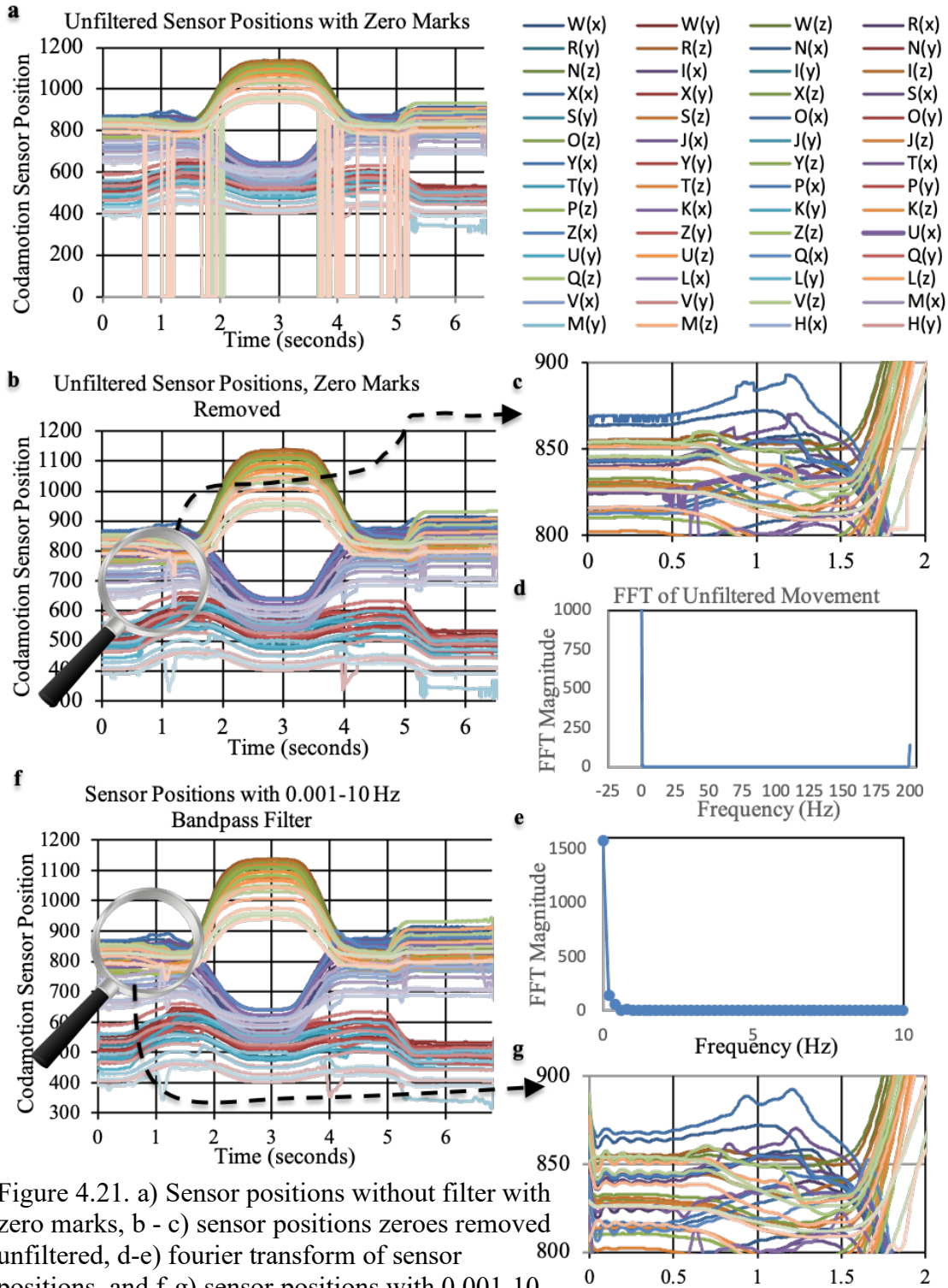


Figure 4.21. a) Sensor positions without filter with zero marks, b - c) sensor positions zeroes removed unfiltered, d-e) fourier transform of sensor positions, and f-g) sensor positions with 0.001-10 Hz bandpass filter

Averages of preceding 5 non-zero data points and succeeding 5 non-zero data points were substituted for the zero points. The interpolated, unfiltered data was observed to have a bit of a

noisy signal which can be observed in Figure 4.21. b-c. Fast Fourier transform was utilized to determine there was significant noise at near 200 Hz and at the 0 Hz frequencies (Figure 4.21. d-e). Researchers in motion capture study have revealed that human movement occurs between the 0-10 Hz range[34, 35]. However, there is also a significant FFT magnitude that occurred directly at the 0 Hz frequency. This signal is interpreted as a DC offset noise signal. Therefore, a bandpass filter was utilized from 0.001 Hz to 10 Hz to remove the DC offset and noise above the 10 Hz frequency. That data was much smoother and can be found in Figure 4.21. f-g.

#### **4.6.2. Can Grasp Motion Capture Data and Discussion**

Table 4.2 provides the angular ROM of all the wrist and hand joints during the can grasp task. As can be seen, mean and standard deviation measures were captured for within subjects (intrasubject) and between subjects (intersubject). Since there is a significant amount of data in Table 4.2, a better understanding of the values can be visualized in Figure 4.22. What can be inferred is that the hand appears to be positioned in a spherical grasp as was hypothesized. When we take a closer look at the data, it is important to maintain a reference of the total joint ROM to understand the importance of standard deviation measures. As a refresher, the standard deviation is the distance or variance from the mean. A value of zero would indicate no variability from the mean. In this research, that would indicate that there is no difference in joint position between trials. A significant intrasubject standard deviation was observed during many of the ROM measurements in subject 1. The most significant deviations occurred in PIP flexion of the index, middle, and ring, thumb CMC flexion and abduction, thumb MCP flexion, and wrist radial deviation. On the surface, this variability could be explained by various methods used to grasp the can by the user during the activity. However, when taking a closer look at the data, it is apparent the data for trial 3 differs significantly from trial one and two. In fact, the data differs

significantly in nearly all the joints for ROM in trial 3 compared to the first two trials. There may be multiple reasons for the data differences. The first reason could be that subject 1 used a different method in trial 3 compared to trials 1 and 2. Although this could be a potential reason, further analysis of the ROM normative data may rule this cause out. A hint is given in PIP flexion ROM. The normative ROM for PIP flexion, as stated previously, is approximately 100°. The motion of 130° captured would require the subject to have access to significant hypermobility of the joint. When comparing this to the ROM of trials 1 and 2, it likely means that the subject most likely did not change his method.

Instead, there are likely two other reasons for this significant difference in trial 3. The second reason is that there could have been a change in position of the sensors for trial 1 and 2 to trial 3. Although the sensors were secured to the glove with tape, the adhesion of the tape could have loosened enough to change the position of the sensors. While movement of the sensors likely

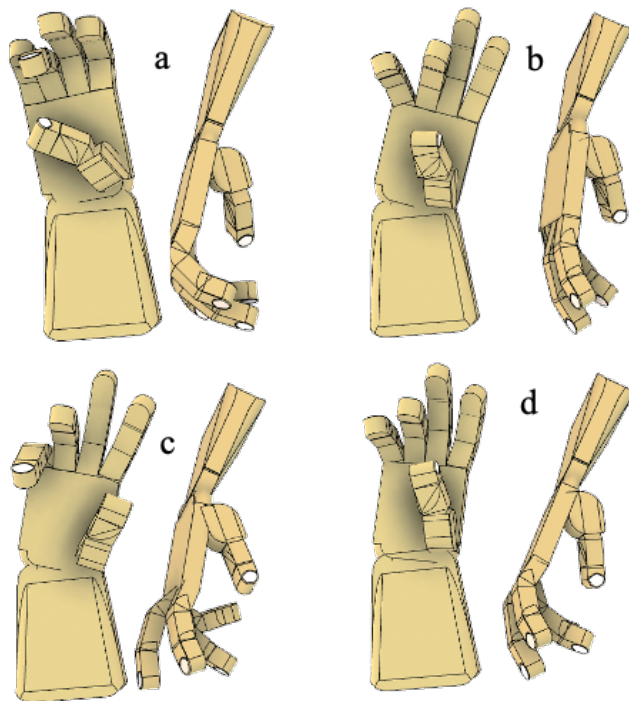


Figure 4.22. Can grasp mean results for a) subject 1, b) subject 2, c) subject 3, and (d) between subjects

Table 4.2. Can Grasp Task

Subject & Trial	Index				Middle			Ring				Little				Thumb				Wrist	
	MCP Abd	MCP Flex	PIP Flex	DIP Flex	MCP Flex	PIP Flex	DIP Flex	MCP Abd	MCP Flex	PIP Flex	DIP Flex	MCP Abd	MCP Flex	PIP Flex	DIP Flex	CMC Abd	CMC Flex	MCP Flex	IP Flex	Rad Dev	Flex
Subject 1, Trial 1	-11.8	-30.1	29.21	19.677	-2.25	35.63	19.018	5.018	10.27	30.15	28.5	21.37	45.27	10.13	17.54	5.564	-3.04	0.6	7.78	-22	-26.7
Subject 1, Trial 2	-12.1	-30.7	27.87	19.358	-8.28	35.96	17.834	4.621	1.042	29.22	28.55	21.47	23.5	32.3	12.14	3.935	1.606	0.268	-2.57	-23.6	-24.6
Subject 1, Trial 3	7.599	30.96	132.7	39.37	61.79	90.52	27.023	-2.28	70.4	90.08	14.4	-28.2	14.3	16.51	20.18	89.48	-62.5	85.95	-0.29	60.35	24.57
Subject 1 Mean Position	-5.45	-9.93	63.26	26.14	17.09	54.04	21.29	2.45	27.24	49.82	23.82	4.90	27.69	19.65	16.62	32.99	-21.31	28.94	1.64	4.90	-8.91
Standard Deviation	11.30	35.41	60.13	11.46	38.83	31.60	5.00	4.10	37.66	34.87	8.15	28.62	15.90	11.41	4.10	48.92	35.74	49.37	5.44	48.02	29.01
Subject 2, Trial 1	-8	1.314	21.6	17.332	-0.27	30.96	17.246	5.389	10.18	24.64	19.3	25.49	2.429	27.83	22.71	20.67	2.27	11.12	-11.9	-18.1	3.596
Subject 2, Trial 2	-10.2	-3.18	20.92	20.534	-14.7	22.2	21.667	1.777	-0.09	34.03	-1.01	51.56	-1.24	39.78	-0.05	49.64	-39.1	25.34	-8.5	-33.1	5.956
Subject 2, Trial 3	-7.64	-10.1	21.39	17.481	-5.1	28.73	18.08	4.78	8.978	19.96	23.47	21.77	-8.85	26.32	15.68	16.17	-0.16	18.39	-20.3	-13.7	-9.79
Subject 2 Mean Position	-8.62	-3.99	21.30	18.45	-6.69	27.30	19.00	3.98	6.36	26.21	13.92	32.94	-2.56	31.31	12.78	28.83	-12.34	18.28	-13.57	-21.66	-0.08
Standard Deviation	1.40	5.75	0.35	1.81	7.35	4.55	2.35	1.93	5.62	7.16	13.10	16.23	5.75	7.37	11.66	18.17	23.23	7.11	6.06	10.15	8.49
Subject 3, Trial 1	-7.64	-10.1	21.39	17.481	-44.6	37.19	21.103	-2.74	-5.75	30.65	10.23	-10.6	38.05	49.6	-4.23	19.45	6.664	-17.7	2.395	-18.2	8.707
Subject 3, Trial 2	-20.8	-28.2	38.94	11.963	-41.1	27.32	22.476	-5.15	-9.9	52.92	15.47	28.91	89.98	22.48	3.702	31.67	-7.81	-7.56	-6.24	-14.4	17.04
Subject 3, Trial 3	-20.6	-11.8	38.41	13.207	-32.7	35.79	18.275	-3.68	3.875	24.75	0.785	16.7	0.795	74.7	-5.81	27.6	27.07	0.44	-6.54	-20.4	19.54
Subject 3 Mean Position	-16.34	-16.70	32.92	14.22	-39.47	33.44	20.62	-3.86	-3.93	36.10	8.83	11.67	42.94	48.93	-2.11	26.24	8.64	-8.27	-3.46	-17.64	15.10
Standard Deviation	7.53	10.00	9.98	2.89	6.14	5.34	2.14	1.22	7.07	14.86	7.44	20.22	44.79	26.12	5.10	6.23	17.53	9.09	5.07	3.04	5.67
Intersubject Mean Position	-10.14	-10.20	39.16	19.60	-9.69	38.26	20.30	0.86	9.89	37.38	15.52	16.50	22.69	33.29	9.10	29.35	-8.34	12.98	-5.13	-11.47	2.04
Standard Deviation	8.37	19.42	35.79	7.95	31.70	20.22	3.13	4.30	23.75	21.85	10.81	23.10	31.23	19.48	10.87	26.44	26.61	30.30	8.24	27.54	18.63

played a part in some of the variance, the most likely explanation for the variance in trial 3 is due to some of the signal artifact and poor acquisition at times. There were significant periods where the signal dropped to a zero level. As mentioned earlier, the signal may have been lost due to the LEDs being hidden from the cameras during movement. The method of averaging previous and post-zero signals may have resulted in inaccurate positions of the sensors compared to sensors that did have signal capture during that period. That could result in significant ROM inaccuracies.

Thankfully, the intrasubject measurements of subjects 2 and 3 did result in lesser standard deviations for all joints for the most part. All those standard deviations were below 30. This results in a greater representation of the wrist and hand between all the subjects tested. In Figure 4.22, the representation of those numbers is exhibited in the wrist and hand positions as a mean within subjects and between each of the subjects.

#### 4.6.3. Key Turn Motion Capture Data and Discussion

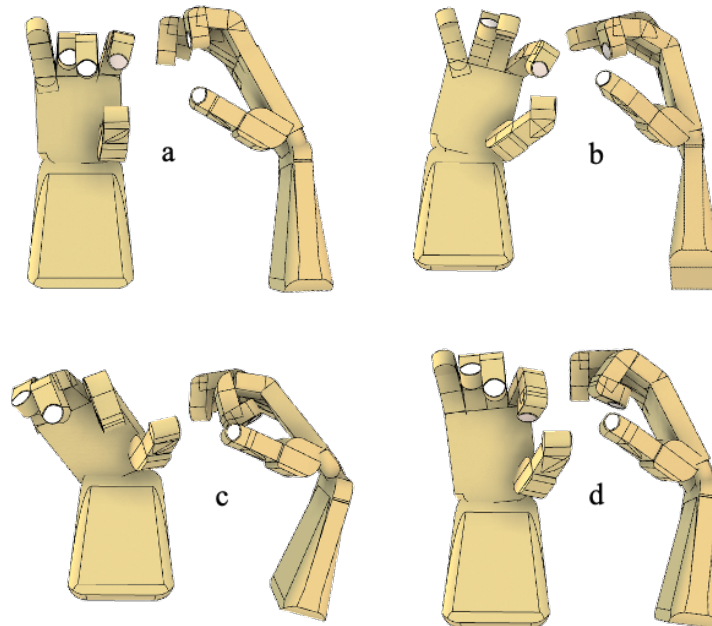


Figure 4.23. Key turn grasp mean results for a) subject 1, b) subject 2, c) subject 3, and (d) between subjects

Table 4.3 provides the angular ROM of all the wrist and hand joints during the key turn task. In this task, it is hypothesized that the lateral pinch grasp would be utilized to turn the key. As can be seen, the standard deviation between subjects is relatively low. In subject 3, there is a standard deviation of 34.21 at the middle DIP joint. This is explained by the fluctuation in the first trial compared to the next 2 trials. This may be related to lack of success during the first trial and flexing the middle finger beneath the index to provide greater stabilization. However, further analysis of the DIP joints of the index, middle, and ring fingers reveals multiple trials where the ROM is greater than 100°. Reviewing goniometric normative ROM, DIP ROM for the index and middle finger is 0-90°. There could be 2 possible reasons for the excessive ROM in these subjects. The least likely reason was that each of the subjects were hypermobile. A recent study has revealed that as many as 12.5% of 18-25 year old young adults tested positive for generalized joint hypermobility [41]. However, this would have required that 100% of this study's test participants be extremely hypermobile. The more likely reason for the findings was that the sensors' positions on the force glove were altered when the fabric was stretched and bent during the test and lead to some inaccuracies in joint position here. For a better view of the positioning of the wrist and hand, refer to Figure 4.23. The results do appear to demonstrate a lateral pinch position in all figures as hypothesized. However, there appears to be a lack of approximation of the thumb and index finger. There are likely three causes for the lack of approximation. First, opposition of the thumb was not truly measured in this experiment. Rotation of the thumb would likely give a better representation of the position of the thumb in relation to the index finger. However, this rotational motion is difficult to measure and would

Table 4.3. Key Turn Task

Subject & Trial	Index				Middle			Ring				Little				Thumb				Wrist	
	MCP Abd	MCP Flex	PIP Flex	DIP Flex	MCP Flex	PIP Flex	DIP Flex	MCP Abd	MCP Flex	PIP Flex	DIP Flex	MCP Abd	MCP Flex	PIP Flex	DIP Flex	CMC Abd	CMC Flex	MCP Flex	IP Flex	Rad Dev	Flex
Subject 1, Trial 1	-14.3	1.289	57.63	91.115	30.77	38.28	99.497	4.074	25.04	11.96	106.7	10.81	-1.85	22.81	2.757	29.98	9.282	0.076	-1.84	5.354	31.85
Subject 1, Trial 2	-14.6	9.774	59.35	121.31	39.2	7.754	104.83	4.178	26.37	-0.1	112.6	6.569	8.051	7.343	6.284	31.37	6.827	3.333	-7.28	-1.7	19.72
Subject 1, Trial 3	-19.2	-3.44	49.54	102.32	19.6	25.04	77.048	2.478	27.01	27.1	78.97	4.352	-3.15	12.95	7.361	34.76	6.68	4.045	-3.98	2.452	32.01
Subject 1 Mean Position	-16.04	2.54	55.51	104.91	29.86	23.69	93.79	3.58	26.14	12.99	99.44	7.24	1.02	14.37	5.47	32.03	7.60	2.48	-4.37	2.04	27.86
Standard Deviation	2.77	6.70	5.24	15.26	9.83	15.31	14.74	0.95	1.00	13.63	17.97	3.28	6.13	7.83	2.41	2.46	1.46	2.12	2.74	3.54	7.05
Subject 2, Trial 1	-23.6	49.85	100.4	122.95	22.07	68.18	103.3	2.141	45.35	-7.26	94.05	34.65	-20.5	8.701	64.93	38.58	32.12	0.548	57.08	-10.3	14.64
Subject 2, Trial 2	-27.6	53	93.31	115.77	22.6	66.48	74.605	2.275	43.79	-7.7	92.64	28.47	-15.3	10.77	63.56	39.71	32.99	0.431	37.76	-13.7	17.64
Subject 2, Trial 3	-28.2	54.97	70.51	81.633	19.37	72.18	77.651	2.626	44.03	-1.54	64.35	24.84	-12.4	15.96	65.42	41.57	33.57	0.68	42.55	-15.9	16.34
Subject 2 Mean Position	-26.46	52.61	88.07	106.78	21.34	68.95	85.18	2.35	44.39	-5.50	83.68	29.32	-16.06	11.81	64.64	39.95	32.89	0.55	45.80	-13.30	16.21
Standard Deviation	2.46	2.58	15.62	22.08	1.73	2.93	15.76	0.25	0.84	3.43	16.76	4.96	4.08	3.74	0.96	1.51	0.73	0.12	10.06	2.84	1.50
Subject 3, Trial 1	-20.5	56.92	111.3	112.33	26.3	16.7	43.739	-3.18	26.82	5.086	57.67	-23.1	33.88	13.23	5.931	38.65	44.45	8.267	15.83	34.24	62.91
Subject 3, Trial 2	-22.3	50.5	116	103.13	26.04	8.55	96.702	-2.87	27.04	7.339	51.95	-21.5	24.55	15.46	2.848	31.64	46.28	2.746	10.59	36.17	59.35
Subject 3, Trial 3	-28.4	36.71	108.2	108.67	20.6	77.81	107.74	-2.55	25.18	18.26	67.24	-20	26.4	19.47	43.41	30.36	37.65	1.002	9.821	21.77	45.93
Subject 3 Mean Position	-23.74	48.04	111.83	108.04	24.31	34.36	82.73	-2.87	26.35	10.23	58.96	-21.52	28.28	16.05	17.40	33.55	42.80	4.01	12.08	30.72	56.07
Standard Deviation	4.13	10.33	3.93	4.63	3.21	37.85	34.21	0.32	1.02	7.05	7.73	1.54	4.94	3.16	22.58	4.46	4.55	3.79	3.27	7.81	8.95
Intersubject Mean Position	-22.08	34.40	85.14	106.58	25.17	42.33	87.23	1.02	32.29	5.90	80.69	5.01	4.41	14.08	29.17	35.18	27.76	2.35	17.84	6.49	33.38
Standard Deviation	5.44	24.79	25.91	13.69	6.44	28.96	20.84	3.01	9.11	11.68	21.87	22.29	19.87	4.98	29.38	4.51	15.90	2.64	22.81	19.87	18.66

likely require more motion sensors. Second, the CAD representation of the hand may not truly represent the actual size of the hand. A better representation would likely reveal that the thumb or index finger are larger than the drawing indicates. Finally, index MCP abduction occurs during each of the trials. Although calibration did occur here, it is still likely that MCP abduction is not fully accounted as there is not truly set origin or 0° point between abduction and adduction. Further studying of abduction/adduction of index, middle, ring, and little fingers are essential in order to obtain a better representation of the hand.

#### **4.6.4. Can Grasp and Key Turn Conclusion**

The hypothesis in performing these two patterns of movement were that two hand postures would be observed: gross grasp for can grasp and lateral pinch for key turn during the largest force producing times. In the case of the can grasp, that is what did occur for the most part. As for the key turn task, the index and middle PIP and DIP joints appear to be flexed in a position that would support force on the of the fingers on the key. However, only the mean of subject 2 (Figure 4.23B) demonstrates that the thumb is in actual physical contact to the index and/or middle fingers. This is a necessity as the thumb must provide an equal and opposite force to the middle and index fingers to statically hold the key in place while the key turns the lock. As stated in Chapter 3, the sensors of the thumb provide a much greater force compared to the index and middle fingers (Figure 3.8). However, this result is more likely a problem in the positioning of the FlexiForce sensors positioning on the palmar portion of the fingers. To record the full force that occurs during this activity. A larger sensor would be required in order to capture the force on the lateral and medial sides of the fingers.

This experiment was somewhat effective in capturing the forces and movements of the fingers that are required during activities of daily living. The results could be utilized to build

biomimetic algorithms for robots and prosthetics. It is believed that central pattern generators exist for activities such as walking [42], breathing and chewing [43], and multiple other activities that are completed on a daily basis by humans. The premise of central pattern generators is that conscious thought is not required to complete these activities. When humans walk, they don't need to plan every step out. Instead, they use spinal and subcortical neurons to complete these tasks. In order to understand the relevance to hand and arm movements, conceptualize placing the hand on a hot object unknowingly. There is a quick instinctive and reflexive reaction to remove the hand from the object. Central pattern generators perform this task without the requirement for conscious thought. This is a protective mechanism. The concept of central pattern generators explains that these reflexive and instinctive actions are occurring throughout daily activities in humans and there are set patterns of movement for activities such as grasping a can and turning a key. When the task is not successful with these stored programs, that is when we, as humans, consciously modify our motions to complete the task. This is the reason why research such as this is so important. As mentioned above, this data can be used to create movement algorithms for robots and prosthetics for a wide range of reasons. The movement patterns can be used to create algorithms to move prosthetics and robotic limbs for those who have neurological paralysis or amputated limbs. These algorithms can also be utilized to determine why some are faster in peeling a crawfish exoskeleton so that a robot can replicate the efficiency without crushing the edible contents.

The limitations in this experiment are multifold. One to the main limitations is the current sensors being employed to perform the current experiments. The FlexiForce sensors utilized were chosen, for the most part, due to financial affordability of the sensors. However, as mentioned, there are multiple problems with use of these sensors. First, these sensors do not

cover the fully used surface area of the fingers and hand utilized by humans on a daily basis. Future sensors for these experiments of this nature should utilize sensors that cover the medial, lateral, and palmar portions of the fingers as well as the palm of the hand. Unfortunate for this project was that sensors were not placed on the palm of the hand for a better understanding of equal and opposite forces of the fingers on the can during can grasp. Another observation is that a grid pattern be utilized in the future to differentiate where the force is being applied. In other words, it appears more likely force would be applied at the lateral/radial side of the index finger and palmar side of the thumb during key turn tasks. Again, this would provide better insight into the equal and opposite nature of the forces of the hand. Lastly for force capture, the FlexiForce sensors required an extensive and arduous amount of calibration when utilized with the Codamotion system.

As for the motion capture portion of the project, the most significant problem encountered was motion capture. An extensive amount of time was utilized to set-up infrared cameras in order to capture movements of the sensors. In spite of this effort, there were still periods of 0 measurements registered by the system that required significant signal analysis and modification. Future endeavors in this research could provide analysis of movement patterns and forces for more normal daily activities such as handwriting, typing, and cooking, etc. It could also reach into work related activities where repetitive stress injuries occur or where some individuals are more efficient and effective at their occupations than others. There could also be potential in leisure and professional activities such as the difference between professional musicians and artists compared to those that perform on a recreational level. This technology could also be utilized to determine the force Odell Beckham utilizes in order to catch a football with the palm of his hand so easily. There could also be importance in determining the most

efficient hand force that Alex Bregman utilizes on a bat to hit a 425-foot homerun so that the correct diameter of the handle is chosen for him. To accomplish these activities, force and motion capture sensors that are more reliable and portable would have to be manufactured.

## **5. Suggestions on Soft Elastomer Sensors and Actuators for the Hand**

### **5.1. Introduction**

The goal of this research project was to create a device capable of moving a paretic wrist and hand. As mentioned previously in Chapter 2, there have been multiple attempts to create orthotics/actuators to assist in moving the paretic hand/wrist. Those attempts have included orthotics that passively move the hand, devices that stimulate the muscles for hand and wrist movement, and devices that do not actually move the hand but instead provide an extra appendage to manipulate objects. However, there is not a widely used commercial product that is utilized in the paretic hand/wrist. In an attempt to characterize such a device, a force glove was fabricated to better understand the movements and forces produced by the normal hand during ADLs. The results of those experiments can be found in chapters 3 and 4. The goal of that research was to create a library of these forces and motions so that device fabrication can implement these concepts into the design of an actuator. Many hand and wrist orthotics are not fully used and often sit on a shelf because the design does not mimic the forces and movements of normal hands. A library of these kinematics would also provide algorithms that would allow the user to control the devices more effectively.

While performing this research, it was determined that there were many limitations in regard to the FlexiForce sensors when attempting to capture force data. In particular, the current sensors lack the ability to record forces that occur on all of the various portions of the fingers and palm. Therefore, research was started to create a device that enables the capture of a larger surface area of the hand. The undertaking of this project to create better sensors and actuators of the hand required endeavors into materials that have properties similar to the skin, creating flexible yet resilient conductive and actuating materials, and fabrication of a small and

lightweight design so that it is wearable for the user. In this chapter, discussion on the fabrication of a flexible sensor with a grid array, soft robotic actuator, and mechanical gear actuator ensues.

## 5.2. Background of a Hand Sensor Design

The hand and wrist are a complex arrangement of 16 freely moveable (diarthrodial) joints that allow us, as humans, to interact with our environment about as well as any animal species. As a result of this mobility, a large arrangement of hand positions can be achieved to manipulate objects as reported in Chapter 2. There is growing

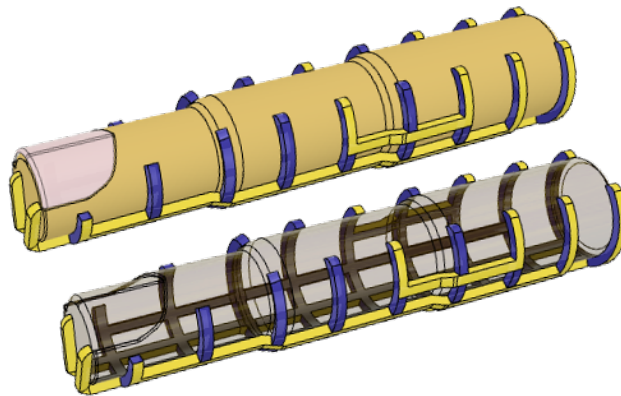


Figure 5.1. CNT finger sensor

desire to understand movement patterns and forces of the hand in order to create biomimetic robots and prosthetics. In Chapters 3 and 4, we presented research where sensors were utilized to capture forces and movement patterns of the hand when subjects performed can grasp and key turning activities. However, there were many limitations with the use of these sensors. Therefore, this research group proposed the fabrication of a sensor comprised of grid patterns to more accurately capture the forces applied to various portions of the fingers and the hand.

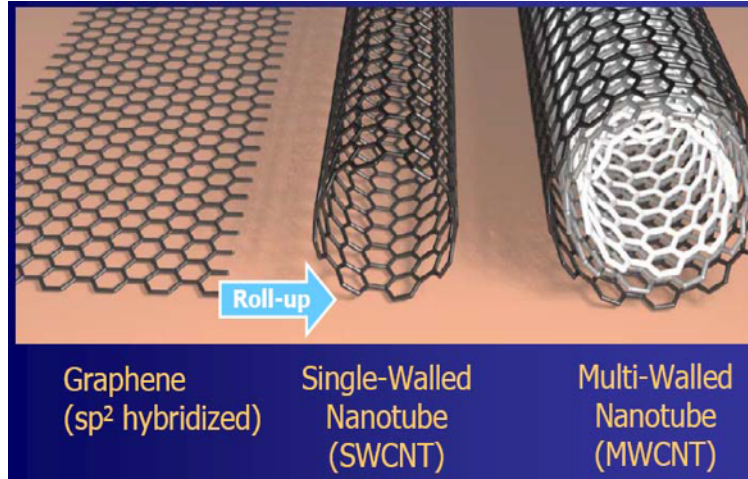


Figure 5.2. Graphene, single-walled, and multi-walled CNT[1]

In order to accomplish this feat, a conductive material was first agreed upon. Previous researchers in the LSU BioMEMS laboratory proposed that carbon nanotubes (CNT) could be utilized to create an array of flexible sensors[44-47]. According to Dresselhaus and Avouris, a carbon nanotube is defined as a sheet of graphene rolled into a cylinder of nanometer size diameter[48]. Graphene is a two-dimensional lattice of carbon – carbon bonds. As can be seen in Figure 5.2, carbon nanotubes are rolled sheets of graphene that are available in two forms: single walled and multiwalled. Single walled (SWCNT) refers to one single layer of graphene while multiwalled (MWCNT) refers to materials that have multiple layers of graphene wrapped together[49]. Carbon nanotubes provide an excellent material for flexible sensors due to their strength, durability, flexibility, and conductivity. Just how strong are carbon nanotubes. Some studies lay claim that CNT based materials may be used one day to create a space elevator! This ladder like projection would attach the surface to the earth to outer space objects such as satellites or even the moon[50]. Current biomedicine has used CNT to improve the process of joint replacement. MWCNTs added to bone ceramics when adhering total joint prosthetics to bone have

proven to lessen bone ceramic fracture occurrence and enhance mechanical compression and bending strengths compared to bone ceramics without MWCNT[51, 52]. Multiple studies have been performed that demonstrate the strength of carbon nanotubes. A comparative study performed by Osmani et al revealed that carbon nanotubes possess significantly greater Young's modulus (SWCNT 1054 GPa and MWCNT 1200 GPa) ratings when compared to steel (208 GPa) and wood (16 GPa) [53]. As can be seen in Figure 5.2, graphene results in a hollow shell when rolled into a CNT. This results in great tensile strength (axial direction). However, studies have demonstrated that CNT may be more susceptible to column buckling during axial compression due to this hollow inner lattice[48, 54]. MWCNT should provide greater resistance to column buckling under axial compression due to the robust cross-sectional surface area [55]. That deformation can lead to transition in the material from a conductor that acts as a metal to a more semiconductor type material[56, 57].

The ultimate importance of this research is to utilize a material that is resistive to both compression and tension and still act as a conductor of electricity. CNTs can be constructed with various lattice formations. The covalent bonds of the carbon – carbon bonds give rise to their conductive nature. According to multiple researchers, there are three geometrical shapes of SWCNT (armchair, zigzag, and chiral) that allow these materials to take on differing semiconductor and metallic properties[48, 58]. MWCNTs maintain a metallic property[59]. In an attempt to further understand the electrical properties of CNTs, a strand of SWCNT was positioned across two metal electrodes and an atomic force microscopy probe contacted the strand causing a deflection. This resulted in a change in conductance that corresponded to the amount of deflection. However, resting

conductance values returned when the force was removed[60]. Inevitably, this research opened the door to electromechanical based CNT sensors in which conductive properties were changed based on mechanical forces such as tension and compression[47, 61, 62].

Fabrication of devices that utilize CNT have recently started to come into commercial use. A product that utilizes a sheet of CNTs termed buckypaper (or Nafion) has been fabricated. This sensor has a property that allows for bending but minimal to no linear translation similar to paper. Therefore, the sensor acts as a cantilever that results in decreased conductance when the sensor is bent[63]. When creating a sensor for biomimetic reasons, it would be optimal to include both bending and translational properties. To accomplish this task, CNTs will have to be combined with a material that allows for this property.

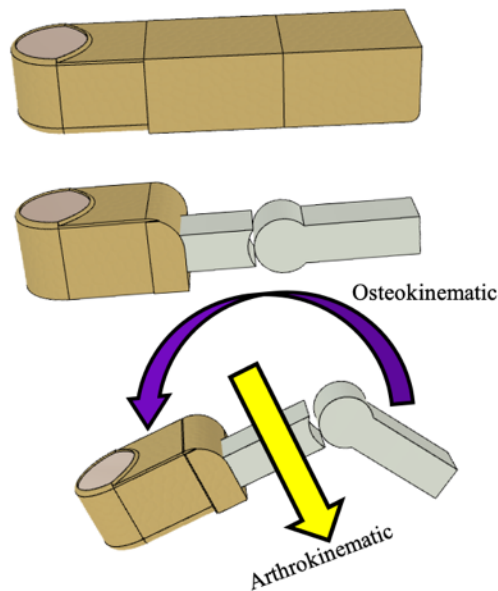


Figure 5.3. Considerable motions of the finger

### 5.3. Sensor Characteristics

To create the devices that mimic human movements (biomimetics), it is important to capture forces applied by the hand on objects during ADLs. The joints of the hand and

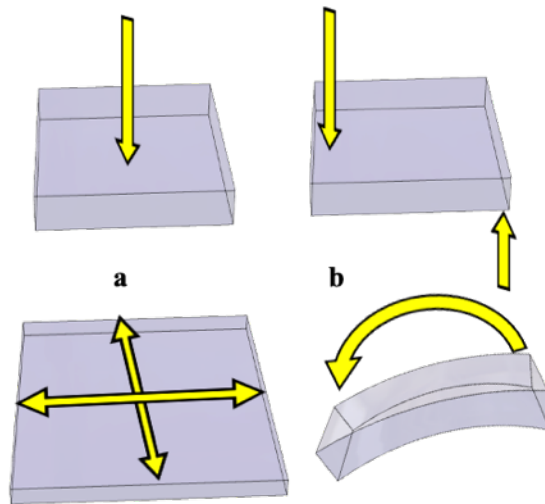


Figure 5.4. Mechanical properties of silicon rubber and skin: a) Translational and b) rotational

wrist contain movements that occur in both rotational planes (osteokinematic movement) and translational planes (arthrokinematic movement). It is important to keep this in mind to avoid bunching of the material near the joint regions. Therefore, the material should be slender and tight-fitting to the skin so as to avoid translational movement of the whole device of the fingers.

Skin and subcutaneous soft tissues of the fingers also demonstrate viscoelastic properties. This results in strains patterns in both the translational and rotational planes in response to forces applied to the skin. Therefore, it is important to create force/pressure sensors that allow for both translational and rotational deformation. Since

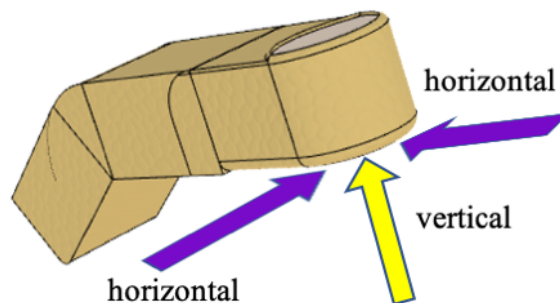


Figure 5.5. Three dimensional forces applied to the finger

there are so many joints in proximity and a large surface area of the fingers used in manipulating an object, it is important to create a grid pattern that differentiates forces occurring at different parts of the fingers. Therefore, this research group attempts to further research studies performed in the LSU BioMEMS laboratory in flexible sensors.

A material that allows for both translational and rotational movements is polydimethylsiloxane (PDMS). Previous studies have created a method of inkjet printing a SWCNT array on a polyester transparency film. However, the transparency allows only for movement in the rotational plane[46]. Therefore, an alternative method of stamp printing utilized a fabricated stamp dipped into a MWCNT solution and stamped onto a glass substrate. Next, a thin layer of PDMS was spin-coated onto the substrate, cured, and then removed creating then PDMS layer embedded with CNTs. Although this technique does create CNT sensors, the process results in inconsistent levels of CNT embedded within the PDMS substrate[45]. Therefore, a transfer printing technique was composed to create a more consistent aggregation of CNT on PDMS. In this technique, MWCNT are initially printed on a transparency. That transparency is then secured inside a spin-coater and PDMS is spun across the transparency. Once cured, the PDMS is then released from the transparency with embedded MWCNT attached securely into the PDMS[47]. This novel technique works well when there is a constant direction in application of force. However, forces on the fingers are not always applied in one direction. The surface area of the finger is so adaptive and robust that it can accommodate to forces in all 3-dimensions. Therefore, a grid pattern must be created to better capture the position of the applied forces.

The flexible substrate chosen for this project was Ecoflex silicon rubber produced by Smooth-On (Smooth-On, Pennsylvania, USA). This substrate was chosen over PDMS

because it can be purchased in an assortment of hardness properties. Each of the products contain datasheets with a plethora of information explaining the properties of the materials such as modulus, tensile strength, specific weight, shore hardness, and elongation percentage. This allowed for a more efficient approach to this research allowing the opportunity to test out multiple materials without having to perform an actual durometer test for each of the materials.

## 5.4. Force Sensor Fabrication, Preliminary Findings, and Encountered Problems

### 5.4.1. Fabrication

#### MWCNT and Printer Cartridge Preparation (Step 1)

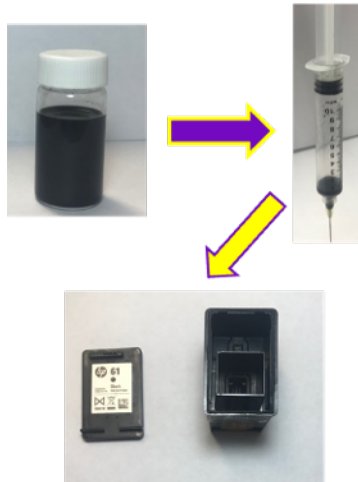


Figure 5.6. CNT solution injected into printer cartridge

Using techniques formulated in previous research[[44](#), [46](#), [47](#)], 45 mg of MWCNT (CheapTubes Inc.), 31.5 mg sodium n-dodecyl sulfate (SDS – Alfa Aesar), and 4.5 ml of DI water were introduced into a vial. The closed vial was placed in a ultrasonic cleaner (Fisher Scientific FS20D) and sonicated for 30 minutes to disperse the CNTs throughout the solution. The solution was then transferred via syringe into centrifuge tubes and spun for 5 minutes at a rate of 12,000 rpm. Once the solid and liquid portions of the solution were separated, a syringe

was utilized to retrieve the aqueous CNT solution leaving the solid content behind. That aqueous ink solution was injected into an HP 61 printing cartridge.

### **Printing MWCNT Solution onto Transparency (Step 2)**

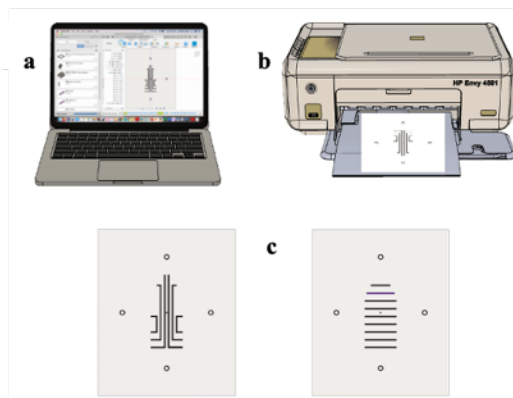


Figure 5.7. a) Grid patterns formulated on Fusion 360, b) printed on inkjet printer, and c) resultant transparencies

Two grid patterns were created in the computer-aided design (CAD) software application Fusion 360. The grid patterns captured the vertical length and horizontal circumference of the middle finger. These two \*.pdf files were opened in the application Inkscape. This allowed for the grids to be colored and fit to an 8"x11" printable file. Those files were then saved and printed on an HP Envy 4501 printer. The grid patterns were printed 30 times on a 7-mil transparency (Inkpress Digital Media). Besides the grids, multiple dot patterns were also printed to align the two transparencies during silicon rubber casting.

### **Laser Printing Aligning Holes and Fabricating Casting Pieces (Step 3)**

After transparencies are fabricated, they are prepared for casting. (To cast a PDMS substrate between the transparencies, a few steps must be undertaken. First, the transparency aligner holes must be cut properly so the grids will line up perfectly. Therefore, an acrylic board is fabricated so that the 8.5"x11" transparencies can be

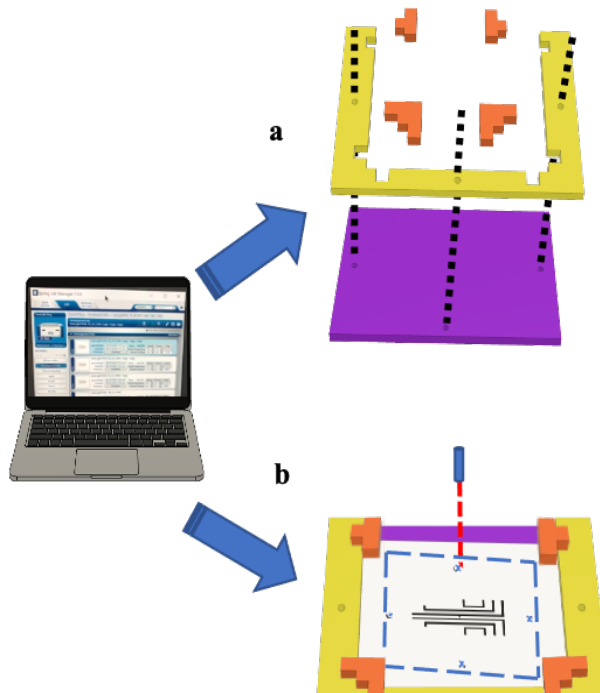


Figure 5.8. a) Laser engraver used to cut out transparency aligner board and b) laser engraver transparency cut

properly placed in the Epilog laser cutter. To accomplish this, an acrylic cutting pattern is created in Fusion 360, exported by the Shaper application into an appropriate .jpeg file, modified into an appropriately sized .pdf file in Inkscape, and printed to the Epilog laser cutter software where the appropriate laser intensity and frequency for cutting can be chosen. An  $\frac{1}{4}$ " thickness acrylic piece is placed in the laser cutter and six acrylic pieces are created from these cuts. Two of the acrylic pieces are epoxied together based on the 3 holes that can be seen in Figure 5.8. Once these 2 pieces are attached, the transparencies can be placed on the board and the four rectangular pieces are set atop the transparencies to prevent them from shifting during the laser cutting process.

Just as with the acrylic pieces, a cutting pattern of the transparencies is created in Fusion 360, exported by the Shaper application into a .jpeg, modified in Inkscape to cut the proper x and y coordinates, and printed to the Epilog laser cutter where the appropriate

frequency and intensity of the laser cutter is set. The result is two transparencies that will properly align into a 3D printed PET structure for silicon rubber casting.

#### Silicon Rubber Casting on Transparencies with 3D Printed Aligner Pieces (Step 4)

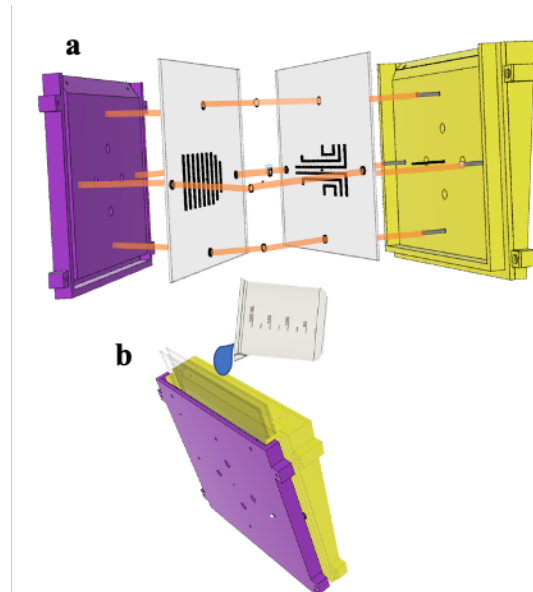


Figure 5.9. a) PLA casting aligners, transparencies, and rings, and b) silicon rubber casting

The flexible substrate chosen here was Ecoflex silicon rubber produced by Smooth-On (Smooth-On, Pennsylvania, USA). This substrate was chosen over PDMS due to the extensive  
Once the transparencies are laser cut, they are ready to be casted with PDMS. In order to align the transparency grid patterns, male and female aligner structures were created in Fusion 360 and printed on Prusament PET plastic with a Prusa I3 MK3 or Prusa I3 MK2 3D printer. Four rods of 3 mm diameter and a 0-80, 1 inch screw were epoxied on the male structure. The rods and screw allow the transparencies and female PET structure to be slid into the proper alignment with the male PET structure. The male portion of the PET structures are fabricated to allow for a 1.5 mm distance between the surfaces of the male and female structures. Five PET rings of 1.5 mm thickness were also printed to

maintain a separation distance of 1.5 mm between the two transparencies. Once these structures were combined, Dragon Skin 35 silicon rubber (SR) mix A and B are combined at a 1:1 mixture ratio. The mixture is degassed and then poured into the 1.5 mm void between the transparencies. In order to ensure curing, the PET structure is placed in an oven and the SR is cooked at 60 ° C for 4 hours.

#### Whole Punching the Transparency/SR Device (Step 5)

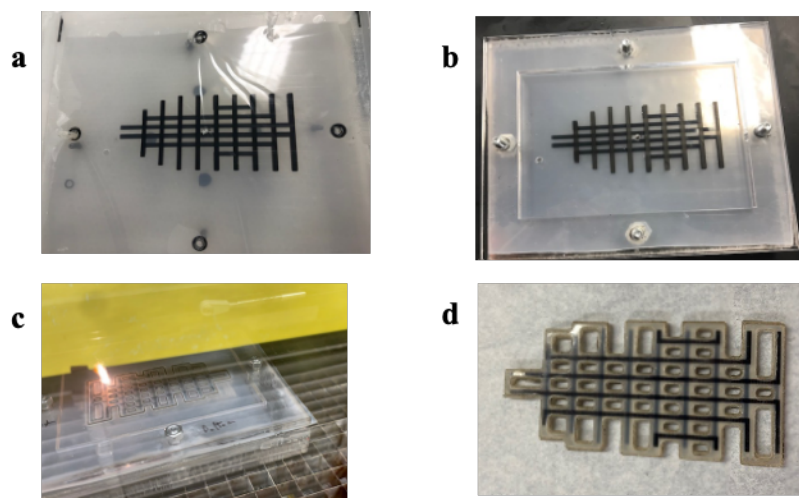


Figure 5.10. a) Transparency/SR released from PLA casting aligner, b) placed in an acrylic aligner, c) laser cut to precision, and d) resultant transparency/SR structure

An important concept to this research is to provide some sensory feedback to the user while wearing this glove. Previous research attempts in capturing forces utilize gloves that fully enclose the hand and fingers and do not allow the skin to actually contact the objects that it is manipulating. This can result in delayed reaction when items are slipping in the hand and possible modification in manipulation techniques to achieve greater sensory feedback.

Therefore, holes were laser cut through the SR/transparency with dimensions as large as 5 mm and as narrow as 2.5 mm. In order to accomplish this task, the transparency was first removed from the PLA casting aligner as can be seen in Figure 5.10. The transparency was then placed in

an acrylic aligner. The acrylic aligner was fabricated with the Epilog laser cutter so that aligner holes would allow for proper placement of the transparency/silicon rubber to later also be cut by the same Epilog laser cutter. A pattern for proper cutting of the transparency/SR was developed in Fusion 360 CAD software, saved in a .dxf file, uploaded to Inkscape software, and saved as a .pdf. That Inkscape software is critical again for alignment of the proper cutting pattern. It also allows for a clean vector cutting of the transparency/SR. That .pdf file was exported to the Epilog laser cutter and the transparency/SR was cut. Figure 5.10d is resultant of the laser cutting process.

### Removing One Side of Transparency and Fixing Small Wiring to CNT (Step 6)

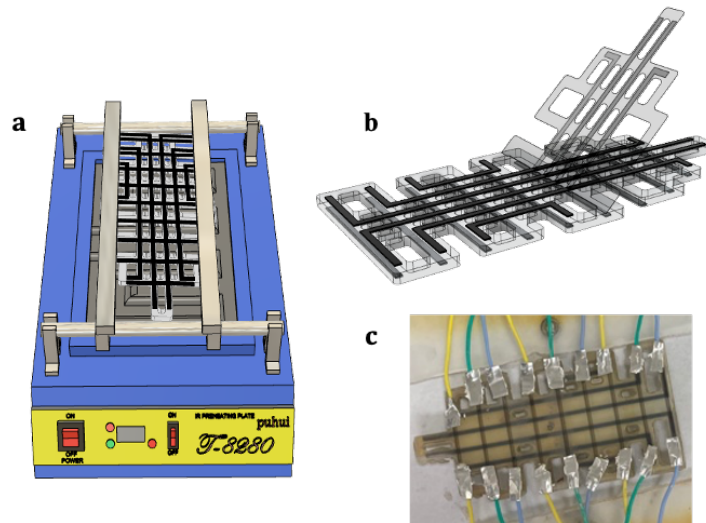


Figure 5.11. a) Infrared heating of SR/ transparency, b) removal of transparency, and c) aluminum wired adhered to SR with silver epoxy and aluminum adhesive tape

After the transparency/SR is cut, one side of the transparency must be removed. When attempting to transfer the greatest amount of CNT onto the SR, heat is applied to the transparency/SR prior to removal of the transparency. Therefore, the transparency/SR was heated at 165° C for a period of 15 minutes and one transparency side was removed. After removal of the transparency, aluminum wires were attached to the CNT pattern on the SR using

a conductive silver epoxy (MG Chemicals 8330) and aluminum adhesive tape (Dexerials AL 7650)

### 2D to 3D Transformation (Step 7)

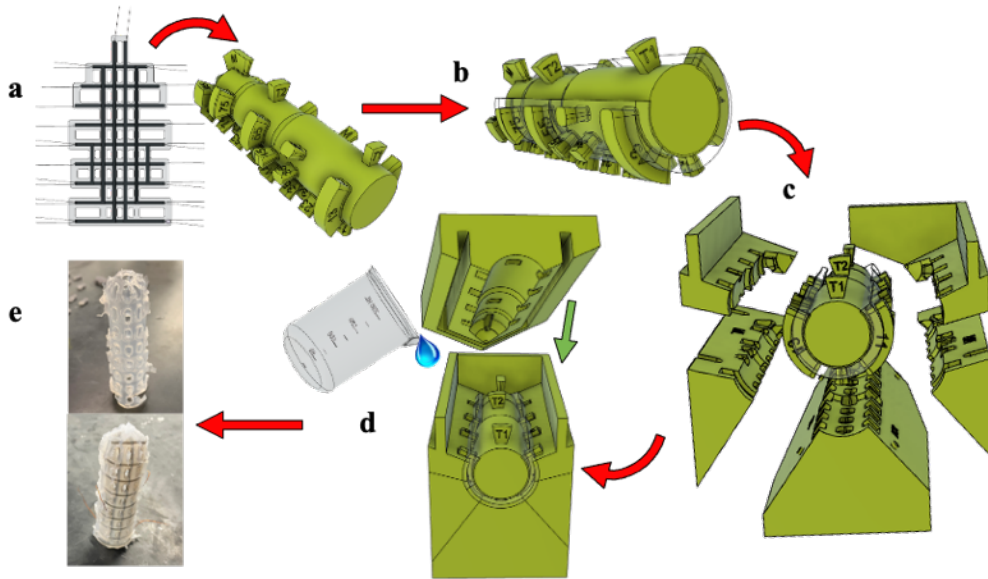


Figure 5.12. 2D to 3D transformation of SR: a) wrap SR on inner PLA device to form b), combine outer shell around inner PLA/SR, d) pour liquid SR, and e) completed cylindrical device

The desire from the beginning has been to create a wearable sensor that is portable and can be used in a multitude of situations. Therefore, this sensor must be cylindrical and fit snugly around the fingers. To accomplish this feat, the SR/CNT structure is initially wrapped around an inner PLA cylinder. The CNT/SR is then sandwiched between the inner and outer PLA pieces. Liquid SR is then poured and the top portion is connected to finish the cylindrical outer form. The cast is allowed to cure for 4 hours and the resultant cylindrical piece is formed which can be seen in Figure 5.13e.

#### 5.4.2. Preliminary Findings

Although there is a plan to incorporate each of the fingers as well as the palm of the hand in this sensor glove, the research has not quite reached that point. However, there

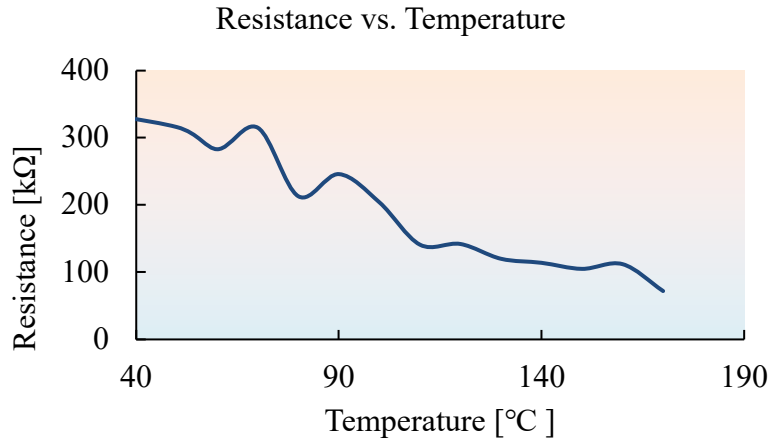


Figure 5.13. Recorded resistances of released CNT/SR device related to IR heat exposure

have been some positive results of note so far. Figure 5.13 reveals that resistance values as low as 72 kΩ have been achieved on the SR/CNT grid after the transparency has been removed. These results are favorable for the current methods. These initial values will provide the ability to measure the device when it is mechanically deformed into translation (compression, traction) or rotational motions. The expectation is that the resistance will increase but still be measurable for all forces on the hand.

### 5.4.3. Encountered Problems

As mentioned previously, future work is planned to create a sensor to incorporate each of the fingers and palm of the hand. Before that can occur, specific testing on the resistance values when the device is under mechanical deformation must occur. Preliminary studies with a strain gauge have started toward collecting resistance values in response to compression forces applied to the sensor grid. However, there have been problems and challenges that have prevented the progression of this research.

An initial problem encountered is the variability in sensor resistance values that occurs during the transfer process when transparency is removed from the silicon

rubber/CNT substrate. There are multiple variables that could be the cause of this. First off, variability has been noted in the amount of CNT that is printed on the transparency by the inkjet printer. It is the belief of this researcher that the variability in the inkjet cartridge pores that the CNT solution is released from could be a major cause. Therefore, techniques such as washing the cartridges in an ultrasonic cleansing bath have been employed to counteract this problem. New cartridges after each printing would be optimal. However, that would also drive the cost of the fabrication process up significantly. Another problem could simply be the variability of transfer of the CNT from the transparency to the silicon rubber during the heating process. More research is being done to determine infrared heating bed temperature and time exposures for optimal transfer of CNT to SR. In spite of the variability, a good sensor can still be created with the correct calibration of resistance rates to force applied. Again, further effort is planned toward strain gauge testing to characterize this device.

The most significant problem at this time is connection of the CNT grid pattern to a controller/data acquisition component. Efforts have been attempted to adhere a conductive wire to the CNT grid. However, silicon rubber is a material that is notoriously difficult to adhere to other materials. This relates to the covalent bonds of silicon that result in a lack of surface energy. Conductive materials such as graphite and silver have surface energies of 1250 and 890 mJ/m<sup>2</sup>, respectively, which allow for great adhesion[64]. In comparison, PDMS has a surface energy of 20.1 mJ/m<sup>2</sup>[65]. Additional problems occur in the interface between the SR and applied conductive adhesives once the materials are cured/adhered. SR materials have a flexible nature and allow elongation as great as 620% before the material fails (Ecoflex Dragon Skin 20 datasheet). In contrast, silver epoxy adhesive (MG Chemicals Silver Conductive Epoxy

Adhesive 8331 datasheet) allow elongation only up to .30% prior to failure. This has resulted in the fracture of multiple wire connections during the recasting method and/or bending of the SR. The most successful attempts, at this time, have occurred when applying silver epoxy and pressure on the wire to the CNT grid with a Dexerials aluminum adhesive sheet. Prior to handling the material, another light coat of SR was applied to prevent risk of CNT/silver epoxy failure.

## **5.5. Devices to Actuate the Hand and Wrist – Soft Robotics and Mechanical Gear Orthosis**

The last part of this research involves the creation of an orthotic that is capable of moving a paretic hand. Multiple methods have been undertaken to create this device. Those attempts include the use of soft robotics and a mechanical gear system. A device still has yet to be applied to a human hand as of the completion of this dissertation. However, this researcher would like to continue working toward a device that could be commercially available.

### **5.5.1. Soft Robotics Background**

Soft robotics are devices that are made of typically involve some form of silicon rubber/polydimethylsiloxane (PDMS). The materials are chosen as a result of their flexible nature. When fabricating a soft robotic, a hollow chamber is designed within the structure. The chamber is connected to a hydraulic or pneumatic pump. As the pump increases pressure within the structure, it behaves like a balloon and expands. If the device is restricted by a material such as a Kevlar thread wrap (which has less elasticity percentage compared to silicon rubber), the material will be restricted and expand more in a translatory fashion. If an additional restriction such as Tyvek fiber is embedded within the SR beneath the hollow chambers, it will create less expansion on inflation of the device. This causes a cantilever effect as that upper portion of the

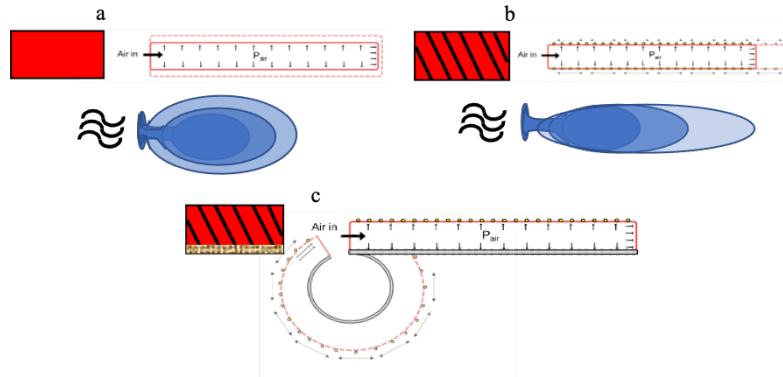


Figure 5.14. Model of soft robotics: a) inflation and expansion of SR, b) encircled SR allowing linear translation, c) restrictive layer creating cantilever (<https://softroboticstoolkit.com>)

device continues to expand. Soft robotics have garnered significant interest in the 21<sup>st</sup> century from use in creating objects that move like sea creatures[66] to early attempts of creating devices that beat like the human heart. The latter attempt embedded cardiac cells in this rubber like material and stimulated the heart cells to contract[67]. This resulted in a pulse-like contraction of the very bendable silicon rubber. Websites such <https://softroboticstoolkit.com> have provided helpful hints and instructions on various projects and outcomes in soft robotics. There is also a plethora on information in regards to characterizing and modeling with soft robotics[68]. There have been some attempts to utilize this material to make hand and wrist motions[69]. However, there is again no such device that is utilized significant by those who experience paresis at the hands and wrist. Therefore, this researcher attempted to create a device with the attempt to move the MCP independently of the PIP/DIP joint.

### 5.5.2. Fabrication of a silicon rubber pneumatic orthotic

While simultaneously working on the previous projects, work was also initiated on a device to passively move a paralyzed hand. Fabrication of this device utilized 3D printed PLA

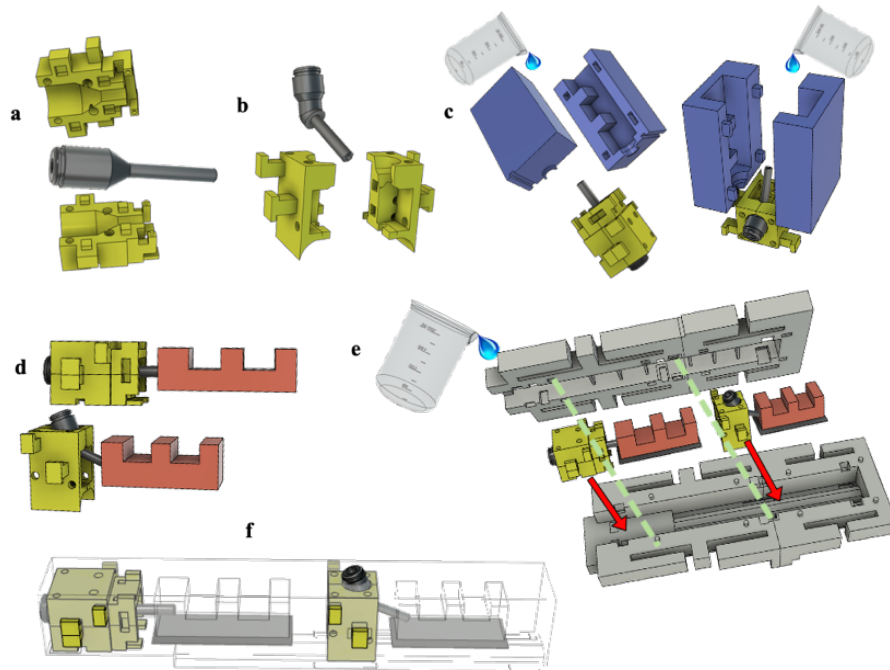


Figure 5.15. Fabrication of SR orthosis: a) MCP PLA piece and valve, b) PIP PLA piece and valve, c) polyethylene glycol (PEG) poured into MCP and PIP cast, d) MCP and PIP with PEG, e) casting with SR, and f) SR completed cast

MCP and PIP device that were utilized to house 1/8-inch straight and 45-degree elbow connectors (McMaster Carr, Illinois, USA) and provided stability to the independent joints.

These pieces were casted in polyethylene glycol (PEG) to provide a frame for casting. A thin layer of Tyvek was adhered to the bottom layer of the MCP/PEG and PIP/PEG structures which were then placed between the upper PLA and lower PLA casting structures. Ecoflex Dragon Skin 30 silicon rubber (Smooth On, Pennsylvania, USA) was poured into the upper PLA structure to cast the MCP and PIP structures. Once the SR was cured, it was removed from the PLA structures and placed in water heated to 65° C. This temperature was chosen to melt PEG but leave the PLA MCP and PIP structures intact (melting temp 100° C, “waxy” temp 85° C). The resultant of this step was to create two hollow chambers that allow air and/or water to be

pumped into the chambers. Tubing of 1/8-inch was then placed into each of the push to connect valves.

The Tyvek piece that was placed below each of the PEG structures remains casted in the silicon rubber. The purpose of this is to create an upper layer of SR above the hollow chamber that has a greater elongation percentage than the lower layer of SR embedded with Tyvek below the hollow chamber. Per datasheets, the SR has an elongation percentage of 364% whereas the Tyvek has an elongation percentage of 16-30%. The difference results in the upper layer having a greater translational elongation than the lower layer. The result of this is a cantilever effect creating a bend of the device. This bending is the proposed method to actuate the fingers of the hand into finger flexion. The current device is only focused on the movement of one finger.

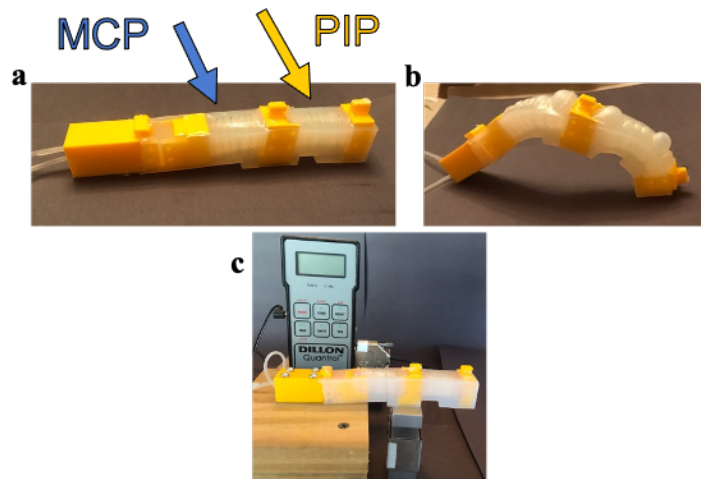


Figure 5.16. SR orthotic: a) independent MCP and PIP chambers, b) inflated device, and c) strain gauge measurements at the distal tip of the PIP/DIP and MCP

However, the device does allow movement to be segmental. That is, the MCP joint moves independent of the PIP/DIP joints (these do move together).

Measurements were taken with a strain gauge placed beneath the distal MCP compartment and the distal PIP/DIP compartment. The greatest forces produced were 0.73 pounds at the MCP and 0.43 pounds at the PIP/DIP. Using a handheld goniometer,

approximately 30 to 45 degrees of motion were the most achieved with max inflation of the device.

Several problems have arisen when attempting to inflate the device. The most frequent problem encountered was leakage of air or water during testing of this device. Multiple attempts have been undertaken to change the design or to create a superior method of sealing the device. However, there was inevitably a leak or rupture of a membrane when testing. The rupture, at times, occurred with minimal bending of the device.

A few problems do require thought when handling and wearing the device. Care must be taken to avoid placing the devices in places that it may be punctured. On a daily basis, the hand comes into contact with many sharp objects. This could possibly lead to a puncture in this device. Therefore, a protective fabric does appear to be imperative if a device such as this is likely to become widely commercial. Another issue with wearing the device is the weight of the device. Those with paretic hand and wrist musculature likely also have some weakness in the proximal upper extremity musculature. The weight of the PLA and silicon rubber is minimal for one finger. However, the weight of the device adds up when considering multiple fingers, some type of microfluidic pump or actuator, a microcontroller and the added weight of air or water being pumped into the hollow chambers.

A final problem with the current device created was the lack of motion and force created by this device. According to the results of the can and key turn experiments in chapters 3 and 4, a force of approximately 20 N (nearly 1 pound) is required for key turn and significant ROM is required for both the can and key turn activities. Considering the capabilities of the hand, can grasp and key turn are activities that require minimal effort. With all of the problems mentioned

above, soft robotic actuators face an uphill battle for extensive commercial use for those who have paretic hands.

### 5.5.3. Mechanical Gear System/Future Work

As a result of the significant challenges with soft orthotics/robotics, an effort has been made to create a mechanical gear device to passively move fingers. At this time, this research is still in the early stages. The goal of this research moving forward is still to create a device that moves the MCP and PIP/DIP joints of the fingers independently, is light weight, and creates biomimetic forces synonymous with the normal hand. The device, as can be seen in Figure 6.4,

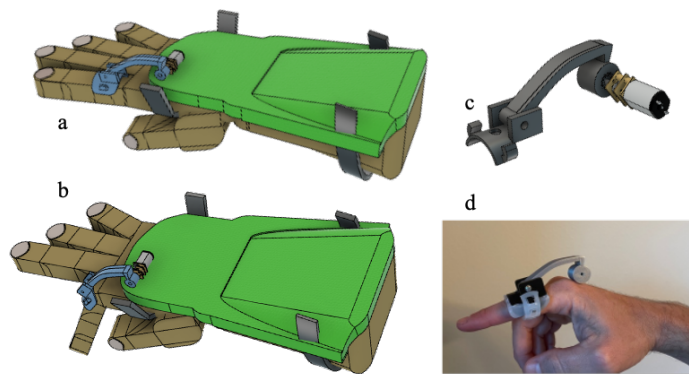


Figure 5.17. Gear orthosis: a) at rest, b) with MCP flexion, c) gearmotor with angle overhang, d) current fabricated device

utilized Fusion 360 CAD software to print a PLA portion to push on the hand. The PLA portions are attached to a 6V 1500 rpm micro metal gearmotor with a gear ratio 10:1. The arc of the PLA arm has been created so that it closely mimics the osteokinematic and arthrokinematics motions that occurs at the hand. Once testing has been completed, further work will be performed on the PIP/DIP portion of the device. After actuation has been characterized, attachment of the SR/CNT sensor grid to this device would provide sensory feedback to the user. Completion of

this project could provide those with paretic hands the ability to live more independently and prevent the necessity of 24-hour supervision.

## **5.6. Summary of Sensors and Actuators**

Advances in electronics are allowing for exploration into small sized devices. These small devices are required for the hand due to the multiple joints and large amount of movement in a small region. An SR force sensor, such as that which is proposed here, could provide many commercial applications for use. Those could include a wearable glove during exercise that communicates with a smart electronic device such as a phone. This device could track progress and make exercise more interactive and rewarding. This device also has potential in ergonomics in tracking the amount of force required to perform various work duties. The potential would be valuable in tracking which activities could be causing work related injuries and possibly developing alternatives such as robotics to complete these activities. Another interesting possibility would be capturing forces in elite performers such as athletes, artists, and musicians. This would be useful in data in determining the difference between elite and non-elite performs when attempting to catch a football, strum a guitar, swing a golf club, throw a baseball, or perform a pommel horse routine.

Most of all, analysis of the hand and wrist is critical for future development of biomimetic orthotics and robotics. There is currently an absence of literature in regard to the movement and forces of the hands that occur during ADLs. More information is required to create algorithms that allow for greater devices and control of those devices that will move paralyzed hands. With greater technology advances, there is a distinct possibility that many individuals with disabilities will be able to return to independent

living. That technology has provided miniature motors and pumps that will allow for selectivity in moving the individual joints of the hand and wrist. However, these devices need to incorporate the normal movement patterns that the predominant normal population uses for everyday activities such as grasping a can or turning a key. Typically, those activities do not require a significant amount of cognitive effort to accomplish. These devices must assist the disabled population also perform these activities with minimal cognitive effort. Otherwise, these somewhat expensive devices will be rendered to a shelf with the user left frustrated and in need of assistance for those everyday tasks. In addition to the movement patterns built into the device, sensors must be incorporated into the device to create a feedback system. This is necessary so that the user is able to adjust forces applied or movement patterns as a result of real time sensory inputs such as shear (slipping of a key out of the fingers) or deformation (compression of a can from too much force).

## 6. Conclusion

Hand paralysis is a debilitating condition that prevents those affected from completing everyday daily activities. This renders those individuals unable to live independently and necessitates 24-hour supervision. Devices such as prosthetics and orthotics have been employed to assist those with this debilitating condition. Science fiction movies such as Terminator and Star Wars have concocted prosthetic hands that provide sensory and actuation components that appear similar to normal human movement. However, there are no widely popular commercial devices that are utilized in reality. This appears related to the lack of true biomimetic components in the current designs.

In this research, basic forces and movement patterns were captured that could assist in building the proper algorithms when fabricating these future devices. While performing these experiments, limitations in the current technology were noted. Therefore, an attempt was undertaken to build a flexible device that is capable of capturing forces over a large surface area of the hands. While the research is incomplete, the method of using a flexible, conductive embedded substrate appears to be a promising venture.

Although effort has also been utilized in creating an actuating device to move the hand, much more effort is required. Early attempts were made with a popular technique of soft robotics. However, it appears that soft robotics may be limited in its functional use due to factors such as weight of the device, limitations in force, and vulnerability to puncture. Another attempt has begun with a mechanical device using a gearmotor. More attention must be focused on modeling to move portions of the fingers independently. However, the goal is still to create a device that moves the hand in a biomimetic fashion and utilize the CNT/SR sensor to provide sensory feedback to the user simultaneously.



## Appendix A. IRB Approval

### dProject Report and Continuation Application

(Complete and return to IRB, 130 David Boyd Hall.

Direct questions to IRB Chairman Dennis Landin,

578-8692.)

IRB#: 3823 Your Current Approval Expires On: 1/19/2018

Review type: Expedited Risk Factor: Minimal Date Sent: 7/17/2021

PI: Sara Winges Dept: Kinesiology

Student/Co-Investigator: Eddie Austin

Project Title: Capturing Measurements of the Phalanges with a Force Glove During ADLs

Number of Subjects Authorized: 20

**Please read the entire application. Missing information will delay approval!**

# LSU

Institutional Review Board  
Dr. Dennis Landin, Chair  
130 David Boyd Hall  
Baton Rouge, LA 70803  
P: 225.578.8692  
F: 225.578.5983

[irb@lsu.edu](mailto:irb@lsu.edu) | [lsu.edu/research](http://lsu.edu/research)

I. PROJECT FUNDED BY: \_\_\_\_\_ LSU proposal # \_\_\_\_\_

II. PROJECT STATUS: Check the appropriate blank(s); and complete the following:

- 1. Active, subject enrollment continuing
- 2. Active, subject enrollment complete
- 3. Active, subject enrollment complete; work with subjects continues.
- 4. Active, work with subjects complete; data analysis in progress.
- 5. Project start postponed
- 6. Project complete; end date 12/31/2017
- 7. Project cancelled: no human subjects used.

III. PROTOCOL: (Check one).

- Protocol continues as previously approved
- Changes are requested\*
  - List (on separate sheet) any changes to approved protocol.

IV. PARTICIPANT ENROLLMENT

- > Number of participants enrolled 10

V. UNEXPECTED PROBLEMS: (did anything occur that increased risks to participants):

- > State number of events since study inception: 0 since last report: 0
- > If such events occurred, describe them and how they affect risks in your study.
- > Have there been any **previously unreported** events? Y/N N  
(if YES, attach report describing event and any corrective action).

VI. CONSENT FORM AND RISK/BENEFIT RATIO:

Does new knowledge or adverse events change the risk/benefit ratio? Y/N N;

Is a corresponding change in the consent form needed? Y/N N

VII. ATTACH A BRIEF, FACTUAL SUMMARY of project progress/results to show continued participation of subjects is justified; or to provide a final report on project findings.

VIII. ATTACH CURRENT CONSENT FORM (only if subject enrollment is continuing); and check the appropriate blank:

- 1. Form is unchanged since last approved
- 2. Approval of revision requested herewith: (identify changes)

Signature of Principal Investigator: \_\_\_\_\_

Date: 11/27/2017

## Appendix B. Questionnaire

General Participant Questionnaire

Date of Data Collection: \_\_\_\_\_

Subject Code: \_\_\_\_\_

---

**Please answer the following questions/check the appropriate boxes.**

Date of Birth: \_\_\_\_\_  
(month /day/ year)

Ethnicity:  
 Hispanic or Latino  
 Not Hispanic or Latino

Height: \_\_\_\_\_ (inches or meters)

Race:

Right or Left Handed: \_\_\_\_\_

American Indian / Alaska Native  
 Asian  
 Native Hawaiian or other Pacific  
 Black or African American  
 White  
 More than one race

Gender:  
Islander

Male  
 Female

Have you ever had any injury that affected the use of your arm or hands? \_\_\_\_\_  
(yes/no)

If yes, please describe: \_\_\_\_\_  
\_\_\_\_\_  
\_\_\_\_\_

## Bibliography

- [1] L. R. Hochberg *et al.*, "Reach and grasp by people with tetraplegia using a neurally controlled robotic arm," (in eng), *Nature*, vol. 485, no. 7398, pp. 372-375, 2012, doi: 10.1038/nature11076.
- [2] P. H. Peckham, J. T. Mortimer, and E. B. Marsolais, "Controlled prehension and release in the C5 quadriplegic elicited by functional electrical stimulation of the paralyzed forearm musculature," *Annals of Biomedical Engineering*, vol. 8, no. 4, pp. 369-388, 1980/07/01 1980, doi: 10.1007/BF02363440.
- [3] B. S. Armour, E. A. Courtney-Long, M. H. Fox, H. Fredine, and A. Cahill, "Prevalence and Causes of Paralysis-United States, 2013," *American Journal of Public Health*, vol. 106, no. 10, pp. 1855-7, Oct 2016, doi: 10.2105/AJPH.2016.303270.
- [4] M. J. DeVivo, Chen, Y., Mennemeyer, S.T., Deutsch, A., "Costs of Care Following Spinal Cord Injury," *Topics in Spinal Cord Injury Rehabilitation*, vol. 16, no. 4, pp. 1-9, 2011, doi: <https://doi.org/10.1310/sci1604-1>.
- [5] A. J. Thurston, "Paré and prosthetics: the early history of artificial limbs," (in eng), *ANZ Journal of Surgery*, vol. 77, no. 12, pp. 1114-9, Dec 2007.
- [6] A. Verkhatsky, O. A. Krishtal, and O. H. Petersen, "From Galvani to patch clamp: the development of electrophysiology," (in eng), *Pflügers Archiv: European Journal of Physiology*, vol. 453, no. 3, pp. 233-47, Dec 2006, doi: 10.1007/s00424-006-0169-z.
- [7] M. Bresadola, "Medicine and science in the life of Luigi Galvani (1737-1798)," (in eng), *Brain Research Bulletin*, vol. 46, no. 5, pp. 367-80, Jul 15 1998, doi: 10.1016/s0361-9230(98)00023-9.
- [8] K. B. Bhattacharyya, "Edgar Adrian and Patrick Merton: Names Blurred with the Passage of Time," *Annals of Indian Academy of Neurology*, vol. 21, no. 1, pp. 19-23, Jan-Mar 2018, doi: 10.4103/aian.AIAN\_271\_17.
- [9] P. H. Peckham, E. B. Marsolais, and J. T. Mortimer, "Restoration of key grip and release in the C6 tetraplegic patient through functional electrical stimulation," *The Journal of Hand Surgery*, vol. 5, no. 5, pp. 462-469, 1980/09/01/ 1980, doi: [https://doi.org/10.1016/S0363-5023\(80\)80076-1](https://doi.org/10.1016/S0363-5023(80)80076-1).

- [10] P. H. Peckham *et al.*, "Efficacy of an implanted neuroprosthesis for restoring hand grasp in tetraplegia: A multicenter study," *Archives of Physical Medicine and Rehabilitation*, vol. 82, no. 10, pp. 1380-1388, 2001/10/01/ 2001, doi: <https://doi.org/10.1053/apmr.2001.25910>.
- [11] G. Alon, A. F. Levitt, and P. A. McCarthy, "Functional electrical stimulation enhancement of upper extremity functional recovery during stroke rehabilitation: a pilot study," (in eng), *Neurorehabilitation and Neural Repair* vol. 21, no. 3, pp. 207-15, May-Jun 2007, doi: 10.1177/1545968306297871.
- [12] M. J. Mulcahey, R. R. Betz, S. H. Kozin, B. T. Smith, D. Hutchinson, and C. Lutz, "Implantation of the Freehand System during initial rehabilitation using minimally invasive techniques," *Spinal Cord*, vol. 42, no. 3, pp. 146-55, Mar 2004, doi: 10.1038/sj.sc.3101573.
- [13] K. D. Runnalls, G. Anson, S. L. Wolf, and W. D. Byblow, "Partial weight support differentially affects corticomotor excitability across muscles of the upper limb," *Physiological Reports*, vol. 2, no. 12, p. e12183, 2014, doi: <https://doi.org/10.14814/phy2.12183>.
- [14] K. D. Runnalls, G. Anson, and W. D. Byblow, "Partial weight support of the arm affects corticomotor selectivity of biceps brachii," *Journal of NeuroEngineering and Rehabilitation*, vol. 12, no. 1, p. 94, 2015/10/26 2015, doi: 10.1186/s12984-015-0085-6.
- [15] M. A. Delph, 2nd, S. A. Fischer, P. W. Gauthier, C. H. Luna, E. A. Clancy, and G. S. Fischer, "A soft robotic exomusculature glove with integrated sEMG sensing for hand rehabilitation," (in eng), *International Conference on Rehabilitation Robotics*, vol. 2013, p. 6650426, Jun 2013, doi: 10.1109/icorr.2013.6650426.
- [16] I. Hussain *et al.*, "Using the robotic sixth finger and vibrotactile feedback for grasp compensation in chronic stroke patients," in *2015 IEEE International Conference on Rehabilitation Robotics (ICORR)*, 11-14 Aug. 2015 2015, pp. 67-72, doi: 10.1109/ICORR.2015.7281177.
- [17] D. Prattichizzo, M. Malvezzi, I. Hussain, and G. Salvietti, "The Sixth-Finger: A modular extra-finger to enhance human hand capabilities," in *The 23rd IEEE International Symposium on Robot and Human Interactive Communication*, 25-29 Aug. 2014 2014, pp. 993-998, doi: 10.1109/ROMAN.2014.6926382.

- [18] T. Feix, J. Romero, H. Schmiedmayer, A. M. Dollar, and D. Kragic, "The GRASP taxonomy of human grasp types," *IEEE Transactions on Human-Machine Systems*, vol. 46, no. 1, pp. 66-77, 2016, doi: 10.1109/THMS.2015.2470657.
- [19] J. R. Napier, "The prehensile movements of the human hand," *The Journal of bone and joint surgery. British volume*, vol. 38-B, no. 4, pp. 902-13, Nov 1956. [Online]. Available: <https://www.ncbi.nlm.nih.gov/pubmed/13376678>.
- [20] N. Salter, "Methods of measurement of muscle and joint function," *The Journal of bone and joint surgery. British volume*, vol. 37-B, no. 3, pp. 474-91, Aug 1955.
- [21] W. N. Bullard, *In A Reference Handbook of the Medical Sciences*. New York: William Wood & Co, 1886.
- [22] R. W. Lovett and E. G. Martin, "Certain Aspects of Infantile Paralysis: With a Description of a Method of Muscle Testing," *Journal of the American Medical Association*, vol. LXVI, no. 10, pp. 729-733, 1916.
- [23] H. Kendall and F. P. Kendall, *Muscles: Testing and Function*. Baltimore: The Williams and Wilkins Company, 1949.
- [24] F. P. Kendall, E. K. McCreary, and P. G. Provance, *Muscles: Testing and Function: With Posture and Pain*. Williams & Wilkins, 1993.
- [25] J. L. Rudd, "A dynamometer and exerciser," *Archives of Physical Medicine and Rehabilitation*, vol. 32, no. 5, pp. 347-8, May 1951.
- [26] C. O. Bechtol, "Grip test; the use of a dynamometer with adjustable handle spacings," *Journal of Bone and Joint Surgery*, vol. 36-A, no. 4, pp. 820-4;, Jul 1954.
- [27] W. R. Russell, "Use of a recording dynamometer in clinical medicine," *British Medical Journal*, vol. 2, no. 4890, pp. 731-2, Sep 25 1954.
- [28] V. Mathiowetz, N. Kashman, G. Volland, K. Weber, M. Dowe, and S. Rogers, "Grip and pinch strength: normative data for adults," *Archives of Physical Medicine and Rehabilitation*, vol. 66, no. 2, pp. 69-74, Feb 1985.

- [29] G. H. Büscher, R. Kõiva, C. Schürmann, R. Haschke, and H. J. Ritter, "Flexible and stretchable fabric-based tactile sensor," *Robotics and Autonomous Systems*, vol. 63, pp. 244-252, 2015/01/01/ 2015, doi: <https://doi.org/10.1016/j.robot.2014.09.007>.
- [30] T. Sagisaka, Y. Ohmura, Y. Kuniyoshi, A. Nagakubo, and K. Ozaki, "High-density conformable tactile sensing glove," *2011 11th IEEE-RAS International Conference on Humanoid Robots*, pp. 537-542, 2011.
- [31] D. S. Asakawa, G. H. Crocker, A. Schmaltz, and D. L. Jindrich, "Fingertip forces and completion time for index finger and thumb touchscreen gestures," *J Electromyogr Kinesiol*, vol. 34, pp. 6-13, Jun 2017, doi: 10.1016/j.jelekin.2017.02.007.
- [32] A. Kargov, C. Pylatiuk, J. Martin, S. Schulz, and L. Doderlein, "A comparison of the grip force distribution in natural hands and in prosthetic hands," *Disability and Rehabilitation*, vol. 26, no. 12, pp. 705-11, Jun 17 2004.
- [33] Tekscan. "FlexiForce™ Standard Model A201"; DS Rev G 062519 datasheet. [www.tekscan.com/flexiforce](http://www.tekscan.com/flexiforce) 2019, Tekscan, Inc.
- [34] R. Bartlett, "Quantative Analysis of Movement," in *Introduction to Sports Biomechanics: Analysing Human Movement Patterns*, T. a. F. Group Ed., Second Edition ed. New York, NY: Routledge, 2007, ch. 4, pp. 114-162.
- [35] S. Schreven, P. J. Beek, and J. B. Smeets, "Optimising filtering parameters for a 3D motion analysis system," *Journal of Electromyography and Kinesiology*, vol. 25, no. 5, pp. 808-14, Oct 2015.
- [36] C. D. Metcalf, S. V. Notley, P. H. Chappell, J. H. Burridge, and V. T. Yule, "Validation and application of a computational model for wrist and hand movements using surface markers," *IEEE Transactions on Biomedical Engineering*, vol. 55, no. 3, pp. 1199-210, Mar 2008, doi: 10.1109/TBME.2007.908087.
- [37] D. M. Alba, S. Moya-Sola, and M. Kohler, "Morphological affinities of the Australopithecus afarensis hand on the basis of manual proportions and relative thumb length," *Journal of Human Evolution*, vol. 44, no. 2, pp. 225-54, Feb 2003, doi: 10.1016/s0047-2484(02)00207-5.
- [38] J. R. Napier, *Hands*. Princeton, New Jersey: Princeton University Press, 1993.

- [39] S. Almecija, J. B. Smaers, and W. L. Jungers, "The evolution of human and ape hand proportions," *Nature Communications*, vol. 6, p. 7717, Jul 14 2015, doi: 10.1038/ncomms8717.
- [40] C. C. Norkin and J. White, *Measurement of Joint Motion: A Guide to Goniometry*, 2 ed. Philadelphia: F. A. Davis Company, 1995.
- [41] P. R. Reuter and K. R. Fichthorn, "Prevalence of generalized joint hypermobility, musculoskeletal injuries, and chronic musculoskeletal pain among American university students," *PeerJ*, vol. 7, p. e7625, 2019, doi: 10.7717/peerj.7625.
- [42] M. R. Dimitrijevic, Y. Gerasimenko, and M. M. Pinter, "Evidence for a spinal central pattern generator in humans," *Annals of the New York Academy of Sciences*, vol. 860, pp. 360-76, Nov 16 1998, doi: 10.1111/j.1749-6632.1998.tb09062.x.
- [43] J. P. Lund and A. Kolta, "Generation of the central masticatory pattern and its modification by sensory feedback," *Dysphagia*, vol. 21, no. 3, pp. 167-74, Jul 2006, doi: 10.1007/s00455-006-9027-6.
- [44] C.-X. Liu and J.-W. Choi, "Patterning conductive PDMS nanocomposite in an elastomer using microcontact printing," *Journal of Micromechanics and Microengineering*, vol. 19, no. 8, p. 085019, 2009/07/14 2009, doi: 10.1088/0960-1317/19/8/085019.
- [45] C.-X. Liu and J.-W. Choi, "Analyzing resistance response of embedded PDMS and carbon nanotubes composite under tensile strain," *Microelectronic Engineering*, vol. 117, pp. 1-7, 2014/04/01/ 2014, doi: <https://doi.org/10.1016/j.mee.2013.11.013>.
- [46] R. P. Tortorich, E. Song, and J.-W. Choi, "Inkjet-Printed Carbon Nanotube Electrodes with Low Sheet Resistance for Electrochemical Sensor Applications," *Journal of the Electrochemical Society*, vol. 161, no. 2, pp. B3044-B3048, 2013/11/28 2013, doi: 10.1149/2.008402jes.
- [47] T. H. da Costa and J.-W. Choi, "A flexible two dimensional force sensor using PDMS nanocomposite," *Microelectronic Engineering*, Article vol. 174, pp. 64-69, 04/25/April 2017 2017, doi: 10.1016/j.mee.2017.02.001.
- [48] M. S. Dresselhaus, G. Dresselhaus, and P. Avouris, C. E. Ascheron, H. J. Kolsch, and W. Skolaut, Eds. *Carbon Nanotubes Synthesis, Structure, Properties, and Application* (Topics in Applied Physics). Germany: Springer, 2001, p. 461.

- [49] S. Carrara, "Nano-Bio-Technology and Sensing Chips: New Systems for Detection in Personalized Therapies and Cell Biology," *Sensors*, vol. 10, no. 1, pp. 526-43, 01/12 2010, doi: 10.3390/s100100526.
- [50] B. C. Edwards, "The space elevator: a new tool for space studies," *Gravitational and space biology bulletin*, vol. 16, no. 2, pp. 101-5, Jun 2003. [Online]. Available: <https://www.ncbi.nlm.nih.gov/pubmed/12959137>.
- [51] Y. Lin and Y. Z. Xu, "Incorporation of MWCNTs to PMMA Bone Cements: Effects on Fatigue Properties," *Advanced Materials Research*, vol. 971-973, pp. 1013-1016, 2014, doi: 10.4028/[www.scientific.net/AMR.971-973.1013](http://www.scientific.net/AMR.971-973.1013).
- [52] S. Soleymani Eil Bakhtiari, S. Karbasi, S. A. Hassanzadeh Tabrizi, R. Ebrahimi-Kahrizangi, and H. Salehi, "Evaluation of the effects of chitosan/multiwalled carbon nanotubes composite on physical, mechanical and biological properties of polymethyl methacrylate-based bone cements," *Materials Technology*, vol. 35, no. 5, pp. 267-280, 2020/04/15 2020, doi: 10.1080/10667857.2019.1678086.
- [53] R. Osmani, A. Kulkarni, A. H. R. Bhosale, P. Ghodake, and B. Harkare, "Carbon nanotubes: an impending carter in therapeutics," *International Journal of Pharmaceutical and Clinical Research*, vol. 6, pp. 84-96, 01/01 2014.
- [54] B. I. Yakobson and P. Avouris, "Mechanical Properties of Carbon Nanotubes," in *Carbon Nanotubes: Synthesis, Structure, Properties, and Applications*, M. S. Dresselhaus, G. Dresselhaus, and P. Avouris Eds. Berlin, Heidelberg: Springer Berlin Heidelberg, 2001, pp. 287-327.
- [55] H. Shima, "Buckling of Carbon Nanotubes: A State of the Art Review," (in eng), *Materials (Basel, Switzerland)*, vol. 5, no. 1, pp. 47-84, 2011, doi: 10.3390/ma5010047.
- [56] C. E. Giusca, Y. Tison, and S. R. Silva, "Evidence for metal-semiconductor transitions in twisted and collapsed double-walled carbon nanotubes by scanning tunneling microscopy," (in eng), *Nano Letters*, vol. 8, no. 10, pp. 3350-6, Oct 2008, doi: 10.1021/nl801782k.
- [57] A. P. Barboza *et al.*, "Deformation induced semiconductor-metal transition in single wall carbon nanotubes probed by electric force microscopy," (in eng), *Physical Review Letters*, vol. 100, no. 25, p. 256804, Jun 27 2008, doi: 10.1103/PhysRevLett.100.256804.

- [58] S. G. Louie, "Electronic properties, junctions, and defects of carbon nanotubes," in *Carbon Nanotubes: Synthesis, Structure, Properties, and Applications*, M. S. Dresselhaus, G. Dresselhaus, and P. Avouris Eds. Berlin, Heidelberg: Springer Berlin Heidelberg, 2001, pp. 113-145.
- [59] E. Tetik, F. Karadağ, M. Karaaslan, and İ. Çömez, "The electronic properties of the graphene and carbon nanotubes: *Ab Initio* density functional theory investigation," *International Scholarly Research Notices Nanotechnology*, vol. 2012, p. 416417, 2012/04/11 2012, doi: 10.5402/2012/416417.
- [60] T. W. Tomblor *et al.*, "Reversible electromechanical characteristics of carbon nanotubes under local-probe manipulation," *Nature*, vol. 405, no. 6788, pp. 769-772, 2000/06/01 2000, doi: 10.1038/35015519.
- [61] G. T. Pham, Y.-B. Park, Z. Liang, C. Zhang, and B. Wang, "Processing and modeling of conductive thermoplastic/carbon nanotube films for strain sensing," *Composites Part B: Engineering*, vol. 39, no. 1, pp. 209-216, 2008/01/01/ 2008, doi: <https://doi.org/10.1016/j.compositesb.2007.02.024>.
- [62] I. Kang, M. J. Schulz, J. H. Kim, V. Shanov, and D. Shi, "A carbon nanotube strain sensor for structural health monitoring," *Smart Materials and Structures*, vol. 15, no. 3, pp. 737-748, 2006/04/25 2006, doi: 10.1088/0964-1726/15/3/009.
- [63] P. J. Cottinet *et al.*, "Strain phenomenon in carbon nanotube buckpaper actuator: Experiments and modeling," *Sensors and Actuators A: Physical*, vol. 194, pp. 252-258, 2013/05/01/ 2013, doi: <https://doi.org/10.1016/j.sna.2013.02.014>.
- [64] A. Kinloch, *Adhesion And Adhesives: Science And Technology*. 1987.
- [65] S. V. Gohil, S. Suhail, J. Rose, T. Vella, and L. S. Nair, "Chapter 8 - Polymers and Composites for Orthopedic Applications," in *Materials for Bone Disorders*, S. Bose and A. Bandyopadhyay Eds.: Academic Press, 2017, pp. 349-403.
- [66] C. Laschi, M. Cianchetti, B. Mazzolai, L. Margheri, M. Follador, and P. Dario, "Soft Robot Arm Inspired by the Octopus," *Advanced Robotics*, vol. 26, no. 7, pp. 709-727, 2012/01/01 2012, doi: 10.1163/156855312X626343.
- [67] C. J. Payne *et al.*, "Soft robotic ventricular assist device with septal bracing for therapy of heart failure," *Science Robotics*, vol. 2, no. 12, p. eaan6736, 2017, doi: 10.1126/scirobotics.aan6736.

- [68] P. Polygerinos *et al.*, "Modeling of soft fiber-reinforced bending actuators," *IEEE Transactions on Robotics*, vol. 31, no. 3, pp. 778-789, 2015, doi: 10.1109/TRO.2015.2428504.
- [69] T. H. Hong, S. Park, J. Park, N. Paik, and Y. Park, "Design of Pneumatic Origami Muscle Actuators (POMAs) for A Soft Robotic Hand Orthosis for Grasping Assistance," in *2020 3rd IEEE International Conference on Soft Robotics (RoboSoft)*, 15 May-15 July 2020 2020, pp. 627-632, doi: 10.1109/RoboSoft48309.2020.9116046.

## Vita

Edward F. Austin, Jr. was born in New Orleans, Louisiana and completed a Bachelor of Science in Occupational Therapy from Northeast Louisiana University. He worked in Baton Rouge, Louisiana for a few years at Our Lady of the Lake Regional Medical Center before pursuing a master's degree. Edward moved to Galveston, Texas and completed a Master of Physical Therapy degree from the University of Texas Medical Branch. On completion, he moved back to Baton Rouge, Louisiana and worked in various outpatient and inpatient physical therapy facilities. Working with patients whose lives were drastically changed as a result of paralysis, Edward sought to gain better engineering-based knowledge in order to build assistive devices. He eventually enrolled in mechanical and electrical engineering courses at Louisiana State University. While attending these courses, Edward maintained a full-time job as a physical therapist at Baton Rouge General Medical Center. Finding similar biomedical interests with mentor and professor Jin-Woo Choi, he joined both the BioMEMS laboratory and electrical engineering graduate school program. On completion of the Doctorate in Philosophy in the field of electrical engineering, Edward has hopes to continue his studies of creating assistive devices for those with paralyzed upper extremities. He also has ambitions to pursue other biomedical devices that can assist in capturing kinematics of disabled, normal, athletic, artistic, and working populations.

